

**INSTITUTO DE QUÍMICA**

**PROGRAMA DE PÓS-GRADUAÇÃO EM GEOCIÊNCIAS - GEOQUÍMICA**

**THIAGO PEREIRA DOS SANTOS**

**SUBTROPICAL WESTERN SOUTH ATLANTIC PALEOCEANOGRAPHY DURING  
THE LAST 190 KYR: EVALUATING MECHANISMS FOR THE BRAZIL CURRENT  
GLACIAL EARLY WARMING AND OCEAN-ATMOSPHERE COUPLING**

**UNIVERSIDADE  
FEDERAL  
FLUMINENSE**

**NITERÓI  
2017**

THIAGO PEREIRA DOS SANTOS

**SUBTROPICAL WESTERN SOUTH ATLANTIC PALEOCEANOGRAPHY DURING  
THE LAST 190 KYR: EVALUATING MECHANISMS FOR THE BRAZIL CURRENT  
GLACIAL EARLY WARMING AND OCEAN-ATMOSPHERE COUPLING**

Tese apresentada ao Curso de Pós-Graduação  
em Geociências da Universidade Federal  
Fluminense, como requisito parcial para a  
obtenção do Grau de Doutor. Área de  
Concentração: Geoquímica Ambiental.

Orientadora:

Prof.<sup>a</sup> Dr.<sup>a</sup> Ana Luiza Spadano Albuquerque

NITERÓI  
2017

UFF. SDC. Biblioteca de Pós-Graduação em Geoquímica

S237 Santos, Thiago Pereira dos.

Subtropical western South Atlantic paleoceanography during the last 190 kyr: evaluating mechanisms for the Brazil Current glacial early warming and ocean-atmosphere coupling / Thiago Pereira dos Santos. – Niterói : [s.n.], 2017.

85 f. : il. ; 30 cm.

Tese (Doutorado em Geociências - Geoquímica Ambiental) - Universidade Federal Fluminense, 2017.

Orientadora: Profª Drª Ana Luiza Spadano Albuquerque.

1. Paleoclimatologia. 2. Paleoceanografia. 3. Foraminíferos planctônicos. 4. Temperatura da água. 5. Produção intelectual. I. Título.

CDD 551.69

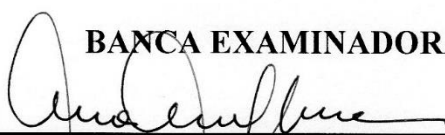
THIAGO PEREIRA DOS SANTOS

**SUTROPICAL WESTERN SOUTH ATLANTIC  
PALEOCEANOGRAPHY DURING THE LAST 180 KYR:  
EVALUATING MECHANISMS FOR THE BRAZIL  
CURRENT GLACIAL EARLY WARMING AND OCEAN-  
ATMOSPHERE COUPLING**

Tese apresentada ao Curso de Pós - Graduação  
em Geociências da Universidade Federal Fluminense,  
como requisito parcial para a obtenção do **Grau  
de Doutor**. Área de Concentração: **Geoquímica  
Ambiental**.

Aprovada em março de 2017.

**BANCA EXAMINADORA**



---

PROFA. DRA. ANA LUIZA SPADANO ALBUQUERQUE  
ORIENTADORA/UFF

---

PROF. DR. CRISTIANO MAZUR CHIESSI  
USP



---

PROF. DR. PEDRO LEITE DA SILVA DIAS  
LNCC



---

PROFA. DRA. CATIA FERNANDES BARBOSA  
UFF



---

PROF. DR. NICOLÁS MISAILIDIS STRÍKIS  
UFF

NITERÓI  
2017

## ACKNOWLEDGEMENTS

First, I thank my parents for their unconditional careful and understanding no matter what I have done along my life. My small but beloved family - my sister, aunts, uncle, nephews, brother-in-law and parents-in-law were all very important during these years. My grandma, who left us long time ago, but planted the most important value of our lives: the power of education to overcome social inequalities.

This path would not be the same without my Juliana. We shared excellent, good and bad moments of real and academic life during the last nine years. I grew up and became a better human being with you and for that, I am deeply grateful. I look forward to realize our future dreams and share more dozens of years at your side. For you all my love.

Complete this work would not be possible without my supervisor Ana Luiza Albuquerque. Our partnership is much longer than these four years and throughout this time, you did not measure efforts to offer me the best conditions for developing my work. Thank you so much for showing me the unknown “paleo-world”, which I am today a real enthusiast.

I thank my Geochemistry friends that directly or indirectly were involved in this work. Special thanks to Igor Venancio for his company in Bremen and constructive discussions and Douglas Lessa for teaching me how to identify the shells many years ago. Thanks to Stephanie Di Chiara and Lu Fontana. I will miss the days with you here. I am grateful to the Geochemistry department employees for all support, particularly Nivaldo and Meiber.

These years living in Niteroi would not be so good without the presence of my biologist friends. Thank you all for our meetings sharing beer, laughter and plans. I hope have you all in my life for many years ahead.

My PhD included one year in Bremen (Germany) which would not have been successful without the contribution of Dr. Stefan Mulitza and Dr. Henning Kuhnert. Thank you for technical support and constructive suggestions. I also thank Prof. Cristiano Chiessi for his valuable contributions and support during first days at MARUM. During this year abroad, Aline Govin provided great improvements to the age model. My year in Bremen would be much harder without the friends I have made there. I thank Fabi and Thomas Kühn and Stephanie for their help in Germany. I hope see you again.

Finally, I am very thankful to Renato Kowsmann and Petrobras/Cenpes for providing sediment core GL-1090 (and others) to make this project available. I also thank David Nielsen by the South Atlantic Convergence Zone data.

## RESUMO

Reconstruções paleoceanográficas da Corrente do Brasil são escassas e carecem da resolução temporal necessária para estudar apropriadamente suas variabilidades durante períodos importantes dos ciclos glaciais-interglaciais. Neste trabalho, é apresentada a primeira reconstrução paleoclimática em alta resolução combinando ferramentas geoquímicas e micropaleontológicas da Corrente do Brasil ao longo dos últimos 185 ka. Durante o último e penúltimo períodos glaciais, a temperatura de superfície (SST) aferida pelo Mg/Ca mostrou um forte resfriamento em 47 ka e 156 ka, que é seguido por uma tendência de aquecimento do final do Estágio Isotópico Marinho (MIS) 3 para o MIS 1 e do final do MIS 6 para o MIS 5e, respectivamente. Além disso, após as baixas SSTs em 47 ka (156 ka) a Corrente do Brasil aqueceu-se ininterruptamente em direção a Terminação I (II), sem apresentar temperaturas mínimas relacionadas ao Último Máximo Glacial (penúltimo máximo glacial). A razão para o forte resfriamento e gradual aquecimento durante o final do MIS 3 e MIS 6 poderiam ser resultado de condições orbitais favoráveis, principalmente condicionadas a obliquidade. No entanto, este mecanismo não é suficiente para sustentar o aquecimento observado para o resto do último e penúltimo períodos glaciais. Propõe-se então que, mudanças na Circulação Meridional do Atlântico (AMOC), descritas na literatura, de um modo “quente” para um modo “frio” para o MIS 2 e MIS 6 é responsável pela acumulação de águas quentes na porção oeste do Atlântico Sul subtropical, evitando a ocorrência de temperaturas mínimas durante o último e penúltimo máximos glaciais. Simultaneamente, temperaturas de subsuperfície (100 m) reconstruídas a partir da assembleia de foraminíferos planctônicos revelam um aquecimento similar em 30 ka, que pode ter sido gradualmente transmitido pela superfície. Como resultado, a porção oeste do Atlântico Sul subtropical já possuía águas em superfície e subsuperfície bastante aquecidas durante o período em que o clima frio do Último Glacial ainda estava aproximando-se do seu máximo (23 – 19 ka). Este fato faz desta região uma potencial fonte de calor necessário para desestabilização do clima glacial durante as Terminações. Modificações no  $\delta^{13}\text{C}$  de foraminíferos bentônicos corroboram que uma alteração fundamental no regime de circulação da AMOC pode ser o gatilho para iniciar a acumulação de calor. Além disso, a temperatura derivada do Mg/Ca também indica uma periodicidade relacionada ao ciclo de precessão que pode ter sido transmitida a superfície oceânica através da forçante atmosférica do Sistema de Monção Sul-americano e da Zona de Convergência do Atlântico Sul. Observações atuais exibem que a cobertura de nuvens associada com a precipitação de verão pode reduzir a incidência de radiação solar de onda longa, diminuindo a temperatura da superfície oceânica. No entanto, análises temporais demonstram que esta forçante não é prevalente para todo o período estudado, mas sim, concentrada entre 130 e 40 ka. Os resultados apresentados nesta tese, portanto, lançam luz sobre os mecanismos responsáveis pelo aquecimento da porção subtropical do Atlântico Sul ao fim dos estágios glaciais e sua possível consequência para desestabilização do clima glacial.

**Palavras-chave:** Aquecimento precoce do Atlântico Sul. Transição glacial-interglacial do Atlântico Sul. Giro subtropical do Atlântico Sul. Acumulação de calor e sal nas baixas latitudes. Transferência de calor inter-hemisférica.

## ABSTRACT

Paleoceanographic reconstructions from the Brazil Current are scarce and lack the required temporal resolution to appropriately represent its variability during key periods of the last glacial-interglacial cycles. Here, we present the first high-temporal resolution reconstruction combining geochemical and micropaleontological proxies based on benthic and planktonic foraminifera of the Brazil Current covering the last 185 ka. During the last and penultimate glacial periods, our Mg/Ca-derived sea surface temperature (SST) record shows a strong cooling at ca. 47 and ca. 156 ka, that is followed by a warming trend from late Marine Isotope Stage (MIS) 3 to MIS 1 and from late-MIS 6 to MIS5e, respectively. Importantly, after the low SST at ca. 47 (ca. 156) ka the Brazil Current warmed uninterruptedly towards Termination I (II) after the low SST at ca. 47 and (ca. 156) ka, with no SST minima during the Last Glacial Maximum or (penultimate glacial maximum). The reason for the strong cooling and the warming trend during late-MIS 3 and late-MIS 6 could reside in the favorable obliquity configuration. However, this mechanism is not sufficient to sustain the warming observed for the rest of the last and penultimate glacial periods. We propose that the change in the Atlantic meridional overturning circulation (AMOC), as described in the literature, from a "warm" to a "cold mode" for MIS 2 and MIS 6 is responsible for the accumulation of warm waters in the subtropical western South Atlantic, preventing SST minima during the last and penultimate glacial maxima in the region. Concurrently, subsurface (100 m) temperature derived from planktonic foraminifera assemblage reveals a similar early warming at ca. 30 ka. As a result of this, the western subtropical South Atlantic already had surface and subsurface waters consistently warmed during the period when Last Glacial climate is approaching its maximum (23 – 19 ka, MIS 2). This fact does the western South Atlantic a potential source of heat for disrupting glacial climate and produce massive melting events during terminations. Changes in benthic  $\delta^{13}\text{C}$  corroborates that a fundamental modification in the AMOC mode might have triggered the heat accumulation. Additionally, Mg/Ca-derived SST also indicates a precessional periodicity likely linked to an atmospheric forcing transmitted by the South America Summer Monsoon (SASM) and South Atlantic Convergence Zone (SACZ). Modern observations exhibit that the cloud cover associated with summer precipitation may reduce the long-wave radiation over the ocean, reducing the surface temperature. However, temporal analysis demonstrates that such forcing is not prevalent during all studied period, but it is concentrated between ca. 130 and 40 ka. The results present in this thesis, therefore, shed light on the mechanisms responsible for subtropical South Atlantic climate amelioration at the end of glacial stages and its possible consequences for the destabilization of glacial climate.

**Keywords:** South Atlantic early warming. South Atlantic glacial–interglacial transition. South Atlantic subtropical gyre. Low-latitude heat and salt accumulation. Interhemispheric heat transfer.

## LIST OF FIGURES

Figure 1 .....	11
Figure 2.....	14
Figure 3.....	18
Figure 4.....	20
Figure 5.....	27
Figure 6.....	29
Figure 7.....	32
Figure 8.....	35
Figure 9.....	38
Figure 10.....	42
Figure 11.....	48
Figure 12.....	50
Figure 13.....	54
Figure 14.....	59
Figure 15.....	61
Figure 16.....	63
Figure 17.....	67
Figure 18.....	68
Figure 19.....	70



## SUMMARY

<b>RESUMO.....</b>	<b>4</b>
<b>ABSTRACT.....</b>	<b>5</b>
<b>LIST OF FIGURES.....</b>	<b>6</b>
<b>1 THESIS PRESENTATION .....</b>	<b>10</b>
<b>2 RESEARCH OBJECTIVES.....</b>	<b>13</b>
<b>3 GEOCHEMICAL AND MICROPALEONTOLOGICAL PROXIES.....</b>	<b>14</b>
3.1 OXYGEN ISOTOPE COMPOSITION ( $\delta^{18}\text{O}$ ).....	14
3.2 CARBON ISOTOPE COMPOSITION ( $\delta^{13}\text{C}$ ).....	15
3.3 MAGNESIUM TO CALCIUM RATIO (Mg/Ca).....	16
3.4 MICROPALEONTOLOGY ASSEMBLAGE .....	17
<b>4 PROLONGED WARMING OF THE BRAZIL CURRENT PRECEDES DEGLACIATIONS .....</b>	<b>18</b>
4.1 INTRODUCTION .....	18
4.2 STUDY AREA .....	19
4.3 MATERIAL AND METHODS.....	21
4.3.1 GL-1090 sampling.....	21
4.3.2 Oxygen and carbon isotopic composition of planktonic and benthic foraminifera	21
4.3.3 Planktonic foraminifera Mg/Ca and ice volume-free seawater oxygen isotopic composition.....	22
4.3.4 Age model .....	23
4.4 RESULTS .....	28
4.4.1 Oxygen and carbon isotopic composition of planktonic and benthic foraminifera	28
4.4.2 Sea surface temperature and ice volume-free seawater oxygen isotopic composition.....	28
4.5 DISCUSSION.....	30
4.5.1 The “low/mid-latitude temperature signal” and the early surface warming at the end of the last glacial cycle.....	30
4.5.2 Is the early warming trend a pervasive feature for glacial stages?.....	36
4.5.3 The vigorous Brazil Current during the last glacial descent (MIS 4).....	39
4.6 REMARKS .....	43

<b>5 WESTERN SOUTH ATLANTIC SUBSURFACE WARMING AS A POTENTIAL SOURCE OF HEAT TO COLD MILLENNIAL-SCALE EVENTS .....</b>	<b>44</b>
5.1 INTRODUCTION .....	44
5.2 SOUTH ATLANTIC THERMOCLINE CIRCULATION .....	45
5.3 MATERIAL AND METHODS.....	46
5.3.1 Planktonic foraminifera census count and subsurface temperature estimation .....	46
5.3.2 <i>Globorotalia inflata</i> carbon isotope composition.....	46
5.4 RESULTS .....	47
5.4.1 Subsurface temperature ( $T_{100m}$ ) .....	47
5.4.2 <i>Globorotalia inflata</i> $\delta^{13}C$ .....	49
5.5 DISCUSSION.....	49
5.5.1 Western South Atlantic as a possible source of heat for the Heinrich stadial events.....	49
5.5.2 Marine isotope stage 3/2 transition: a new subsurface temperature baseline and its implication.....	52
5.6 REMARKS .....	56
<b>6 PRONOUNCED THERMOCLINE COOLING OF THE WESTERN SOUTH ATLANTIC DELAYED <math>\Delta^{18}O</math> SHIFT DURING LAST INTERGLACIAL .....</b>	<b>57</b>
6.1 INTRODUCTION .....	57
6.2 MATERIAL AND METHODS.....	58
6.3 RESULTS .....	58
6.4 DISCUSSION.....	59
6.5 REMARKS .....	64
<b>7 EVALUATING THE REGIONAL FORCING ASSOCIATED WITH THE 21-KYR PRECESSIONAL CYCLE AND THE SOUTH AMERICAN SUMMER MONSOON .</b>	<b>66</b>
7.1 INTRODUCTION .....	66
7.2 ATMOSPHERIC CIRCULATION .....	66
7.3 MATERIAL AND METHODS.....	67
7.4 RESULTS .....	68
7.5 DISCUSSION.....	69
7.6 REMARKS .....	71
<b>8 CONCLUSIONS AND FUTURE CHALLENGES .....</b>	<b>73</b>
<b>9 REFERENCES .....</b>	<b>75</b>

## 1 THESIS PRESENTATION

During the last century, subtropical western boundary currents warmed faster than the mean global ocean and, as a consequence, these currents increased their mid-latitude extensions towards the polar regions (WU et al., 2012). Over the South Atlantic, the western boundary domain is represented by the Brazil Current. The warming of this current during the last century acted compressing polar climate, which leads to a poleward shift of the zonally averaged zero-curl line (the separation between subtropical and subpolar regimes) by about  $2^\circ \pm 0.6^\circ$  (WU et al., 2012). These results highlight the crucial work of the western subtropical currents, promoting interaction among low and high latitudes. This pattern in response to a warmer planet may have been repeated during Quaternary time-scale, contributing for the glacial climate expansion or contraction. Into this context, paleoceanography studies in western boundary currents are essential to appropriately fulfill the gap in the knowledge where the human record is no longer present.

In the Brazilian margin, paleoceanography investigations have been conducted usually focused in the Last Glacial Maximum (LGM) and last deglaciation (e. g. ARZ et al., 1999; WELDEAB et al., 2006). Such works indicate that sea surface temperature (SST) was slightly colder during LGM, by around  $1 - 2^\circ\text{C}$  (CHIESSI et al., 2015), which is significantly less prominent than the outstanding cooling of more than  $6^\circ\text{C}$  experienced by the Subantarctic Atlantic (CORTESE et al., 2007). Concerning the salinity content, sea surface salinity (SSS) estimations predict a saltier Brazil Current by  $1 - 2$  psu during the LGM (TOLEDO et al., 2007; CARLSON et al., 2008). All these valuable efforts contributed to enhance the notion that this area may work as a buffer during glacial periods, trapping heat and salt in its surface waters. However, glacial periods were not all of equal magnitude (BARD; RICKABY, 2009) and even an unique glacial interval can present extremely variable patterns throughout its duration. Thus, a full glacial cycle reconstruction with properly resolution is necessary to clarify in depth the patterns of the Brazil Current during distinct climate background. Furthermore, deeper layers of the subtropical western South Atlantic (subsurface/thermocline and mid-depth) were poorly investigated, as well as, the paleoclimate teleconnection with continental reconstructions.

Therefore, in this thesis we applied geochemical and micropaleontological proxies to explore the amplitude and timing of climate change in the subtropical portion of the Brazil Current at  $24^\circ\text{S}$  at high resolution and long time-scale. This approach is included within the

CAPES/*Paleocean* project, which gathers a group of ocean sedimentary records distributed between 20° and 35° S (Figure 1). This project represents the main Brazilian scientific effort in order to produce high-resolution paleoclimate data about the Brazil Current.

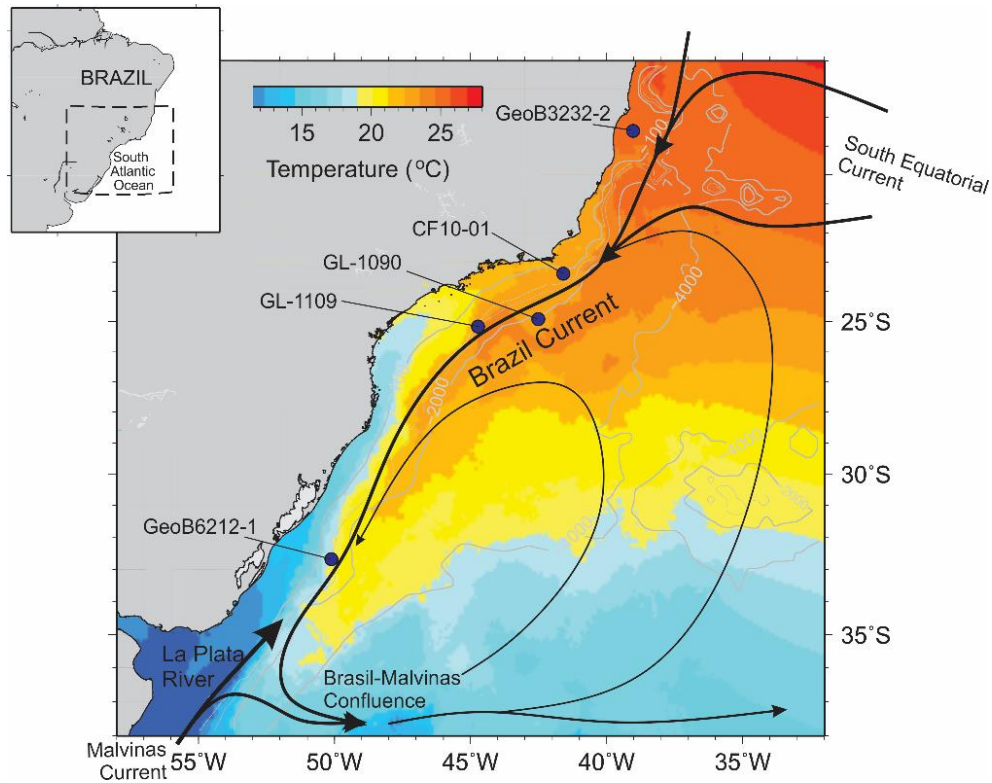


Figure 1 – Distribution of sediment cores included within the CAPES/*Paleocean* project. Core GL-1090 was applied in this work.

For this work, we used core GL-1090 that covers the last 185 ka (Figure 1). The thesis is organized in four chapters. Chapter 1 deals with the surface temperature and mid-depth ventilation proxies to show that a warming trend commencing significantly prior to the last two deglaciations dominated the SST and because of that the minimum of temperature associated with glacial climate is necessarily out-of-phase with the conventional LGM (23 – 19 ka). These findings were recently published in *Earth and Planetary Science Letters* (SANTOS et al., 2017). Chapter 2 explores the subsurface temperature for the last 45 kyr and a possible association between subsurface heat and abrupt climate change at higher latitudes. This draft is passing through internal revision and will be shortly submitted. Chapter 3 and 4 investigate other interesting findings related to core GL-1090 and their ideas will be further developed in future works. Chapter 3 investigates the difference between Termination I and

Termination II and show that a strong thermocline cooling delayed the  $\delta^{18}\text{O}$  shift during the Last Interglacial. Finally, Chapter 4 is dedicated to build a bridge between the South American Summer Monsoon (the main atmospheric system responsible for precipitation in southeastern Brazil) and the surface ocean in long time-scale. We believe that the results presented here will be extremely useful for paleoclimatologists and climate modelers further understand the role of the subtropical western boundary currents on global climate change.

## **2 RESEARCH OBJECTIVES**

The study aims to reconstruct the conditions of surface, thermocline and mid-depth evolution in the western subtropical South Atlantic during the last two glacial-interglacial cycles. Additionally, into this topic the following themes will be explored:

- The timing and mechanisms responsible for subtropical warming at the end of glacial stages.
- The sequence of events surrounding the penultimate and last deglaciations in a subtropical western boundary current.
- A plausible negative feedback between atmosphere circulation related to South America Summer Monsoon and adjacent ocean surface.

### 3 GEOCHEMICAL AND MICROPALAEONTOLOGICAL PROXIES

This topic provides supporting information about the main geochemical and micropaleontological proxies employed in this thesis and states their potential limitations. In terms of geochemical analysis, it was applied benthic (*Cibicides wuellerstorfi*) and planktonic (*Globigerinoides ruber* and *Globorotalia inflata*) foraminifera. Over these species, it was performed oxygen and carbon isotope composition, as well as, elemental ratio measurements. Figure 2 bellow shows the three foraminifera species analyzed here.

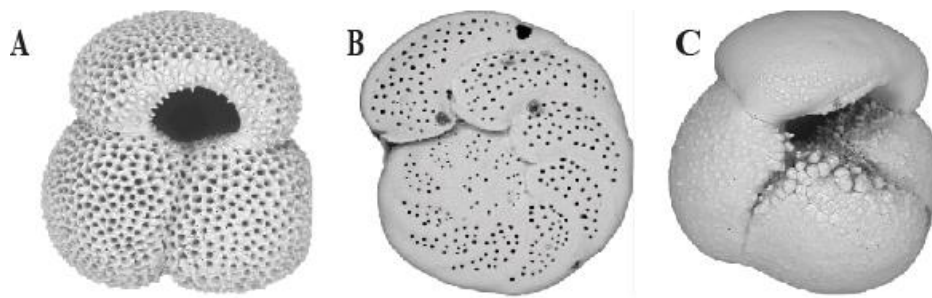


Figure 2 - The three main foraminifera species employed in this study in order to develop oxygen and carbon and elemental ratio measurements. A: *Globigerinoides ruber* white (250-300  $\mu\text{m}$ ). B: *Cibicides wuellerstorfi* (250 – 300  $\mu\text{m}$ ). C: *Globorotalia inflata* (250-300  $\mu\text{m}$ ).

#### 3.1 OXYGEN ISOTOPE COMPOSITION ( $\delta^{18}\text{O}$ )

The oxygen isotope composition ( $\delta^{18}\text{O}$ ) from the shell of planktonic and benthic foraminifera is the most traditional and widely used proxy in paleoceanography. It has been executed since 1950, when Cesare Emiliani analyzed a variety of planktonic foraminifera species from downcore records of the Caribbean Sea. His studies found evidence for many glacial-interglacial cycles over the last half million years, in which the tropical temperature would have varied between 6 – 8  $^{\circ}\text{C}$ . These advances were crucial to establish the isotope stage stratigraphy system, today commonly referred as Marine Isotope Stages (MIS) (BASSINOT, 2007). Today we know that the two stable isotopes of oxygen considered in the  $\delta^{18}\text{O}$  ratio ( $^{18}\text{O}$  and  $^{16}\text{O}$ ) vary according to the ratio in seawater and the temperature at which the carbonate is secreted. The seawater  $\delta^{18}\text{O}$  is sensitive to climate and particularly to the amount of ice stored in continental ice-sheets.  $\delta^{18}\text{O}$  variations found in marine sediments are thus related to climate, and the variation through time are dominated by cycles that can be correlated with the orbital variations in solar radiation (ANDERSON, 2007).

Therefore, in a long time-scale framework heavier values of carbonate  $\delta^{18}\text{O}$  is observed during glacial climate, when considerable amounts of  $^{16}\text{O}$  are trapped in ice-sheets. The opposite is observed during warmer periods, when the ice melts and release the  $^{16}\text{O}$  previously trapped. Consequently,  $\delta^{18}\text{O}$  variability across glacial-interglacial cycles are also strongly linked with sea-level variations, since expansion and retraction of ice-caps is one of the main sea-level modulators (MURRAY-WALLACE, 2007). However, studies of living foraminifera showed that these protozoa not necessarily calcify in equilibrium with ambient seawater and that the stable isotope composition of their test is influenced not only by climatic effects but also by numerous other chemical (e.g., pH, carbonate ion concentration) and biological (e.g., symbiont photosynthesis, metabolic activity, test weight) factors (MULITZA et al., 2003; PADOS et al., 2015). Combination of these and other forcings might make the fossil record difficult to interpret.

### 3.2 CARBON ISOTOPE COMPOSITION ( $\delta^{13}\text{C}$ )

Foraminifera  $\delta^{13}\text{C}$  composition are generally assumed to reflect changes in paleoproductivity and ambient water ventilation. Into the oceans,  $\delta^{13}\text{C}$  is controlled by competing process of  $\text{CO}_2$  exchange with the air, removal of carbon in solids by export production and re-supply of dissolved carbon by subsurface waters (MORTYN AND MARTÍNEZ-BOTÍ, 2007). The net result of these processes is that surface waters are generally enriched in  $^{13}\text{C}$  relative to deeper waters. Planktonic foraminifera  $\delta^{13}\text{C}$  records reflect conditions in a thin surface layer with a high potential variability on regional scales, while benthic foraminifera  $\delta^{13}\text{C}$  are more indicative of long-term stabilized properties in the oceanic deep water reservoir that forms  $> 75\%$  of the global ocean volume (HOOGAKKER et al., 2006). Consequently, the benthic foraminifera  $\delta^{13}\text{C}$  signal is much more used in spite of planktonic foraminifera  $\delta^{13}\text{C}$  signal (HODELL et al., 2009; LOUBERE et al., 2011; PETERSON et al., 2014).

The existing body of foraminiferal isotopic records from deep sea sediment cores provides a picture of glacial deep ocean circulation and ventilation that is dramatically different from the modern ocean (NINNEMANN AND CHARLES, 2002). Glacial reconstruction in the Atlantic demonstrate that a nutricline developed between intermediate and deep waters (2 – 2.5 km) (HODELL et al., 2003) causing a large decrease in  $\delta^{13}\text{C}$  during the last deglaciation. This distribution apparently arose in response to both a reduction of North Atlantic Deep Water and the production of nutrient depleted intermediate depth water



in the North Atlantic (CURRY AND OPPO, 2005). However, new insights from Brazilian margin and other Atlantic cores suggest that reduced ventilation due to a weakened but still active Atlantic Meridional Overturning Circulation also contributed to the low  $\delta^{13}\text{C}$  values during Heinrich stadial 1 (OPPO et al., 2015). It appears that  $\delta^{13}\text{C}$  behaved non-conservatively during the last deglaciation, preventing the conservative mixing between northern and southern water masses to explain the South Atlantic  $\delta^{13}\text{C}$  evolution (TESSIN AND LUND, 2013). Evidence based on neodymium isotopes and therefore, not influenced by carbon cycle variations, corroborate that organic matter remineralization is the dominant cause of the benthic  $\delta^{13}\text{C}$  lowering (HOWE et al., 2016). In this way, the depth of the deep northern-southern water mass interface and the volume of northern sourced waters during the last glacial were not grossly different from that of modern day (GEBBIE, 2014). For the purposes of this work, the benthic  $\delta^{13}\text{C}$  signal is interpreted as a proxy for the Atlantic overturning intensity, since a sluggish overturning cell enables a greater accumulation of nutrients and  $^{13}\text{C}$ -depleted waters in lower North Atlantic.

### 3.3 MAGNESIUM TO CALCIUM RATIO (Mg/Ca)

Among elemental ratios based on geochemistry of foraminifera tests, Mg/Ca is one of the most widely used. The Mg/Ca ratio in planktonic foraminifera is a temperature proxy and its greatest advantage is the need for no other parameters to calculate the temperature (like the seawater  $\delta^{18}\text{O}$  in the case of carbonate  $\delta^{18}\text{O}$ ). The ratio of magnesium to calcium is nearly constant throughout the ocean, and the residence time for both elements is longer than a million years. Such characteristic turn this proxy very robust on glacial-interglacial time-scale (MORTYN; MARTINEZ-BOTI, 2007). Other clear advantage of this carbonate-based thermometer is that coupling  $\delta^{18}\text{O}$  and Mg/Ca potentially provides a novel way to adjust for the temperature dependency of  $\delta^{18}\text{O}$  and isolate the record of seawater  $\delta^{18}\text{O}$ , which can then be used to reconstruct local changes in salinity and evaporation/precipitation balance and provide valuable information about continental ice-volume (ROSENTHAL AND LINSLEY, 2007).

The substitution of magnesium into foraminifera calcite is associated with change in enthalpy or heat of reaction, which is sensitive to temperature. As the substitution of magnesium into calcite is an endothermic reaction, the Mg/Ca ratio is expected to increase with increasing temperature (ROSENTHAL AND LINSLEY, 2007). Alternative environmental controls, like pH and salinity, are also invoked to be a play in magnesium

incorporation. ARBUSZEWSKI et al. (2010) found a 27 % increase in *G. ruber* Mg/Ca ratios per 1 salinity unit increase for seawater salinities above 35.5. However, newer study show that regional differences in preservation, rather than salinity, significantly affects *G. ruber* Mg/Ca-SST in the Atlantic, supporting results that found salinity only has minor influence on Mg/Ca ratios (HERTZBERG AND SCHMIDT, 2013). Indeed, core top studies along bathymetric transects indicate a systematic decrease in Mg/Ca ratios with increasing depth, thereby suggesting that foraminifera Mg/Ca is altered by post-depositional dissolution on the seafloor driven by depth-dependent decrease in carbonate saturation level (DEKENS et al., 2002). Despite this potential biases, here we follow results that interpret *G. ruber* Mg/Ca-SST as reflecting preferentially surface temperatures.

### 3.4 MICROPALAEONTOLOGY ASSEMBLAGE

The microfossil assemblage can be used for a variety of targets, which includes biostratigraphy chronology, temperature, water column stratification and productivity estimations (KUCERA et al., 2005; MORTYN AND MARTÍNEZ-BOTÍ, 2007; BOUDAGHER-FADEL, 2012). Planktonic foraminifera assemblage often is applied in transfer function, a statistical method to reconstruct an environmental parameter of interest, which commonly is the temperature (TELFORD AND BIRKS, 2005). The Modern Analogue Technique is an example of transfer function. This technique attempts to match a geological sample from the past with a set of modern samples containing a similar faunal assemblage through statistical measures known as coefficient of dissimilarity. Disadvantages of this method rely on the assumption that assemblage variability is only affected by water temperature (TELFORD et al., 2004), which is not necessarily true, since other factors such as food availability, light and preferential dissolution can alter the final assemblage composition. In this work, transfer function established with planktonic foraminifera assemblage was employed to estimate the subsurface temperature (100 m), where the *G. ruber* Mg/Ca-SST is not able to detect. Additionally, relative abundance of individual species was used as a secondary proxy to infer conditions related to water column structure taking into account their well-known ecological preferences.

## 4 PROLONGED WARMING OF THE BRAZIL CURRENT PRECEDES DEGLACIATIONS<sup>1</sup>

### 4.1 INTRODUCTION

The ultimate pacing of glacial-interglacial variations is linked to cyclic changes in the Earth's orbital parameters, but orbital variations are insufficient to drive the large amplitude of climatic cycles (SIGMAN AND BOYLE, 2000). Internal feedback mechanisms such as atmospheric CO<sub>2</sub> concentrations, the growth and decay of continental ice sheets and the meridional circulation must amplify the climate response to orbital forcing (Figure 3). In order to better explain the role of each internal mechanism it is fundamental to determine the timing when the distinct natural archives initiated their transition to a subsequent climate pattern. For the South Atlantic and Southern Ocean, available time series indicate that their altered sea surface temperature (SST) precedes North Atlantic SST warming and ice-volume decay at all orbital frequencies by thousands of years (MULITZA et al., 2007). However, the underlying mechanisms for this remain poorly understood, mainly in southern subtropical gyres. Paleoceanographic studies in subtropical regions, therefore, are crucial to accurately determine the causes of this early response and its possible consequences, since low-latitude oceans provide heat and moisture to high latitudes.

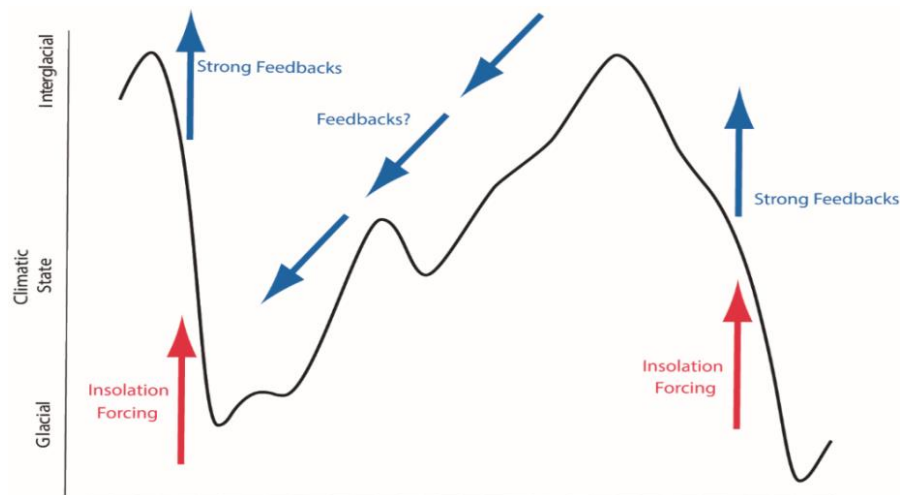


Figure 3 - Schematic example of saw-toothed climatic response, with fast feedbacks that cause rapid deglaciations after long-term ice build-up (modified from RUDDIMAN, 2006).

<sup>1</sup> SANTOS, T. P.; LESSA, D. O.; VENANCIO, I. M.; CHIESSI, C. M.; MULITZA, S.; KUHNERT, H.; GOVIN, A.; MACHADO, T.; COSTA, K. B.; TOLEDO, F.; DIAS, B. B.; ALBUQUERQUE, A. L. S. Prolonged warming of the Brazil Current precedes deglaciations. **Earth and Planetary Science Letters**, v. 463, p. 1–12, 2017. DOI: 10.1016/j.epsl.2017.01.014. Normalizado segundo as normas do periódico.

In the South Atlantic subtropical gyre, the western branch is dominated by the Brazil Current. Millennial-scale paleoceanographic reconstructions show that the southward-flowing Brazil Current may have stored and redirected part of the excess heat and salt of the South Atlantic during periods of reduced Atlantic meridional overturning circulation (AMOC) (e.g., CARLSON et al., 2008). Such periods, like Heinrich stadial (HS) 1, led to a warming of the surface layer in the BC (e. g. CHIESSI et al., 2015). Moreover, benthic foraminifera  $\delta^{13}\text{C}$  reveals that the deep Brazil margin received an input of carbon from a  $^{13}\text{C}$ -depleted reservoir during HS 1 (TESSIN AND LUND, 2013). These findings show that shifts in the SST might be coeval with changes in mid-depth ocean ventilation. The association between ocean interior circulation and surface temperature proxies in a long subtropical record could provide important information about climate transitions and reveal the role of ocean circulation in driving subtropical warming.

Here, we present a high-temporal resolution paleoceanographic reconstruction of the subtropical western South Atlantic for the last two glacial cycles. Our results show that the Brazil Current SST record fits into the subtropical southern hemisphere pattern described by PAHNKE AND SACHS (2006), whereby a strong cooling around 47 ka is followed by a warming trend during late-MIS 3. Nonetheless, the warming trend initiated in late-Marine Isotope Stage (MIS) 3 evolved uninterruptedly towards Termination I, with no temperature minimum observed during the Last Glacial Maximum (LGM). This feature led to a substantial early warming trend, which also took place during the penultimate glacial (MIS 6). Furthermore, during the last glacial inception (MIS 4), our SST and salinity records demonstrate a sudden transition to a warmer and saltier period that lasted for 10 ka. Together with other studies, we show that MIS 4 was not a period of globally in-phase cold conditions as previously thought. In this way, our findings shed light on the mechanisms responsible for subtropical South Atlantic warming at the end and onset of glacial stages.

## 4.2 STUDY AREA

The uppermost circulation (0-600 m) in the subtropical western South Atlantic is dominated by the southward-flowing Brazil Current (BC) (STRAMMA AND ENGLAND, 1999). The BC originates at ca. 10 °S from the southern branch of the bifurcation of the South Equatorial Current that is also the source of the northward-flowing North Brazil Current (PETERSON AND STRAMMA, 1991) (Figure 4). The BC shows its highest intensity during austral spring and summer when the Intertropical Convergence Zone (ITCZ) shifts southward

and the northeasterly trade-winds are stronger (RODRIGUES et al., 2007). Due to the high incoming solar radiation and excess evaporation that characterize the tropical South Atlantic, the BC at the surface is composed of warm ( $> 20^{\circ}\text{C}$ ) and saline ( $> 36$ ) Tropical Water. Around  $38^{\circ}\text{S}$ , the BC collides with the northward-flowing Malvinas Current, producing the Brazil-Malvinas Confluence (Figure 4). Most of the South Atlantic Central Water (SACW) is formed at the Brazil-Malvinas Confluence (PETERSON AND STRAMMA, 1991). The SACW is colder ( $\sim 6 - 20^{\circ}\text{C}$ ), less saline ( $34.6 - 36$ ) and richer in nutrients than the Tropical Water. SACW is then incorporated into the permanent thermocline of the South Atlantic subtropical gyre (PETERSON AND STRAMMA, 1991), which is transported southwards by the BC below the Tropical Water at our study site. Deeper in the water column, the western South Atlantic is bathed by the upper portion of the North Atlantic Deep Water (NADW), originating from the northern North Atlantic and circulating between 1200 m and 2500 m (STRAMMA AND ENGLAND, 1999).

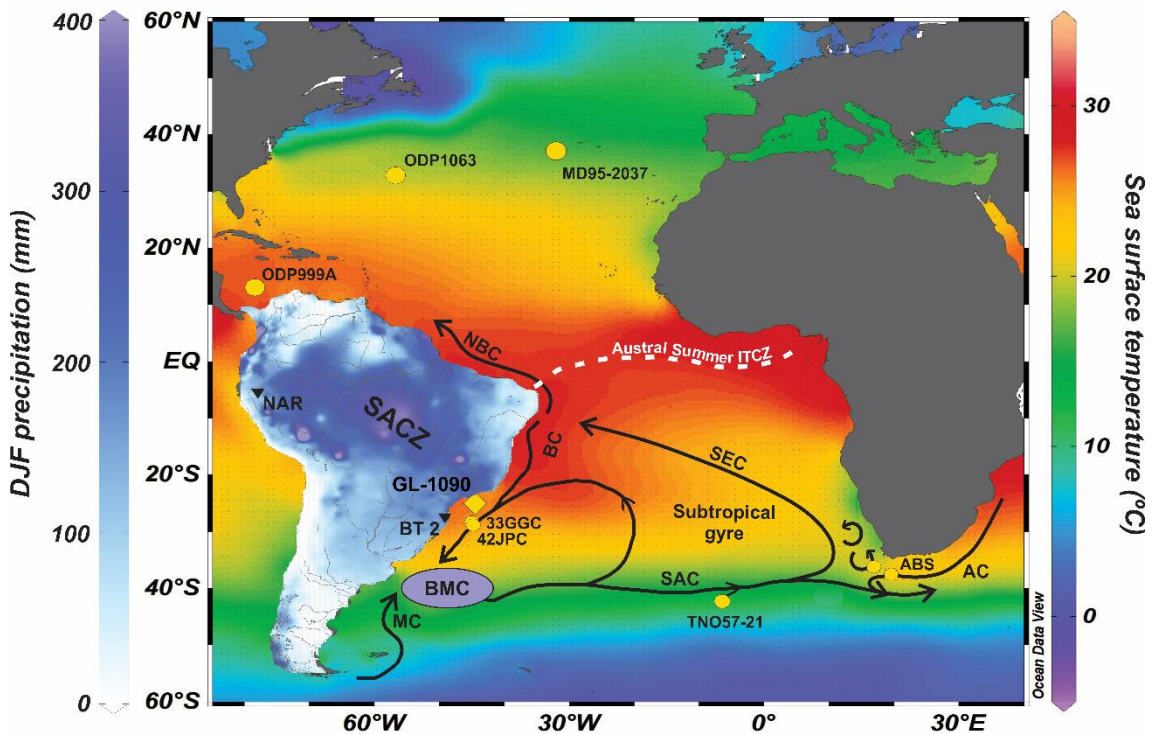


Figure 4 - Position of core GL-1090 (this study) and other records discussed in this work. 33GGC (2082 m) and 42JPC (2500 m) (TESSIN AND LUND, 2013), TNO57-21 (4981 m) (BARKER AND DIZ, 2014), Agulhas Bank Splice (ABS) formed by the cores MD96-2080 (2488 m) and MD02-2594 (2440 m) (Martínez-Méndez et al., 2010), ODP999A (2827 m) (SCHMIDT AND SPERO, 2011), ODP1063 (4584 m) (BÖHM et al., 2015), MD95-2037 (CALVO et al., 2001), BT2 (Botuverá cave, 230 m above sea level) and NAR (Cueva del Diamante, 960 m above sea level) Thick black lines represent the main surface currents of interest. AC: Agulhas Current, BC: Brazil Current, MC: Malvinas Current, NBC: North Brazil Current, SAC: South Atlantic Current and SEC: South Equatorial

Current. The purple ellipse indicates the region of the Brazil-Malvinas Confluence (BMC). Dashed white line shows the austral summer mean position of Intertropical Convergence Zone (ITCZ). Sea surface temperature refers to January-March temperature from 1955 to 2012.

## 4.3 MATERIAL AND METHODS

### 4.3.1 GL-1090 sampling

Core GL-1090 was collected by the Petrobras oil company in the western South Atlantic (24.92 °S, 42.51 °W, 2225 m water depth, 1914 cm long) (Figure 4). The core was sampled at approximately 2 cm resolution. GL-1090 consists mostly of greenish to olive glacial sediments somewhat rich in foraminifera-bearing silty clay. Carbonate-rich Holocene and Last Interglacial sediments are represented by more reddish-brown and whitish clays, respectively. From each sample, 10 cm<sup>3</sup> of sediment was wet-sieved over a 150-µm mesh. The residual material was oven-dried for 24 h at 50 °C. The dried material was handpicked with a stereomicroscope to select ideal shells of benthic and planktonic foraminifera (Figure 2) for the geochemical analysis described below (Table 1).

### 4.3.2 Oxygen and carbon isotopic composition of planktonic and benthic foraminifera

Benthic foraminifera oxygen ( $\delta^{18}\text{O}$ ) and carbon ( $\delta^{13}\text{C}$ ) stable isotope analyses were performed on 438 samples. In most cases (373 samples), analyses were conducted on the species *Cibicides wuellerstorfi* (250-300 µm size fraction). For those samples with insufficient *C. wuellerstorfi* (65 samples), we employed the species *Uvigerina peregrina* (250-300 µm). Planktonic foraminifera analyses were conducted on 832 samples of the species *Globigerinoides ruber* (white variety, *sensu stricto*, 250-300 µm). For both benthic and planktonic foraminifera samples, around ten shells of each species were selected. The *C. wuellerstorfi*  $\delta^{18}\text{O}$  measurements were converted to *U. peregrina*  $\delta^{18}\text{O}$  by adding 0.69 ‰, according to the offset proposed by ZAHN et al. (1986).  $\delta^{13}\text{C}$  values of the endobenthic *U. peregrina* were not considered. All analyses were performed at the MARUM – Center for Marine Environmental Sciences, University of Bremen, Germany using a Finnigan MAT251 gas isotope ratio mass spectrometer coupled to a Kiel III automated carbonate preparation device. Data were calibrated against an in-house standard (Solnhofen limestone). The results are reported in per mil (‰, parts per thousand) versus Vienna Peedee belemnite (VPDB). The

standard deviation based on replicate measurements of the in-house standard was 0.06 ‰ and 0.04 ‰, for  $\delta^{18}\text{O}$  and  $\delta^{13}\text{C}$ , respectively.

#### 4.3.3 Planktonic foraminifera Mg/Ca and ice volume-free seawater oxygen isotopic composition

Mg/Ca analyses were performed on samples comprising 30 shells of *G. ruber* (white, *sensu stricto*, 250-300  $\mu\text{m}$ ) that were gently crushed and cleaned following the procedure described by Barker et al. (2003). Before dilution, samples were centrifuged for 10 minutes to exclude any remaining insoluble particles from the analyses. The diluted solutions were analyzed with an ICP-OES Agilent Technologies 700 Series with an autosampler (ASX-520 Cetac) and a micro-nebulizer at MARUM. After every five samples, instrumental precision was monitored by analyzing an in-house standard solution of 2.93 mmol/mol Mg/Ca. Each Mg/Ca estimate is an average of three replicate analyses. Standards and replicate runs showed a mean reproducibility of  $\pm 0.03$  mmol/mol (0.07%). Only samples with Al/Ca  $< 0.5$   $\mu\text{mol/mol}$  were used, resulting in 606 samples. To convert Mg/Ca ratios into SST, we applied the *G. ruber* calibration [ $\text{Mg/Ca} = 0.38 \exp 0.09 \cdot (\text{SST} - 0.61)$ ] from DEKENS et al. (2002) for records shallower than 2.8 km.

The temperature- $\delta^{18}\text{O}$  relationship for *G. ruber* (white) [ $\text{SST} = 14.2 + 4.44(\delta^{18}\text{O}_{\text{C}} - \delta^{18}\text{O}_{\text{SW}})$ ] from MULITZA et al. (2003) was employed to estimate the seawater  $\delta^{18}\text{O}$  composition ( $\delta^{18}\text{O}_{\text{SW}}$ ) of surface waters. A conversion factor of 0.27 ‰ was applied to convert the values from VPDB to Vienna Standard Mean Ocean Water (VSMOW) (HUT, 1987). The effect of changes in global sea level was subtracted from  $\delta^{18}\text{O}_{\text{SW}}$  by applying the sea level correction of WAELBROECK et al. (2002) between 185 and 150 ka and GRANT et al. (2012) for the last 150 ka. This produced an ice volume-free seawater oxygen isotopic composition ( $\delta^{18}\text{O}_{\text{IVF-SW}}$ ) as a proxy for changes in sea surface salinity (SSS).  $\delta^{18}\text{O}_{\text{IVF-SW}}$  error estimation takes into account an uncertainty of 1.2 °C for the Mg/Ca-SST equation from DEKENS et al. (2002), which is equivalent to 0.26 ‰  $\delta^{18}\text{O}$  change (MULITZA et al., 2003) and an analytical error for  $\delta^{18}\text{O}$  of 0.06 ‰. Hence, the propagated cumulative error estimated for the  $\delta^{18}\text{O}_{\text{IVF-SW}}$  was  $\pm 0.27$  ‰. Considering the regional  $\delta^{18}\text{O}_{\text{SW}}$  SSS relationship proposed by TOLEDO et al. (2007), our  $\delta^{18}\text{O}_{\text{IVF-SW}}$  mostly predicts a fluctuation of 2 salinity units throughout the studied period. Culture experiments have shown a salinity effect on Mg/Ca in the order of 4 salinity units per °C (DUEÑAS-BOHÓRQUEZ et al., 2009). Thus, the effect of salinity on our Mg/Ca data would result in an error of 0.5 °C or less. HÖNISCH et al. (2013)

suggest that to a large extent the Mg/Ca salinity sensitivity derived from Atlantic core-top sediments is not a direct effect of salinity, but rather the result of the dissolution correction often applied to Mg/Ca data, which can lead to significant overestimation of temperatures. Therefore, we consider that salinity plays a minor role on the control of Mg incorporation in GL-1090 *G. ruber*.

Table 1 - Geochemical and micropaleontological proxies applied in this work with their respective amount and mean temporal resolution along core GL-1090.

Proxy	Species	Total	Mean resolution (ka)
$\delta^{18}\text{O}/\delta^{13}\text{C}$	<i>G. ruber</i>	832	0.22
$\delta^{18}\text{O}/\delta^{13}\text{C}$	<i>G. inflata</i>	818	0.22
$\delta^{18}\text{O}/\delta^{13}\text{C}$	<i>C. wuellerstorfi/U. peregrina</i>	438	0.42
Mg/Ca SST - $\delta^{18}\text{O}_{\text{IVF-SW}}$	<i>G. ruber</i>	606	0.30

#### 4.3.4 Age model

The chronology of core GL-1090 was obtained through the combination of AMS  $^{14}\text{C}$  ages and benthic foraminifera  $\delta^{18}\text{O}$  tie-points (Table 2 and 3) aligned to two reference curves (LISIECKI AND RAYMO, 2005; GOVIN et al., 2014). The complete age-depth model (Figure 5) was built within the software Bacon v.2.2, which uses Bayesian statistics to reconstruct Bayesian accumulation histories for sedimentary deposits (BLAAUW AND CHRISTEN, 2011). For the first 327 cm, we selected ten samples for AMS  $^{14}\text{C}$  dating (Table 2). Each sample was composed of about 500 tests of *G. ruber* (white), which were collected from the residue of the  $> 150\ \mu\text{m}$  mesh after wet sieving and oven drying. The AMS  $^{14}\text{C}$  ages were performed at BETA Analytic (Miami, USA). The  $^{14}\text{C}$  ages were calibrated with the curve Marine13 (REIMER et al., 2013) applying a reservoir age effect of  $407 \pm 59$  years and a  $\Delta R$  of  $7 \pm 59$  (ANGULO et al., 2007). A reversal was identified at 327 cm (Table 2). BLAAUW AND CHRISTEN (2011) explain that Bacon v.2.2 is not affected by outlying dates, since the dates are modeled using a Student  $t$  distribution with wide tails, thereby making the chronological modeling process much more robust against outlying dates. Despite this, we observed that our model presents an improved chronological fit around the negative



excursion of benthic  $\delta^{13}\text{C}$  related to HS 5 without this reversal. Therefore, the final age-model (Figure 5) does not consider the reversal at 327 cm.

Between 327 cm and 1914 cm, the chronology was determined by benthic  $\delta^{18}\text{O}$  correlation (Figure 5A-C and Table 3). The section from 327 cm to 1578 cm was correlated to core MD95-2042, whose chronology has been modified by GOVIN et al. (2014) using the most recent AICC2012 ice core chronology (BAZIN et al., 2013, VERES et al., 2013). This record was used as a reference because of its higher temporal resolution for the last 135 ka, which results in reduced age uncertainties when defining the tie-points. The section from 1578 cm to 1914 cm was correlated to the LR04 benthic  $\delta^{18}\text{O}$  stack of LISIECKI AND RAYMO (2005).

Table 2 - The  $^{14}\text{C}$  ages were calibrated with the curve Marine13 (REIMER et al., 2013) applying a reservoir age effect of  $407 \pm 59$  years and a  $\Delta R$  of  $7 \pm 59$  (ANGULO et al., 2007).

Lab Code	Depth (m)	Age ka $^{14}\text{C}$	Age ka error	cal ka	Lower ka	Upper ka
<b>BETA-404133</b>	0.007	6.69	0.03	7.23	7.16	7.27
<b>BETA-404134</b>	0.017	9.12	0.03	9.88	9.74	9.95
<b>BETA-404135</b>	0.023	11.35	0.04	12.79	12.89	12.72
<b>BETA-404136</b>	0.033	13.76	0.04	16.07	15.97	16.17
<b>BETA-404137</b>	0.061	17.58	0.06	20.69	20.56	20.86
<b>BETA-404138</b>	0.151	25.26	0.11	28.85	28.68	29.08
<b>BETA-404139</b>	0.204	28.36	0.13	31.59	31.41	31.92
<b>BETA-404140</b>	0.243	33.29	0.21	36.77	36.33	37.66
<b>BETA-404141</b>	0.286	37.93	0.35	41.94	41.45	42.36
<b>BETA-404142</b>	0.327	37.69	0.36	41.78	41.25	42.23

Error estimations of  $\delta^{18}\text{O}$  tie-points take into account the mean resolution of the GL-1090 benthic  $\delta^{18}\text{O}$  record around the tie-point depth, the mean resolution of the reference curve around the tie-point age, a matching error visually estimated when defining the tie-points, and the absolute age error of the time-scale used for the reference record. Beyond the  $\delta^{18}\text{O}$  tie-point error estimation, the age model calculated within Bacon v. 2.2 also issues the maximum

and minimum error estimation for the interpolation between two consecutive tie-points along the core (Figure 5E).

Table 3 - Tie-points between GL-1090 *Cibicides wuellerstorfi*  $\delta^{18}\text{O}_c$  and the two reference curves adopted to build the remaining age-depth model. The first curve was applied between 3.27 m and 15.78 m and was extracted from MD95-2042 improved by GOVIN et al. (2014) using the most recent AICC2012 ice core chronology (VERES et al., 2013).

Depth (m)	Tie-point age	Correlated curve	Reference	Estimated error (ka)
<b>3.67</b>	47.32	MD95-2042	Onset of D/O 13	2.2
<b>4.25</b>	51.07	MD95-2042	End of D/O 14	2.3
<b>5.19</b>	58.36	MD95-2042	End of D/O 17	2.7
<b>6.17</b>	62.23	MD95-2042	End of MIS4	1.6
<b>8.47</b>	71.21	MD95-2042	End of D/O 19	1.8
<b>10.53</b>	85.82	MD95-2042	End of D/O 21	1.7
<b>11.58</b>	93.71	MD95-2042	MIS5b/MIS5c	1.8
<b>12.75</b>	102.84	MD95-2042	Onset of D/O 23	1.8
<b>13.20</b>	105.87	MD95-2042	Onset of D/O 24	2.0
<b>13.46</b>	111.23	MD95-2042	Onset of MIS5d	2.4
<b>13.81</b>	126.94	MD95-2042	Onset of MIS5e	2.5
<b>14.03</b>	133.94	MD95-2042	Onset of penultimate deglaciation	2.3
<b>16.86</b>	165.61	LR04	-	4.6

According to our age-depth model, core GL-1090 covers the last 185 ka (Figure 4). Benthic foraminifera  $\delta^{18}\text{O}$  presents a well-defined marine isotope stage sequence, with lightest values occurring during MIS 5e and MIS 1 (3.0 ‰ and 3.2 ‰, respectively). The greatest values of approximately 5.0 ‰ occurred at the end of MIS 6 and MIS 2. The mean sedimentation rate for the whole core is 13 cm/ka. This provides a mean temporal resolution for the planktonic foraminiferal  $\delta^{18}\text{O}$  record of 0.2 ka and for the Mg/Ca and  $\delta^{18}\text{O}_{\text{IVF-SW}}$  records of 0.3 ka. The highest resolution period spans from MIS 5c to MIS 2, with an interval between adjacent samples of 0.07 ka during MIS 4 when the sedimentation rate reaches 24

cm/ka. In contrast, MIS 5e, MIS 5d and MIS 1 recorded the lowest temporal resolution, with intervals between adjacent samples reaching 1.2 ka and sedimentation rates as low as 3 cm/ka.

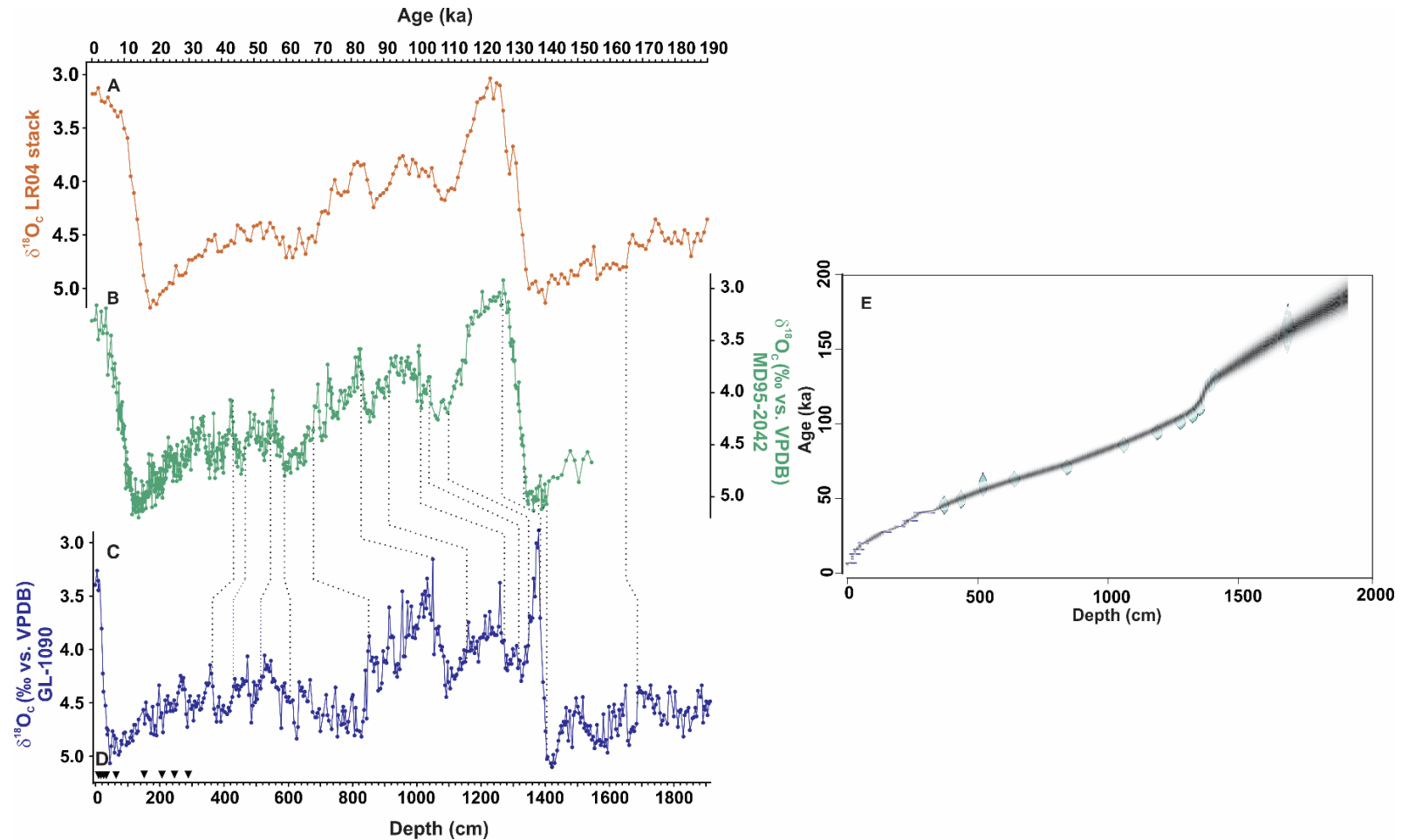


Figure 5 - Reference curves and age-depth model of core GL-1090. A: LR04 benthic foraminifera  $\delta^{18}\text{O}$  stack LR04 (LISIECKI AND RAYMO, 2005). B: MD95-2042 benthic foraminifera  $\delta^{18}\text{O}$  plotted with the age-depth model of GOVIN et al. (2014). C: GL-1090 benthic foraminifera  $\delta^{18}\text{O}$ . D: GL-1090 calibrated  $^{14}\text{C}$  ages. E: Age-depth model based on Bacon v. 2.2 (BLAAUW AND CHRISTEN, 2011). Symbols in panel E represent the positions of calibrated  $^{14}\text{C}$  ages and benthic  $\delta^{18}\text{O}$  tie-points. Error estimations of  $\delta^{18}\text{O}$  tie-points take into account the mean resolution of the GL-1090 benthic  $\delta^{18}\text{O}$  record around the tie-point depth, the mean resolution of the reference curve around the tie-point age, a matching error visually estimated when defining tie-points, and the absolute age error of the time-scale used for the reference record.

## 4.4 RESULTS

### 4.4.1 Oxygen and carbon isotopic composition of planktonic and benthic foraminifera

*G. ruber*  $\delta^{18}\text{O}$  varies between -1.31 ‰ and 0.95 ‰ (Figure 6A). The lowest values occurred during MIS 5e and MIS 1 (-1.24 ‰ and -1.31 ‰, respectively). The highest  $\delta^{18}\text{O}$  values of approximately 0.5 ‰ occurred around the final portion of glacial MIS 6 and MIS 2, as well as during late MIS 4. The penultimate and last deglaciations recorded the highest amplitudes of  $\delta^{18}\text{O}$  change of approximately 2.0 ‰ and 1.7 ‰, respectively. The glacial inception during the MIS 5a/4 transition is represented by an increase of around 0.9 ‰ in  $\delta^{18}\text{O}$  (Figure 6A).

Benthic  $\delta^{13}\text{C}$  varies between -0.6 ‰ and 1.4 ‰ (Figure 6D). Long-term negative excursions (as large as 0.8 ‰) occurred during the latter parts of the penultimate and last glacials, from ca. 150 ka and 40 ka, respectively, as well as during the descent into the last glaciation of MIS 4 when  $\delta^{13}\text{C}$  was lower than 0.2 ‰. Low benthic  $\delta^{13}\text{C}$  values are also present during the MIS 5d/5c and MIS 5b/5a transitions, but these excursions were of shorter duration. The highest  $\delta^{13}\text{C}$  values of around 1.0 ‰ or even higher occurred during MIS 5e, 5c and 5a and MIS 3 and MIS 2 (Figure 6D).

### 4.4.2 Sea surface temperature and ice volume-free seawater oxygen isotopic composition

The mean SST for core GL-1090 was 25.6 °C (Figure 6B). During the last glacial, the lowest SST value (24 °C) occurred at ca. 47 – 45 ka. After 45 ka, SST abruptly increased by 2 °C and remained relatively stable until ca. 32 ka, when a new and more gradual warming initiated (Figure 6B). This warming trend remained constant from late-MIS 3 towards the last deglaciation, elevating the SST by 1 °C. At the MIS 2/1 transition, the SST increased by another 1 °C. After the strong cooling at 47 – 45 ka, the SST in the region was raised by about 4 °C until the early-Holocene. Other SST minima occurred earlier at mid-MIS 6 (ca. 156 ka), MIS 5b and the MIS 5a/4 transition. Similar to the SST evolution observed during the last glacial, cooling during mid-MIS 6 was also followed by a gradual and constant warming trend that was initiated prior to the penultimate deglaciation (Figure 6B). After this long-term warming, the highest SST values (ca. 30 °C) were recorded during the last interglacial (MIS 5e). The last glacial inception between 70 and 60 ka was marked by a strong increase in SST after the low values recorded at the end of substage MIS 5a.

Changes in  $\delta^{18}\text{O}_{\text{IVF-SW}}$  were similar to those registered by the SST record, with high variability within MIS 6 (Figure 6C). The highest  $\delta^{18}\text{O}_{\text{IVF-SW}}$  values, corresponding to the

highest surface water salinity, were identified during the warm intervals MIS 5e, MIS 5c, MIS 5a and MIS 1, but also during MIS 4 and at the end of the penultimate glacial (MIS 6) (Termination II) (Figure 6D). All fluctuations in SST and  $\delta^{18}\text{O}_{\text{IVF-SW}}$  discussed below are larger than the associated methodological uncertainties.

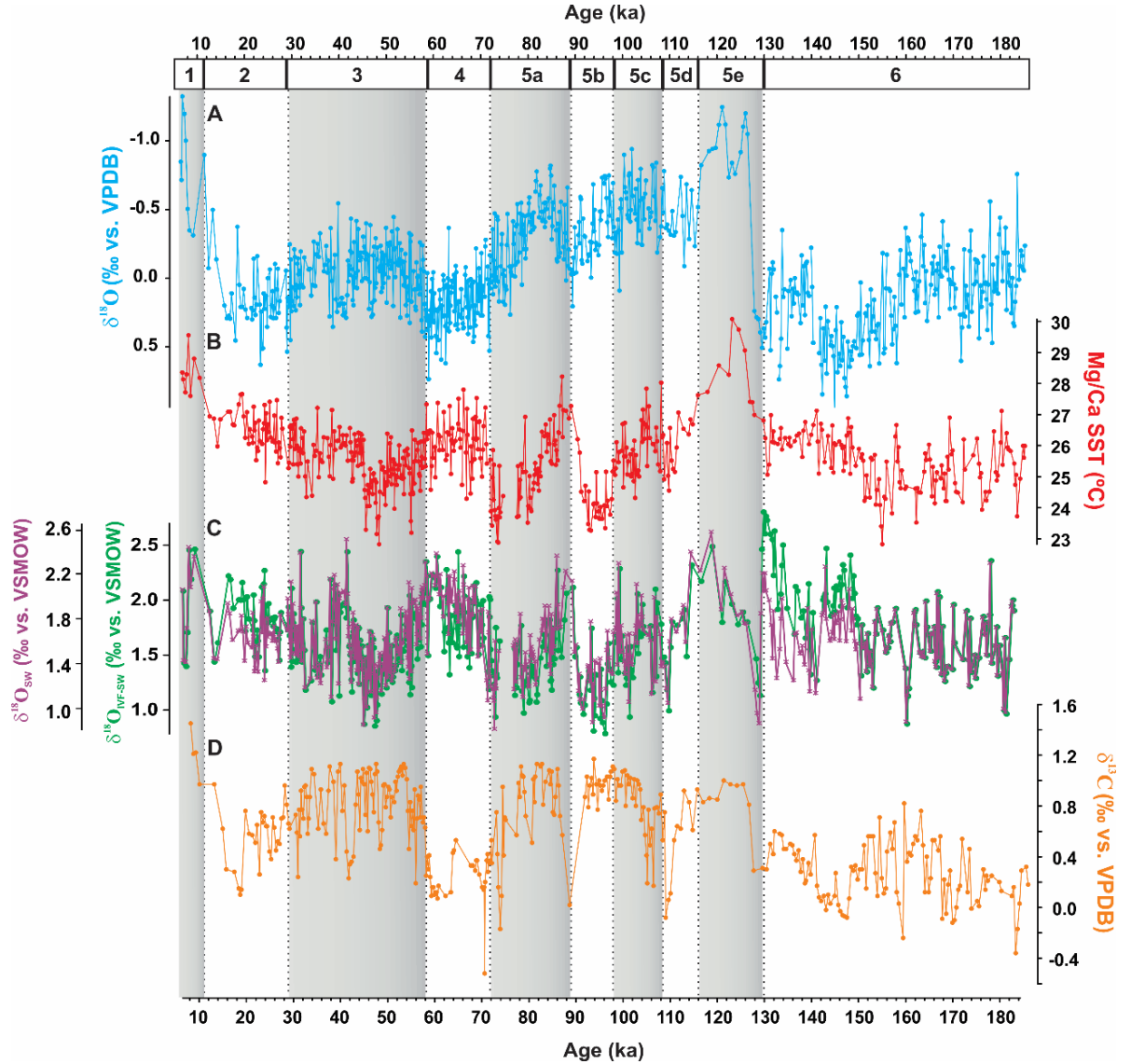


Figure 6 - Main results from core GL-1090 involving ocean surface and mid-depth ventilation. A: *Globigerinoides ruber*  $\delta^{18}\text{O}$ . B: *G. ruber* Mg/Ca sea surface temperature (SST) ( $^{\circ}\text{C}$ ) applying the calibration equation of DEKENS et al. (2002) for *G. ruber* (white). C:  $\delta^{18}\text{O}_{\text{IVF-SW}}$  reconstructed with *G. ruber*  $\delta^{18}\text{O}$  and Mg/Ca SST ( $^{\circ}\text{C}$ ). Green line is the  $\delta^{18}\text{O}_{\text{SW}}$  with ice-volume correction and purple line is the  $\delta^{18}\text{O}_{\text{SW}}$  without ice-volume correction. D: *Cibicides wuellerstorfi*  $\delta^{13}\text{C}$  (*Uvigerina peregrina*  $\delta^{13}\text{C}$  was not considered for the  $\delta^{13}\text{C}$  record). Grey bars highlight warm marine isotopic stages.

## 4.5 DISCUSSION

### 4.5.1 The “low/mid-latitude temperature signal” and the early surface warming at the end of the last glacial cycle

The last glacial portion of our SST record is similar to what PAHNKE AND SACHS (2006) describe as a “low/mid-latitude temperature signal”. This signal is formed by a substantial cooling at ca. 47 ka followed by a warming trend until ca. 23 ka (PAHNKE AND SACHS, 2006). The good agreement of GL-1090 SST to the compilation shown in PAHNKE AND SACHS (2006) demonstrates that our record is unlikely to reflect local SST patterns, but, in fact, presents a characteristic signal of subtropical latitudes (Figure 7).

According to PAHNKE AND SACHS (2006), the subtropical cooling at ca. 47 ka and the progressive warming that followed was caused by orbital forcing, leading to changes in insolation. The high obliquity at 47 ka resulted in decreased mean annual insolation in subtropical regions between 43 °N/S and may have had a significant impact on decreased surface layer temperature, as the upper ocean integrates the mean annual insolation changes over several years (Figure 7A). Moreover, the eccentricity minimum at this time boosted the contribution of obliquity-driven changes by dampening the precessional amplitude (PAHNKE AND SACHS, 2006). The GL-1090 SST cooling between 47 - 45 ka and the subsequent warming was probably controlled by a similar mechanism. The main difference between our reconstruction and the pattern postulated by PAHNKE AND SACHS (2006) is the absence of a clear temperature minimum around the LGM (23-19 ka) (Figure 7A-C). Thus, a very early warming trend starting thousands of years prior to the last deglaciation dominated the temperature evolution of the subtropical portion of the BC. The spliced Agulhas Bank (ABS) (cores MD95-2080 and MD02-2594) record (MARTÍNEZ-MÉNDEZ et al., 2010) also presents a Mg/Ca-derived SST pattern similar to the “low/mid-latitude temperature signal”. Their reconstruction shows an early warming trend starting ~ 3 kyr after GL-1090 warming,

but still thousands of years prior to the last deglaciation. The same pattern is present in the alkenone-derived SST of PAHNKE AND SACHS (2006), where the cooling during MIS 3 is more pronounced than the one that occurred during the LGM, i.e. the period with the largest sea and continental ice volume of the last glacial period. These pieces of evidence indicate that the minimum SST in southern subtropical latitudes could have occurred considerably out-of-phase with glacial maxima of higher latitudes. Therefore, the decrease in obliquity between  $\sim 45$  and 29 ka could be responsible for the increase in mean annual insolation in the subtropics, increasing the SST during late-MIS 3 after the strong cooling at ca. 47 – 45 ka. With the same reasoning, the increased obliquity from 29 ka on should have led to a decrease in subtropical mean annual insolation, decreasing the SST during MIS 2. However, this is not the case, as we observe a SST increase until about 16 ka. Orbital forcing cannot explain the sustained warming through the remaining glacial cycle and another mechanism is necessary to explain the persistent SST increase (Figure 7A). Based on this, we further explored the potential of internal climate mechanisms related to AMOC interhemispheric heat distribution and mid-depth ventilation to explain the progressive warming occurring after ca. 45 ka and the absence of a SST minimum during the LGM in core GL-1090.

Here, we adopted the definition presented by BÖHM et al. (2015) for core ODP1063 (Bermuda Rise) to classify the different AMOC conditions throughout the Last Glacial cycle. In this work, the AMOC “warm mode” concerns the full activity of deep water convection in the high latitude North Atlantic, when the NADW deeply fills the North Atlantic and recirculates near depths of 3 km towards Antarctica. The AMOC “off mode” describes the complete shutdown of the NADW convection and is restricted to some strong abrupt stadial events (BÖHM et al., 2015). Finally, the AMOC “cold mode” is an intermediary between the “warm” and “off” modes, and defines the state when sea-ice is sufficiently extensive to affect



deep water convection, but the NADW continues recirculating in the top 2 km (BÖHM et al., 2015).

Nutrient-related proxies, like benthic  $\delta^{13}\text{C}$ , are useful tools to investigate changes in deep water circulation. However, the  $\delta^{13}\text{C}$  signal can be severely biased by changes in the end-members of source water masses and the addition of respired organic carbon due to biological processes along the advection pathway (OPPO et al., 2015). Terrestrial carbon

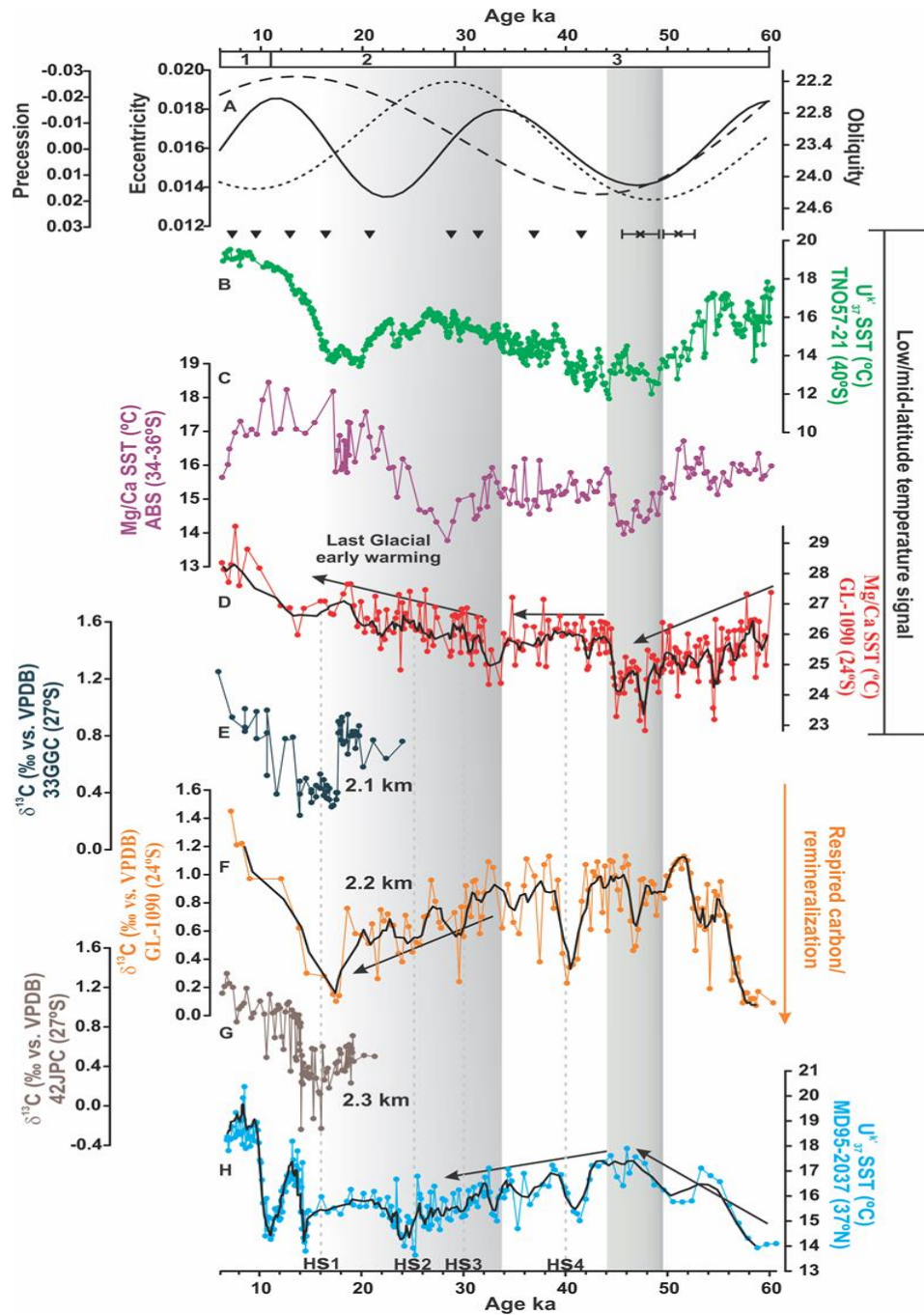


Figure 7 - The “low/mid-latitude temperature signal” and the state of mid-depth ocean ventilation and orbital configuration during the last glacial. A: Precession (thick black line), obliquity (short dashed

line) and eccentricity (long dashed line). B: Alkenone-derived sea surface temperature (SST) of TNO57-21 (40 °S) (PAHNKE AND SACHS, 2006). C: *Globigerina bulloides* Mg/Ca-derived SST for the Agulhas Bank Splice (ABS) formed by cores MD96-2080 and MD02-2594 (34-36 °S) (MARTÍNEZ-MÉNDEZ et al., 2010). D: *Globigerinoides ruber* Mg/Ca-derived SST of GL-1090 (this study). E: *Cibicidoides*  $\delta^{13}\text{C}$  of core 33GGC (TESSIN AND LUND, 2013). F: *Cibicides wuellerstorfi*  $\delta^{13}\text{C}$  of core GL-1090 (this study). G: *Cibicidoides*  $\delta^{13}\text{C}$  of core 42JPC (Tessin and Lund, 2013). H: Alkenone-derived SST of core MD95-2037 (CALVO et al., 2001). Grey bars indicate the strong cooling during MIS 3 and the early warming trend in the southern subtropical records for the last glacial. Black triangles position the calibrated  $^{14}\text{C}$  ages and black crosses depict the benthic  $\delta^{18}\text{O}$  tie-points used to construct the age-depth model of GL-1090.

uptake also has the capacity to alter seawater  $\delta^{13}\text{C}$  (HOOGAKKER et al., 2016). Application of the LGM  $\delta^{13}\text{C}$  end-members of CURRY AND OPPO (2005) to our mean LGM  $\delta^{13}\text{C}$  value indicates a 44 % contribution of northern component waters against a 56 % contribution of Antarctic Bottom Water. During HS 1, this contribution would be even smaller because of the abrupt  $\delta^{13}\text{C}$  decrease at  $\sim 18$  ka. Comparison of our data with the values found further south by TESSIN AND LUND (2013) (Figure 7E-G) for cores 33GGC and 42JPC suggests that the depletion in benthic  $\delta^{13}\text{C}$  during HS 1 is larger by about 0.2 ‰ each 100 m between 2.1 km and 2.3 km.

LGM GL-1090 foraminifera- $\epsilon_{\text{Nd}}$  (not affected by carbon cycle dynamics) suggests that bottom waters at the core site were formed by 78 % of northern component waters (HOWE et al., 2016). For the Holocene,  $\delta^{13}\text{C}$  and foraminifera- $\epsilon_{\text{Nd}}$  indicate very similar proportions of the northern component water of 94 and 93 %, respectively. Furthermore, other LGM  $\epsilon_{\text{Nd}}$  results across the Atlantic require the presence of Glacial North Atlantic Intermediate Water (GNAIW) in the upper 2.5 km (HOWE et al., 2016). Thus, the most likely cause of the strong glacial reduction in  $\delta^{13}\text{C}$  in GL-1090 is related to a weakening of the AMOC (“cold mode”) and the accumulation of  $^{13}\text{C}$ -depleted carbon in the upper 2.5 km (LUND et al., 2015; HOWE et al., 2016). When the AMOC returns to its “warm mode”, the NADW flushes the respired carbon from the mid-depth South Atlantic, and the  $\delta^{13}\text{C}$  and  $\epsilon_{\text{Nd}}$  are again in good agreement.

Under an AMOC “cold mode” scenario, it is expected that the southern hemisphere would trap warm waters mostly in the first 1000 m of the water column (STOCKER AND JOHNSEN, 2003). The warming trend initiated during late-MIS 3 was accompanied by a long-term reduction in benthic  $\delta^{13}\text{C}$ , which culminated in the extremely depleted values during HS 1 (Figure 7D and F). The progressive AMOC slowdown highlighted by decreasing benthic  $\delta^{13}\text{C}$  suggests a reduced efficiency in heat and salt transport from the South to the

North Atlantic. Likely, these conditions sustained the surface warming trend observed at the GL-1090 location (Figure 7A, D and F).

This configuration could also explain the absence of a clear SST minimum during the LGM at our study site (Figure 6D). Previous works that provide SST reconstructions from the subtropical western South Atlantic suggested a surface warming from the LGM to HS 1 of around 1 °C (e. g. CARLSON et al., 2008; CHIESSI et al., 2015). Despite the lower temporal resolution for this interval, GL-1090 also exhibits a temperature increase slightly lower than 1 °C during the LGM/HS 1 transition. However, considering our data, it is difficult to affirm that this small warming was the consequence of reduced AMOC during HS 1 (Figure 7D). In our view, the HS 1 warming is the result of heat accumulation in the surface ocean throughout late-MIS 3/2, which is coeval with the progressive depletion of benthic  $\delta^{13}\text{C}$  caused by the sluggish overturning cell. Interestingly, other earlier HS (HS 6 – 2), which are better defined in our record, are not characterized by significant SST changes (Figure 7D). Therefore, our data suggest that millennial-scale events play a marginal role in the SST evolution of the western subtropical South Atlantic, and the long-term trend dominates the variability of the surface ocean in this region. Despite this, rapid negative excursions are present in the benthic  $\delta^{13}\text{C}$ , especially during HS 4 (Figure 7D). Therefore, HS represent intervals when mid-depth remineralization of organic carbon was abruptly stronger and the surface ocean kept its gradual warming trend (Figure 7D, F).

Despite the damped surface millennial-scale SST variability, our data shows a long-term thermal asynchrony with North Atlantic SST records (Figure 7D, H) (e.g., CALVO et al., 2001), which is usually associated with abrupt millennial events. A clear opposing SST pattern is present in our record compared to the North Atlantic record from core MD95-2037 (CALVO et al., 2001) (Figure 7D, H). This opposing long-term trend could relate to the fact that such interhemispheric temperature contrast would not require a total shutdown of the AMOC, and the gradual progression of glacial conditions at high northern latitudes, with advancing sea-ice cover, is sufficient to produce wide reorganizations in ocean heat distribution. A recent model study showed that an unstable AMOC regime is present during glacial conditions (SÉVELLEC AND FEDOROV, 2015). This unstable mode depends on the North Atlantic sea-ice extent, which can shift the formation site of the GNAIW southwards (SÉVELLEC AND FEDOROV, 2015). Under this scenario, mid-depth convection of the GNAIW can remain active, as suggested by HOWE et al. (2016), but with instabilities that create a thermal contrast across the equator. Thus, the gradual increase of sea-ice in the

northern hemisphere during late-MIS 3/2 might have limited the transport of warm waters from the western subtropical South Atlantic and contributed to the > 10 kyr-long warming period observed in our record.

In summary, the last glacial GL-1090 SST agrees with the subtropical temperature pattern described by PAHNKE AND SACHS (2006), in which a strong cooling occurred between 47 and 45 ka. This low temperature interval is likely associated with the glacial maximum conditions in the BC and other southern subtropical regions (Figure 7B-D). Subsequently, a warming trend dominated the surface layer and preceded by thousands of years the increase in greenhouse gases and the onset of the last deglaciation. From late-MIS 3, this warming is coeval with a decrease in benthic  $\delta^{13}\text{C}$  likely due to remineralization of organic matter (Figure 8), which indicates a fundamental change in AMOC. Therefore, we suggest that the warming of the subtropical western South Atlantic is more influenced by the AMOC state itself rather than other climate forcing. Additionally, the warm water reservoir developed by the subtropical western South Atlantic may have worked as a source of moisture contributing to the growth of the Antarctica ice-sheet, as proposed by ice-core water isotope measurements (STENNI et al., 2004).

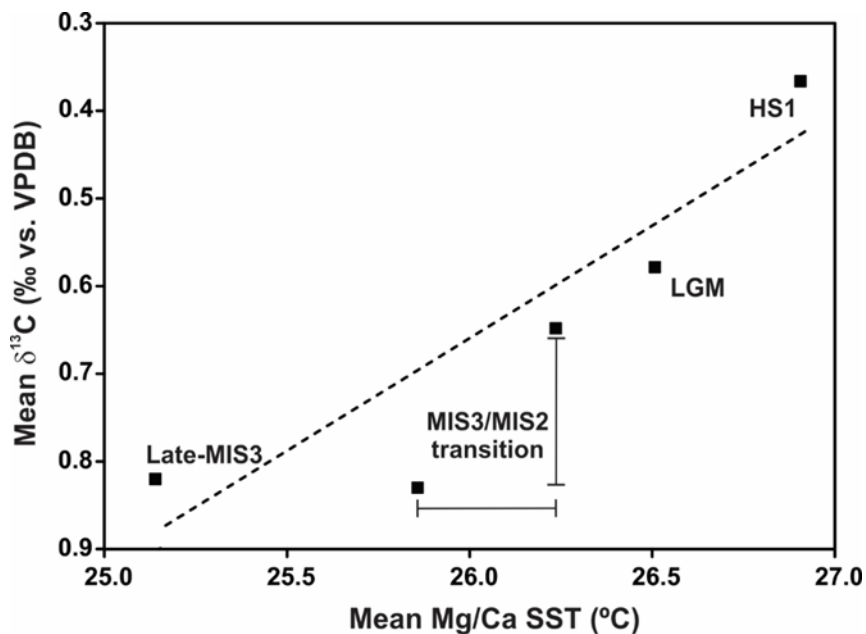


Figure 8 - Mean *Cibicides wuellerstorfi*  $\delta^{13}\text{C}$  against mean *Globigerinoides ruber* Mg/Ca-derived SST from the late-MIS 3 towards the Heirinch stadial 1 (HS 1). The MIS3/2 transition records a pronounced shift in benthic  $\delta^{13}\text{C}$ . After that, the depletion in benthic  $\delta^{13}\text{C}$  and the gradual SST increase followed a quasi-linear trend. Dashed-line indicates linear regression.

#### 4.5.2 Is the early warming trend a pervasive feature for glacial stages?

The early warming trend in core GL-1090 could be interpreted as a feature related to exclusive boundary conditions for the last glacial period. However, a rather similar pattern occurred during the latest portion of the penultimate glacial (MIS 6), raising the possibility that this is a pervasive feature present in the western subtropical South Atlantic. Early-MIS 6 (ca. 185 –160 ka) is characterized by a much higher SST variability not observed in any part of MIS 3. Subsequently, i.e. between 156 and 152 ka, the coldest temperature for MIS 6 was recorded. The pattern of the SST record here is less prominent than the decreasing trend from 60 ka that culminated in the strong cooling between 47 and 45 ka. Nonetheless, SST during this timeframe achieved values slightly lower than 23 °C, i.e. as cold as the SST minimum of the last glacial period (Figure 9B).

The distinct pattern of the MIS 3 and MIS 6 SST minima might be related to the totally different orbital configuration. The minimum SST of MIS 6 is coeval with low obliquity and considerably wider precessional amplitude, which could result in stronger insolation and seasonality. Despite the less marked SST minimum, the early warming trend initiated after 152 ka is quite clear and occurred again thousands of years earlier than the Termination II that culminated in the highest SST recorded during the Last Interglacial MIS 5e at 121 ka. Repetition of this glacial early warming was also observed in the spliced Agulhas Bank SST record, where the authors showed a clear increment in the temperature initiated at early-MIS 6, with a steeper evolution after ~ 152 ka (Figure 9C) (MARTÍNEZ-MÉNDEZ et al., 2010). In that study, SST during the end of the penultimate glacial was even warmer than the temperature of the Last Interglacial (MARTÍNEZ-MÉNDEZ et al., 2010) (Figure 9C). The authors explained their results for *Globigerina bulloides* Mg/Ca based on the increased influence of Agulhas waters during the winter, and the east-west migration of the Agulhas retroflection.

Our depleted benthic  $\delta^{13}\text{C}$  together with Mg/Ca SST could provide an additional explanation. In general, MIS 6 benthic  $\delta^{13}\text{C}$  is marked by lower values compared with the Last Glacial. The early- to mid-MIS 6  $\delta^{13}\text{C}$  record is characterized by higher variability, reaching peaks of 0.7 ‰ (0.3 ‰ lower than the peaks during MIS 3) (Figure 9D). From 152 ka (late-MIS 6), the variability decreases and much depleted values of 0.0 ‰ occurred simultaneously with the onset of surface warming. As the benthic  $\delta^{13}\text{C}$  data strongly indicate a connection between mid-depth ocean ventilation and surface heat distribution, the depletion

of benthic  $\delta^{13}\text{C}$  from late-MIS 6 likely marks the time when the rate of interhemispheric heat transfer slowed down and the residence time of the GNAIW increased (Figure 9B and D).

The  $\epsilon\text{Nd}$  record from Bermuda Rise (Figure 9E) indicates that late-MIS 6 (and also MIS 2) was a period of AMOC “cold mode” (BÖHM et al., 2015). Likely, this “cold mode” is the condition associated with the sustained heat accumulation and depletion of benthic  $\delta^{13}\text{C}$  in the western subtropical South Atlantic that triggered an early warming trend during the final portion of the last two glacial cycles. The beginning of an AMOC “cold mode” period inhibits the western subtropical South Atlantic from recording low SST coeval with glacial maxima at higher latitudes. Thus, the SST minima during glacial stages in the BC region should necessarily occur prior to the onset of the “cold mode”, i.e. when the AMOC is still in “warm mode” (BÖHM et al., 2015) and the western subtropical South Atlantic is shedding heat towards higher latitudes of the North Atlantic through the subtropical gyre recirculation cell. Therefore, we suggest that, if all recent glacial stages have an AMOC “cold mode”, this would likely result in an early glacial cooling that is immediately followed by an early warming trend in the western subtropical South Atlantic.

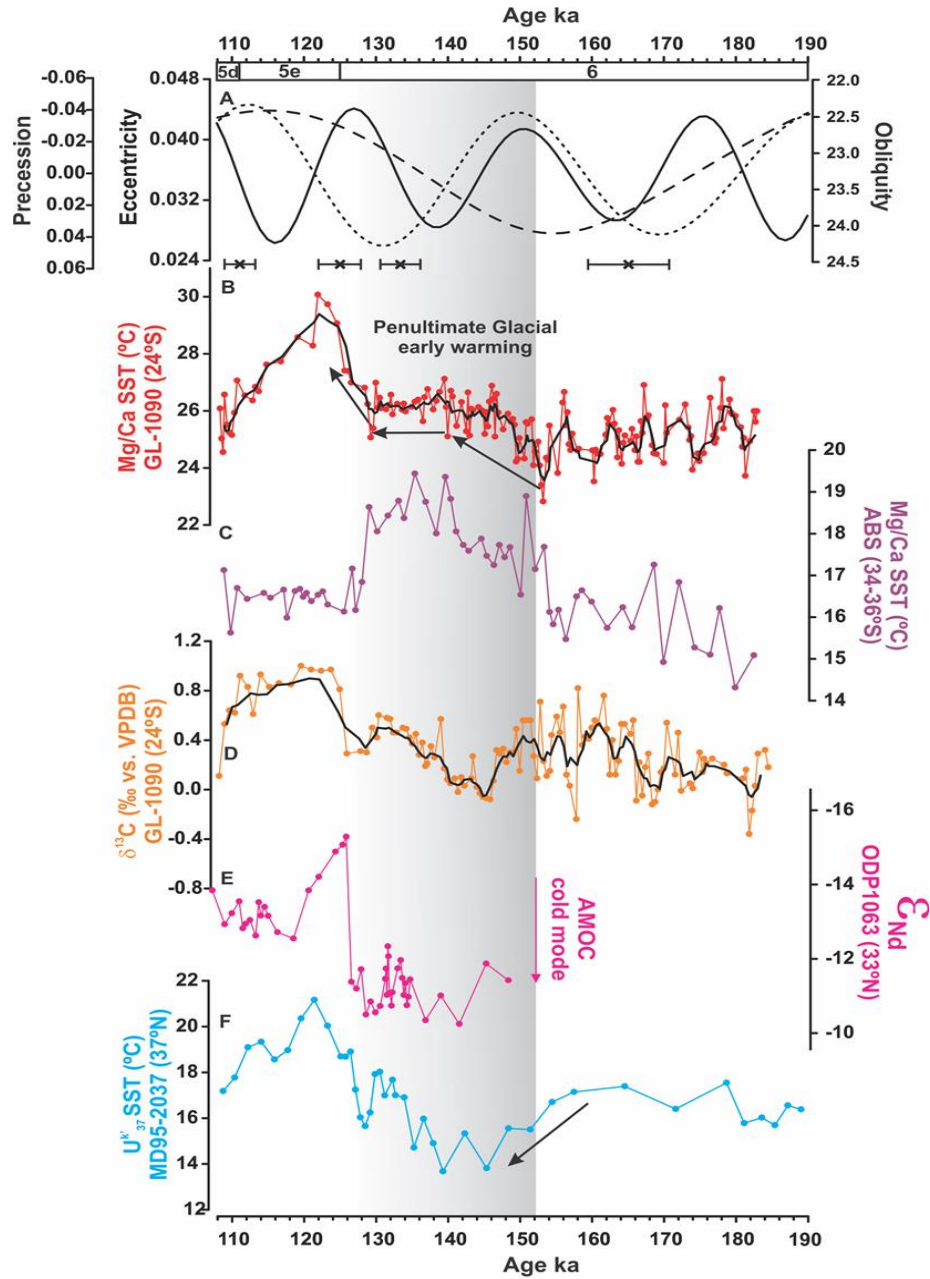


Figure 9 - The state of mid-depth ocean ventilation and orbital configuration during the penultimate glacial A: Precession (thick black line), obliquity (short dashed line) and eccentricity (long dashed line). B: *Globigerinoides ruber* Mg/Ca-derived SST of GL-1090 (this study). C: *Globigerina bulloides* Mg/Ca-derived SST for the Agulhas Bank Splice (ABS) formed by cores MD96-2080 and MD02-2594 (34-36 °S) (MARTÍNEZ-MÉNDEZ et al., 2010). D: *Cibicides wuellerstorfi*  $\delta^{13}\text{C}$  of core GL-1090 (this study). E:  $\epsilon_{\text{Nd}}$  record of core ODP1063 (BÖHM et al., 2015). F: Alkenone-derived SST of core MD95-2037 (CALVO et al., 2001). Grey bar indicates the beginning of early warming trend for the penultimate glacial for the southern subtropical records. Black crosses position the benthic  $\delta^{18}\text{O}$  tie-points.

#### 4.5.3 The vigorous Brazil Current during the last glacial descent (MIS 4)

The interval between 60 and 70 ka represents the transition into full glacial conditions. BARKER AND DIZ (2014) suggest that the transition in the Earth's climate during this period was globally synchronous, generating in-phase cold conditions between southern and northern high latitudes. However, a slightly different picture might emerge as high-temporal resolution records from subtropical latitudes are produced.

In core GL-1090, SST reached  $\sim 27^{\circ}\text{C}$  during substage MIS 5a and then decreased progressively towards the MIS 5a/4 transition (Figure 10E). However, after 70 ka, SST rose abruptly and achieved values similar to peak conditions during substages MIS 5a and 5c, remaining elevated throughout MIS 4. The explanation for this long and stable warming in our record could reside in the complex combination of (i) shifts associated with the Antarctic Circumpolar Current (ACC) and the entire subtropical gyre, (ii) mid-depth ocean circulation and (iii) orbital configuration.

A temperature record from the SE Pacific suggests that the enhanced cooling during MIS 4 was caused by a  $5\text{--}6^{\circ}$  northward shift of the ACC/subtropical gyre system (KAISER et al., 2005). This movement of the subtropical gyre and its associated currents would likely affect the position of the SEC bifurcation in the western South Atlantic. A numerical model study observed that seasonal variation at the latitude where the bifurcation is located partially controls the strength of the NBC and the BC (RODRIGUES ET AL., 2007). In this case, if the bifurcation moved northward together with the ACC/subtropical gyre system, transport of the BC would increase at the expense of a reduction in transport of the NBC. Northward displacement of the bifurcation is also favored by a southward movement of the local wind stress of the marine ITCZ (RODRIGUES et al., 2007). Tropical rainfall reconstructions indicate a relatively southerly position of the ITCZ between 60 and 70 ka, and even further south when HS 6 was initiated during the final period of MIS 4 ( $\sim 64$  ka) (DEPLAZES et al., 2013). Thus, this period combined optimal conditions for the northernmost position of the SEC bifurcation, strengthening the transport of the BC and increasing SST and salinity over site GL-1090 (Figure 10E and F). Likely, this mechanism is also active when climate approach the maximum glacial conditions during the end of MIS 2 and MIS 6. Similarly to HS of MIS 3 and 2, it is difficult to identify a specific response of our SST record to HS 6, given that the abrupt temperature increase was initiated clearly prior to the onset of HS 6 (Figure 10e). The northward movement of the ACC/subtropical gyre also shifts the strong SST gradient formed at the Subtropical Front. This interpretation fits with the observations of



BARKER AND DIZ (2014) that called for an enhanced latitudinal temperature gradient within the South Atlantic/Southern Ocean to explain the low values of *G. bulloides*  $\delta^{18}\text{O}$  within this interval in core TNO57-21. Notably, a warm glacial inception is not an exclusive feature of GL-1090. The Caribbean Sea core ODP999A, despite its lower temporal resolution for this interval, also shows a clear warming trend demonstrated by high Mg/Ca-derived SST during MIS 4 (Figure 10D) (SCHMIDT AND SPERO, 2011). Furthermore, a pronounced thermal gradient between cold air temperatures and a warm subtropical North Atlantic has been proposed as the mechanism for fast ice sheet expansion at this time in Greenland and northern Europe (SÁNCHEZ GOÑI et al., 2013). This evidence reinforces the argument that the BC, and other subtropical gyre currents, might have stored warm and salty waters during such transitions while the climate system transitioned into a glacial background at higher latitudes (Figure 10B-H).

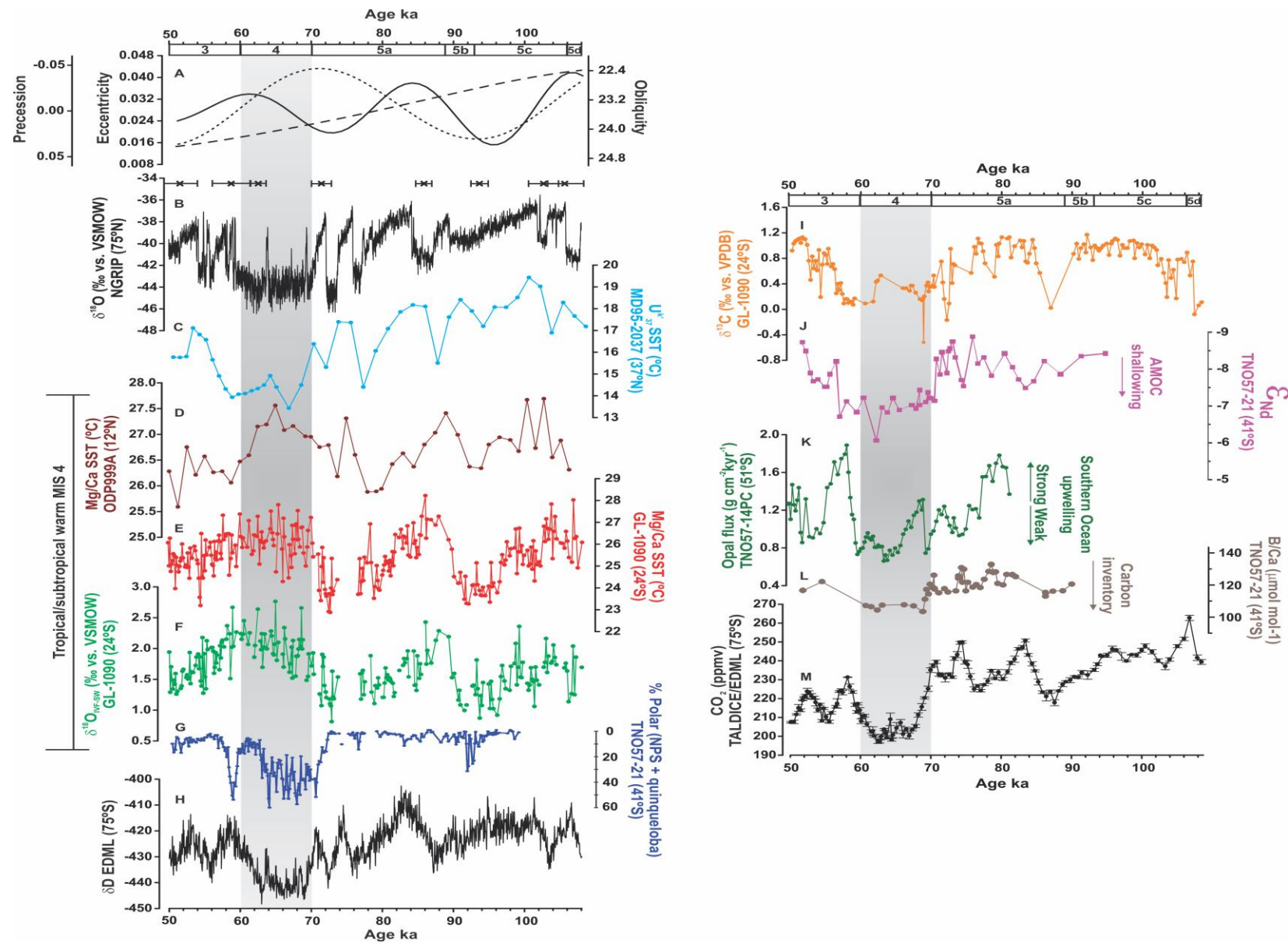


Figure 10 - Comparison of last glacial descent (MIS 4) between low and high latitude records (left hand panel) and state of mid/deep ocean ventilation as well as atmospheric carbon dioxide concentration (right hand panel). A: Precession (thick black line), obliquity (short dashed line) and eccentricity (long dashed line). B: Northern Greenland Ice Core Project  $\delta^{18}\text{O}$  (NGRIP COMMUNITY MEMBERS, 2004) plotted on AICC2012 time-scale (BAZIN et al., 2013; VERES et al., 2013). C: Alkenone-derived sea surface temperature (SST) of core MD95-2037 (CALVO et al., 2001). D: *Globigerinoides ruber* Mg/Ca-derived SST of ODP999A (SCHMIDT AND SPERO, 2011). E: *G. ruber* Mg/Ca-derived SST of GL-1090 (this study). F:  $\delta^{18}\text{O}_{\text{IVF-SW}}$  of GL-1090 (this study). G: Relative abundance of *Neogloboquadrina pachyderma* sinistral and *Turborotalia quinqueloba* of TNO57-21 (BARKER AND DIZ, 2014). H: Antarctica  $\delta\text{D}$  of Dronning Maud Land (EPICA COMMUNITY MEMBERS, 2004) plotted on AICC2012 time-scale (BAZIN et al., 2013; VERES et al., 2013). I: *Cibicides wuellerstorfi*  $\delta^{13}\text{C}$  of core GL-1090 (this study). J:  $\epsilon\text{Nd}$  record of core TNO57-21 (PIOTROWSKI et al., 2005). K: Opal flux of TNO57-13 and TNO57-14 (ANDERSON et al., 2009). L: B/Ca ratio of core TNO57-21 (YU et al., 2016). M: Carbon dioxide in TALDICE/EDML ice-cores (BEREITER et al., 2012). Grey bar in the left-hand panel highlights the contrasting MIS 4 pattern of low and high latitude. Grey bar in the right-hand panel indicates the strong benthic  $\delta^{13}\text{C}$  depletion of core GL-1090 (this study) compared with other studies of Southern Ocean/Antarctica that point for a AMOC shoaling and  $\text{CO}_2$  sequestration into the deep ocean. The black crosses position the benthic  $\delta^{18}\text{O}$  tie-points.

Regarding ventilation of the ocean interior, the MIS 5a/4 transition reveals important changes. GL-1090 benthic  $\delta^{13}\text{C}$  exhibits an abrupt shift from 70 ka, showing extremely depleted values of 0.1 ‰ or even lower (Figure 10I). These values are comparable to those of HS 1, but were produced considerably faster compared with the gradual decrease that occurred from late-MIS 3 up to HS 1 (Figure 7). Obviously, the same processes potentially affecting HS 1  $\delta^{13}\text{C}$  values (see section 5.1) are also at play during the MIS 5a/4 transition, which could overestimate the shallow flow of the GNAIW. However, MIS 4 is characterized by a period of strong  $\text{CO}_2$  sequestration (BEREITER et al., 2012), which requires an expansion of Antarctic Bottom Water to accommodate a larger amount of respired carbon in the deep ocean (MENVIEL et al., 2012). Southern Atlantic  $\epsilon\text{Nd}$  has shown higher radiogenic values from about -8.3 (late-MIS 5a) to -7.3 (MIS 4), indicating a retraction of the GNAIW (Figure 10J) (PIOTROWSKI et al., 2005). Opal flux in the Southern Ocean accounts for a rather reduced upwelling in this period, which increases stratification and retains the carbon in deep layers (Figure 10K) (ANDERSON et al., 2009). Benthic foraminifera B/Ca ratios indicate that enhanced deep carbon storage by at least 50 Gt reduced the carbonate ion concentration by around  $25 \mu\text{mol kg}^{-1}$  during MIS 4 (Figure 10L) (YU et al., 2016). This set of findings, combined with the abrupt nature of our benthic  $\delta^{13}\text{C}$ , may indicate that, at least in part, a shoaling of AMOC could have contributed to the severe  $\delta^{13}\text{C}$  depletion (Figure 10J-N).

Finally, the warm MIS 4 may also have had an orbital component associated. During the MIS 5a/4 transition obliquity changed to very low values, opposite to what is found during

the strong cooling at 47 ka (Figure 10A). This low obliquity resulted in high mean annual insolation between 43 °N/S, consequently warming the subtropical surface ocean. Therefore, MIS 4 gathered ideal conditions for the establishment of a strong, warm and salty BC. However, more high-temporal resolution records are needed to accurately determine the role of low-latitude subtropical regions in long time-scale transitions and decouple the factors behind the strong  $\delta^{13}\text{C}$  lowering during this period.

#### 4.6 REMARKS

The results presented in this chapter exhibit the first high-resolution reconstruction for the last two glacial-interglacial cycle for the BC. Our findings suggest that when AMOC approximates its “cold mode” the subtropical western South Atlantic starts a gradual warming build up that is not only connected to millennial-scale HS 1, as previously thought, but was initiated thousands of years prior to the last deglaciation. Consequently, minimum SST coeval with LGM cannot happen and the coldest SST related to glacial climate is necessarily out-of-phase with maximum glacial cooling of higher latitudes. The presence of this pattern during penultimate glacial enhance that such pattern is a pervasive feature of glacial stages in the BC. The begging of the warming trend at the final portion of glacial stages simultaneous with  $\delta^{13}\text{C}$  depletion strongly suggest that the initial increase in surface temperature is inherently related to deep water convection. In this way, the AMOC reduction is the major forcing for triggering western South Atlantic warming, starting the glacial-interglacial transition in this region. In this scenario, greenhouse gases forcing would take place in a second moment, since their major increase occur later in deglaciations.

## 5 WESTERN SOUTH ATLANTIC SUBSURFACE WARMING AS A POTENTIAL SOURCE OF HEAT TO COLD MILLENNIAL-SCALE EVENTS

### 5.1 INTRODUCTION

Instrumental observations have shown the crucial role of ocean subsurface temperatures for climate variability (ZHANG, 2008). Nowadays, subsurface heat transport from lower to higher latitudes in the middle of winter has the capacity to shorten the ice build-up season (WOODGATE et al., 2010). Paleoclimate reconstruction has systematically shown that ice-sheet disturbs can interfere in deep-water convection associated with Atlantic Meridional Overturning Circulation (AMOC) and trigger regional and global abrupt climate change (BOND et al., 1997; ALLEY et al., 2003; GOTTSCHALK et al., 2015).

Such abrupt climate change severely marked the last glacial period (SKINNER AND ELDERFIELD, 2007), and ocean sediment and ice-core records give us the opportunity to investigate the natural character of these oscillations. Termed as Dansgaard-Oeschger cycles (D-O), these centennial- to millennial-scale events are associated with warm interstadials or cold stadial in Greenland, with some dramatic temperature shifts of more than 11 °C in few years (KANFOUSH et al., 2000; BLUNIER AND BROOK, 2001). A number of explanations, which include solar forcing and volcanism (BAY et al., 2004; BRAUN et al., 2008), were thought as forcing mechanism for that. However, recent works point toward that changes in AMOC play a central role for millennial-scale instabilities and occurred slightly previous than the massive ice-sheet discharge that accompanied the strongest stadial events named as Heinrich stadial (HS) (BARKER et al., 2015; HENRY et al., 2016).

Those changes in the mode of oceanic circulation favor a reduction in North Atlantic Deep Water formation and are apparently followed by a large subsurface warming, increasing the rate of basal melting under the Labrador ice-shelf (ALVAREZ-SOLAS et al., 2013). In this scenario, the iceberg melting may have provided a positive feedback mechanism to accelerate and deepen the initial AMOC slowdown, rather than being the cause of the circulation disruption. At the end of stadial event, subsurface temperatures are equally important, since the stronger it is the vertical temperature gradient in North Atlantic during the stadial the faster will be the rate of the AMOC recovery during the interstadial (MIGNOT et al., 2007).

As important as determine the forcing mechanisms behind millennial-scale changes is also crucial identify the possible regions where subsurface warm waters might accumulate

and be transmitted to northern Atlantic. Therefore, in order to explore the role of southern latitudes during stadial-interstadial oscillation, we present a record exploring the subsurface temperature variability from the western subtropical South Atlantic during the last 45 ka. Our results agree with previous investigation that subsurface warming is coeval or anticipated strong Heinrich stadial (HS) events. Furthermore, a sharp subsurface temperature shift occurred in the transition between MIS 3 and 2, which could have favored the occurrence of the massive HS 1.

## 5.2 SOUTH ATLANTIC THERMOCLINE CIRCULATION

Along the western portion of the South Atlantic subtropical gyre, the Brazil Current transports in the mixed layer the Tropical Water, characterized by intensive radiation, excess of evaporation and poor nutrient concentration with temperature and salinity above 25 °C and 36.5, respectively (CAMPOS et al., 2000). On its way southwards, the surface layer of the Brazil Current gradually loses its heat to the atmosphere, and consequently, its density increases (EMÍLSSON, 1961). Between 34 °S and 43 °S the southward flow of Brazil Current finds the northward flow of the cold and fresh Malvinas Current. The Malvinas Current originates as a branch of the Subantarctic Front, which is the northernmost front associated with the Antarctic Circumpolar Current in the Drake Passage. Both currents turn out the sea in a region of complex mixing zone known as the Brazil-Malvinas Confluence (BMC) (OLSON et al., 1988; GORDON et al., 1992). In this zone the cold, fresh and nutrient-rich South Atlantic Central Water (SACW) is formed. After the confluence the Malvinas and Brazil currents separate from the coast and enter the South Atlantic interior in a series of large amplitude meanders associated with the South Atlantic Current (OLSON et al., 1988). The South Atlantic Current is an eastward current flowing just to the northern limit of the Subtropical Front (PETERSON AND STRAMMA, 1991). When SACW subducts to water depths between 100-600 m in the BMC, it is transported within the South Atlantic Current toward Africa, where a part of it contributes directly to the Benguela Current and then to the South Equatorial Current flowing back toward the Brazilian margin. On the bifurcation of the South Equatorial Current, the SACW can flow south together with the Brazil Current, or crossing the equator associated with the North Brazil Current and North Brazil Undercurrent (STRAMMA AND ENGLAND, 1999). Additionally, according to Tomczak and Godfrey (1994), part of the SACW is not subducted at the Atlantic but is, in fact, Indian Ocean Central Water brought into the South Atlantic by the eddies related to the Agulhas Current intrusions.

In this case, the BMC and the Agulhas leakage region represent the major areas for the formation of the SACW and, therefore, they are crucial for much of the South Atlantic thermocline ventilation (GORDON, 1981).

### 5.3 MATERIAL AND METHODS

#### 5.3.1 Planktonic foraminifera census count and subsurface temperature estimation

Planktonic foraminifera assemblage was analyzed with a mean resolution of 4 cm. We washed 10 cm<sup>3</sup> of sediment in a 150 µm sieve and dried the residuals at 50°C for 24h. The residuals were split until remaining 300 – 500 individuals for identification at specific level in order to determine the planktonic foraminifera assemblage of each sample. Then, the relative abundances was used to estimate paleotemperatures through the Modern Analog Technique (MAT) (HUTSON, 1980). For that, we used the MARGO dataset (KUCERA et al., 2005) with 891 core top of planktonic foraminifera assemblages and temperature values from the Equatorial and South Atlantic. Temperature values of 100 m water depth were extracted for each core top from the World Ocean Atlas (WOA) 2013 (LONCARNINI et al., 2013) using the Ocean Data View software (SCHLITZER, 2002). The MAT model is based on calculations of dissimilarity between the downcore assemblage (fossil) and the core-tops dataset (HUTSON, 1980). The MAT method was performed within the C2 software. The efficiency of the MAT models in reconstructing paleotemperatures were cross-validated using the leave one out method, the analogs dissimilarity was calculated using the Square Chord matrix and the estimated paleotemperature was obtained by the weighted mean from the ten least dissimilar core tops (best analogs).

#### 5.3.2 *Globorotalia inflata* carbon isotope composition

Carbon isotope ( $\delta^{13}\text{C}$ ) analyses were performed on 144 samples of *Globorotalia inflata*. This is a well-known thermocline dweller species of the South Atlantic, but is also very abundant in transitional areas (FAIRBANKS et al., 1980). Previous studies in the South Atlantic successfully applied this species to reconstruct past conditions of the thermocline and migration of mid-latitudes oceanic fronts (CHIESSI et al., 2008; GROENEVELD AND CHIESSI, 2011). For every sample, between 5 and 10 shells of *G. inflata* from 250 – 300 µm size-fraction were handpicked with a stereomicroscope. The analyses were performed at the MARUM – Center for Marine Environmental Sciences, University of Bremen, Germany using a Finnigan MAT251 gas isotope ratio mass spectrometer attached to a Kiel III

automated carbonate preparation device. Data were calibrated against an in-house standard (Solnhofen limestone). The results are reported in per mil (‰, parts per thousand) versus Vienna Peedee belemnite (VPDB). The standard deviation based on replicate measurements of the in-house standard was 0.04 ‰.

## 5.4 RESULTS

### 5.4.1 Subsurface temperature ( $T_{100m}$ )

The mean GL-1090  $T_{100m}$  for the last 45 ka was of 19.4 °C, but accentuated variability marked the record generating temperatures that overcame 23 °C (Figure 11A). At the beginning of this interval,  $T_{100m}$  was relatively low, reaching 17.1 °C at 42.7 ka. Subsequently, the  $T_{100m}$  gradually warmed up to 41.3 ka, where an abrupt peak occurred, leading the  $T_{100m}$  to 22.7 °C at 39.3 ka. Right after this peak, the  $T_{100m}$  abruptly dropped and remained as low as 15 °C up to 31.1 ka. This interval between 39.3 and 31.1 ka (late-MIS 3) showed the lowest  $T_{100m}$  for the last 45 ka and then was initiated the main shift in the  $T_{100m}$  during the transition MIS 3/2. This shift is marked by a progressive increment in the subsurface temperatures up to 27.3 ka. From ~ 29 ka on, the  $T_{100m}$  remained considerably stable around 21 °C, dropping below 20 °C only between 15.5 and 12.8 ka (Figure 11A).



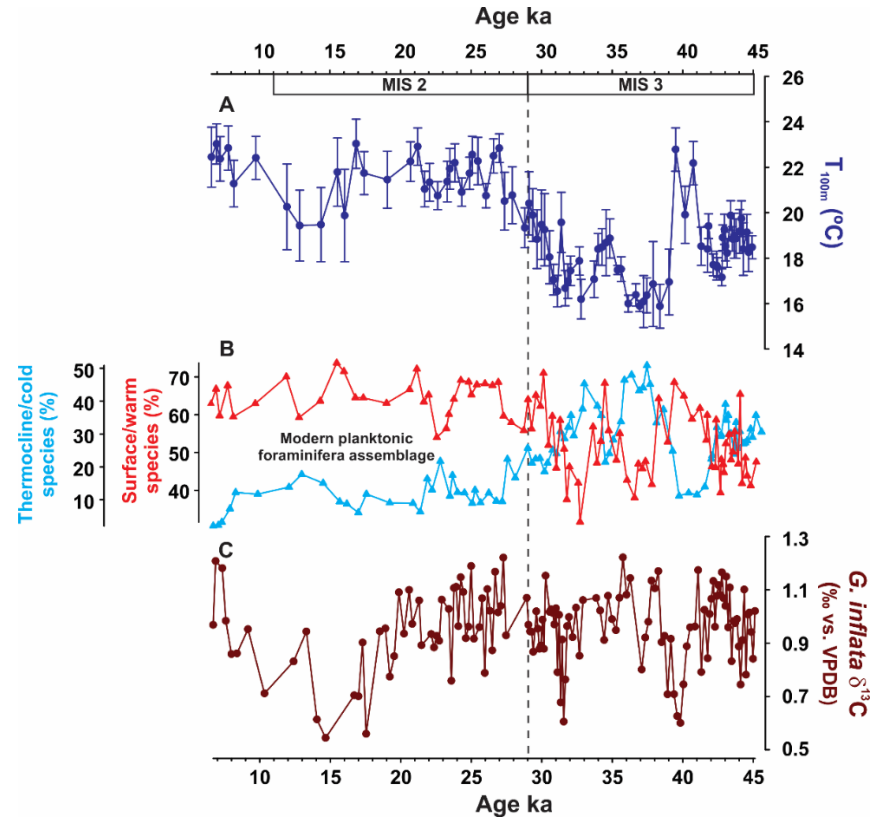


Figure 11 - Main results from core GL-1090 involving ocean subsurface/thermocline layer for the last 45 kyr. A: Subsurface temperature ( $T_{100m}$ ) derived from Modern Analogue Technique (MAT). B: Surface/warm (*Globigerinoides ruber* (white and pink variants), *Globigerinoides sacculifer* (with and without sac), *Globigerinella siphonifera* and *Globoturborotalita rubescens*) and thermocline/cold (*Globigerina bulloides*, *Globorotalia truncatulinoides* (left and right coiling), *G. inflata* and *Neogloboquadrina durtetrei*) species groups. C: Thermocline dweller *Globorotalia inflata*  $\delta^{13}C$ .

Figure 11B presents the relative abundance of the main surface/warm and thermocline/cold species in core GL-1090. These two groups are formed by the four most common species that compose the surface and thermocline layers and had the highest weight for the temperature calculation. Usually, the two groups represent more than 70 % of the all assemblage. The warm/surface group is represented by *Globigerinoides ruber* (white and pink variants), *Globigerinoides sacculifer* (with and without sac), *Globigerinella siphonifera* and *Globoturborotalita rubescens*. The cold/thermocline group is formed by *Globigerina bulloides*, *Globorotalia truncatulinoides* (left and right coiling), *G. inflata* and *Neogloboquadrina durtetrei*. These groups have clear opposite ecological preferences and because of that, the cold late-MIS 3 exhibited the highest abundances of thermocline/cold species, reaching almost 50 % of the planktonic foraminifera assemblage. Contrastingly, the transition to MIS 2 marks the time when the warm/surface group fairly dominated the

assemblage and the strong variability that characterized MIS 3 substantially decreased (Figure 11B). From this point, the modern planktonic foraminifera assemblage is mostly determined.

#### 5.4.2 *Globorotalia inflata* $\delta^{13}\text{C}$

*G. inflata*  $\delta^{13}\text{C}$  ranged between 1.2 and 0.5 ‰ during the study period (Figure 11C). Strong millennial-scale negative excursions of approximately 0.6 ‰ occurred coeval with HS 4 and 1. HS 3 and 2 were simultaneous with smaller amplitude  $\delta^{13}\text{C}$  change. From ~ 25 ka a long term  $\delta^{13}\text{C}$  lowering was initiated, creating a long period of relatively reduced  $\delta^{13}\text{C}$  during the last deglaciation. Last glacial-interglacial transition presented an increase of 0.7 ‰ in the *G. inflata*  $\delta^{13}\text{C}$ .

### 5.5 DISCUSSION

#### 5.5.1 Western South Atlantic as a possible source of heat for the Heinrich stadial events

Subtropical western South Atlantic SST reconstruction showed that the surface layer of the Brazil Current at 24 °S was marginally affected by abrupt millennial-scale variability during the last glacial cycle (SANTOS et al., 2017). However, the  $T_{100\text{m}}$  reconstruction exhibits a considerably distinct pattern concerning millennial-scale variability. For example, during HS 4 GL-1090 Mg/Ca-derived SST oscillation was not higher than 1 °C (SANTOS et al., 2017), whereas the subsurface reconstruction indicates an increase of more than 4 °C during the same event (Figure 12). Eastern South Atlantic  $\text{TEX}^{\text{H}}_{86}$ , a proxy for subsurface (0 – 200 m) temperature, also presents an increment in the subsurface temperature of 3 °C during this event (KIM et al., 2012) (Figure 12). Apparently, eastern and western subsurface South Atlantic present similar sensibility to such events, although western South Atlantic shows warmer values. Other HS (HS 3, 2 and 1, as well as *Younger Dryas*) were equally coeval with rising in western South Atlantic subsurface temperature. All these warming during HS events agree well with high values of  $^{231}\text{Pa}/^{230}\text{Th}$ , connecting them to the largest reductions of AMOC that accompany these episodes (HENRY et al., 2016) (Figure 12).

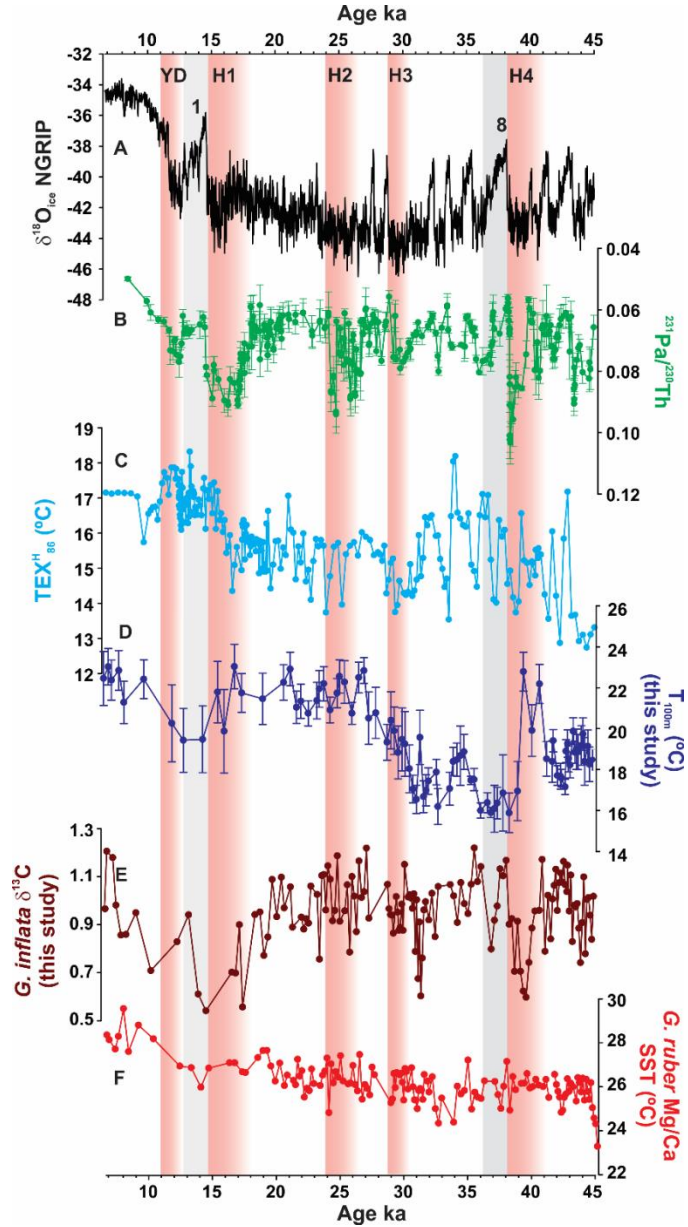


Figure 12 – Subsurface millennial-scale events of western and eastern South Atlantic during the last glacial cycle. A: NGRIP  $\delta^{18}\text{O}$  (NGRIP COMMUNITY MEMBERS, 2004). B:  $^{231}\text{Pa}/^{230}\text{Th}$  of core KNR191-CDH19 (HENRY et al., 2016). C:  $\text{TEX}_{86}^{\text{H}}$  ( $^{\circ}\text{C}$ ) of core GeoB7926-2 (KIM et al., 2012). D: GL-1090 subsurface temperature ( $T_{100\text{m}}$ ) ( $^{\circ}\text{C}$ ) (this study). E: *Globorotalia inflata*  $\delta^{13}\text{C}$  (this study). F: *Globigerinoides ruber* Mg/Ca SST ( $^{\circ}\text{C}$ ) (this study).

Cold stadial conditions have been commonly attributed to the cause of AMOC collapse during last glacial (e. g. BROECKER, 1994). More recently this view has changed due to studies that found a temporal offset of more than 200 years between abrupt cooling and the arrival of ice-rafted debris layers (e. g. BARKER et al., 2015). In this way, build-up of subsurface heat has been proposed as the main cause of the increase in ice-sheet destabilization and calving. MARCOTT et al. (2011) showed that subsurface temperatures gradually warmed prior to the appearance of ice-rafting, with the start of the warming

beginning approximately 1 – 2 kyr before each Heinrich event. Similarly, paleotemperature estimation based on *Neogloboquadrina pachyderma* Mg/Ca and foraminifera census count developed by JONKERS et al. (2012) indicate that many of the ice-rafting events were characterized by increasing subsurface temperatures that started before or at least simultaneously with ice-rafting.

Specifically for the HS 4, JONKERS et al. (2012) exhibited that during this event subsurface temperature of northern North Atlantic increased considerably to more than 5 °C. Taking into account age-model uncertainties, our census-count  $T_{100m}$  estimation display a previous subsurface warming of approximately 2 °C (Figure 12). This warming is then followed by the main shift of the  $T_{100m}$  during HS 4 where the subsurface temperature abruptly increased from ~ 18 °C to 22 °C, reaching one of the highest  $T_{100m}$  of GL-1090 for the last 45 ka (Figure 12). Those findings are rather similar to the pattern proposed by Marcott et al. (2011) with warming initiating previously to the HS event. Warm subsurface waters in the western subtropical South Atlantic could recirculate within the South Atlantic subtropical gyre and eventually be transported beyond the equator at thermocline depths via North Brazil Undercurrent (STRAMMA AND ENGLAND, 1999). Warm subsurface waters recirculating within subtropical gyre could also explain the similar response of western and eastern (KIM et al., 2012) South Atlantic at this time. The northward heat transport from the South Atlantic is supported by the fact that the South Atlantic is the only ocean basin that transport heat equatorward through the subtropical gyre (TALLEY, 1999).

Therefore, we suggest that warm subsurface waters from low latitude western South Atlantic could be, at least, partially involved in the amount of heat required for triggering ice-berg melting at high latitude North Atlantic. Recently, RASMUSSEN et al. (2016) demonstrated that surface and intermediate-depth water south of Iceland warmed gradually synchronously with the Antarctic warming and surprisingly out of phase with the abrupt warming of the nearest Nordic Seas and Greenland. Those results indicate a direct southern influence on the paleoceanography of the northern Atlantic and raise a regenerated interpretation where the South Atlantic and perhaps other southern hemisphere basins may not only react passively to the climate variability identified at northern Atlantic (RASMUSSEN et al., 2016), but, in fact, they could be the source of such anomalies.

The warm subsurface water flowing continuously from South Atlantic would be insulated from the surface by the strong halocline developed during HS events, losing almost no heat as it moves northward (EZAT et al., 2014). However, after a critical point this

warming would promote the abrupt collapse of the halocline and the transition to interstadial conditions. This rapid emptying of subsurface heat could be instrumental in reinvigorating the AMOC and explain the intense warming associated with DO events (JONKERS et al., 2010). Interestingly, near the end of HS 4 GL-1090  $T_{100m}$  abruptly cooled more than 6 °C suggesting that a climate change already started during HS 4 (Figure 12). The subsurface then remained very cold during the subsequent interstadial DO 8. In the eastern South Atlantic, the peak of DO 8 was also followed by a reducing of subsurface temperature of 2 °C (KIM et al., 2012). The relatively strong DO 8, therefore, represents a time when the AMOC is reestablished and the subsurface northern Atlantic releases its heat content to the atmosphere. Consequently, this promotes a sharp reinvigoration of South Atlantic thermocline ventilation, dropping the subsurface temperatures. Likely, the DO 8 and the sequence of shorter DO interstadials (DO 7, 6 and 5) contributed to keep the low  $T_{100m}$  between ~ 38 – 30 ka (Figure 12).

A more ventilated and colder thermocline during DO 8 is supported by the simultaneous high value of *G. inflata*  $\delta^{13}C$  (Figure 12). Planktonic foraminifera  $\delta^{13}C$  can be affected by multiple factors still poorly constrained, like the carbonate ion concentration, nutrient availability, foraminifera respiration and endosymbionts photosynthesis and air-sea exchange (LYNCH-STIEGLITZ et al., 1995; BIJMA et al., 1998). However, recent biogeochemistry modelling efforts suggest that AMOC weakening (strengthening) causes a decrease (increase) of the biological pump efficiency, leading to an increase (decrease) in atmospheric  $CO_2$ . This promotes a particularly strong decrease of surface South Atlantic  $\delta^{13}C$  (SCHMITTNER AND LUND, 2015) that could also affect the subsurface layer. Therefore, the warm subsurface western South Atlantic during HS is connected with a poorly ventilated thermocline denounced by  $\delta^{13}C$  values as low as 0.6 ‰ (Figure 12). Oppositely, during DO interstadials the western subsurface South Atlantic thermocline is strongly ventilated and cold, which is consequently apparent in  $\delta^{13}C$  values as high as 1.2 ‰ (Figure 12).

### **5.5.2 Marine isotope stage 3/2 transition: a new subsurface temperature baseline and its implication**

In late-MIS 3 a new rise in GL-1090  $T_{100m}$  was initiated, interrupting the cold conditions prevalent between ~ 38 and 30 ka. The subsurface temperatures increased approximately 5 °C, similar to the raise regarding HS 4. However, after overcome the value of 20 °C the  $T_{100m}$  did not suffer any considerable reduction, excepting the slight decrease of 2 °C during interstadial D-O 1 (Bølling-Allerød). This means that during almost the entire duration

of MIS 2 the subsurface western South Atlantic was exceptionally warm, with average  $T_{100m}$  of 20.8 °C (1.4 °C warmer than the average  $T_{100m}$  for the last 45 ka). This different baseline of the subsurface temperature indicates that a new thermocline circulation pattern started at this transition.

The MIS 2 was the time when global climate approached the Last Glacial Maximum (LGM). Between 23 – 19 ka the northern North Atlantic sea-ice cover achieved its maximum extension, reducing the strength of AMOC to 20 – 40 % of its interglacial mode (WEBER et al., 2006). The AMOC weakening would not have led merely reduction in deep water convection but also a broad reorganization in Atlantic heat balance. Indeed, in Chapter I we demonstrated that the surface western subtropical South Atlantic warmed considerably earlier than the beginning of Termination I in face of advances of glacial climate during late-MIS 3 and MIS 2. Thus, when AMOC falls in its “cold mode” (BÖHM et al., 2015) the western subtropical South Atlantic becomes a warm pool reservoir, keeping stored the warm waters not transported equatorward. Likely, the heat retained in the surface could be gradually transmitted into the ocean, warming the thermocline layers across late-MIS 3 and MIS 2 (Figure 13).

The AMOC “cold mode” is likely followed by a reduction of the cross-equatorial heat transport which leads to a surface and subsurface warming in the South Atlantic, as demonstrated through coupled climate models of intermediate complexity (e. g. MIGNOT et al., 2007). In this mode, the northern and southern Atlantic subtropical intergyre connection is strongly reduced as compared with AMOC active mode, but still exists supported by the wind-induced circulation which enables ventilation in the tropical and subtropical Atlantic and northward heat transport. This relatively warm water coming from the south penetrates to a high northern latitude beneath the halocline and induces a strong vertical temperature inversion between the surface and intermediate depth (MIGNOT et al., 2007).

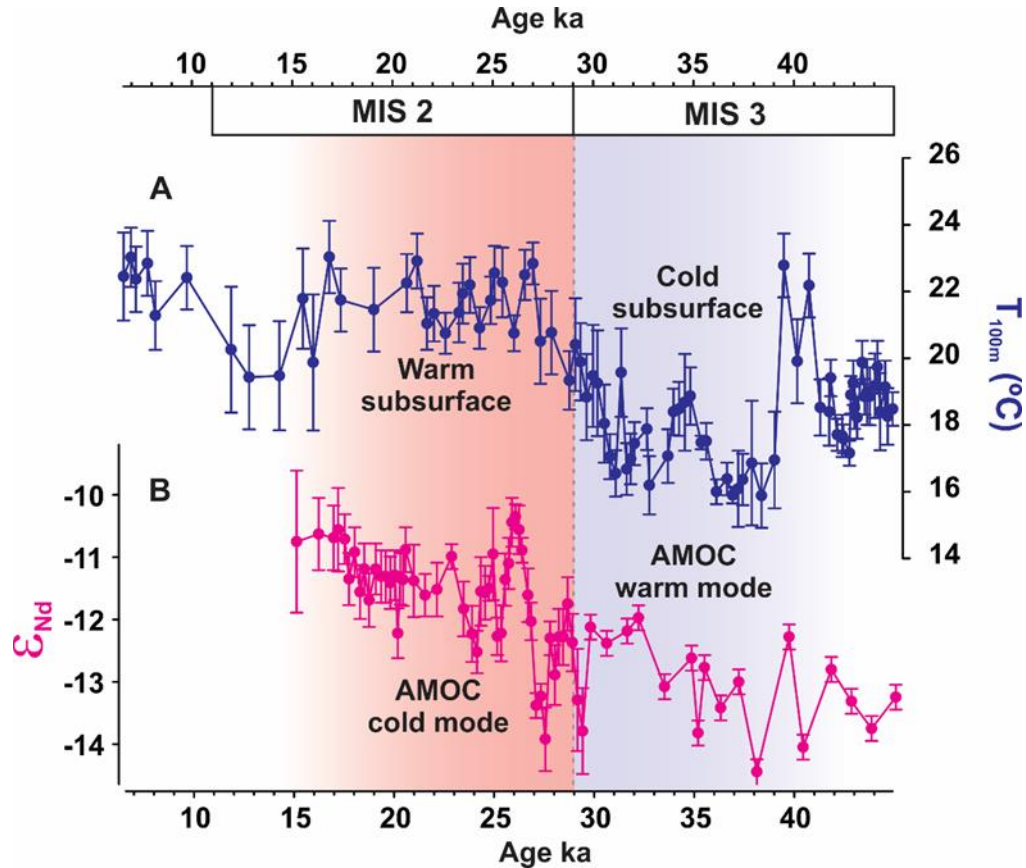


Figure 13 – Transition MIS 3/2 where the AMOC changed from “warm” to “cold mode”. A: GL-1090 subsurface temperature ( $T_{100m}$ ) (°C) (this study). B:  $\epsilon_{Nd}$  record of core ODP1063 (BÖHM et al., 2015). Blue bar highlights the interval of strong AMOC and cold subsurface western South Atlantic. Red bar highlights the interval of weak AMOC and warm subsurface western South Atlantic.

This warmed subsurface may have had important consequences for the remaining glacial climate. If the hypothesis that warm subsurface waters affected the stability of ice-sheet is correct (MARCOTT et al., 2011) this means that a larger amount of heat was available to feed HS events that occurred after the transition MIS 3/2. A warmer and stable source of heat could account for the severity of HS 2 and 1. BÖHM et al. (2015) classified the HS 2 as a period of AMOC “off mode”, wherein the discharge of ice-bergs was intense enough to shut down the circulation. But controversy evidence exists about the scale of HS 2 (LYNCH-STIEGLITZ et al., 2014). However, regarding the HS 1, a wider consensus is in vogue that this episode was the strongest stadial of the last glacial cycle, melting enough ice to significantly disturb the AMOC (HEMMING, 2004; MCMANUS et al., 2004; BRADTMILLER et al., 2014). The very large ice-sheet of LGM would require higher amounts of heat to be melted during HS 1, therefore, we suggest that warm subsurface waters from western South Atlantic continuously flowing northward after be released from South

Atlantic subtropical gyre may have worked as one of the sources of heat to disrupt the ice-cover in northern Atlantic high latitudes. The activity of this subsurface heat source for more than 10 kyr may have produced a cumulative effect, contributing for the wider extension of HS 1 compared to other HS events.

Furthermore, the frequency of DO interstadials dramatically reduced after MIS 3/2 transition. As mentioned previously, during DO events the subsurface heat contained in subsurface layers was released to the atmosphere (JONKERS et al., 2010), reinvigorating the AMOC and relieving the warm stored in southern Atlantic. Without this mechanism, the subsurface western South Atlantic remained warm and poorly ventilated throughout MIS 2, recording the highest  $T_{100m}$  of the last 45 ka (23 °C) during HS 1 (16.8 ka). Thus, the glacial subsurface South Atlantic might be understood as a capacitor; storing energy when deep water convection slowdown or releasing energy when convection resume (Figure 13). This conceptual model agrees well with the “push and pull” system proposed by (RASMUSSEN et al., 2016). “Pull” during interstadials, when convection in the Nordic Seas was active (cold subsurface South Atlantic) and “push” during stadials, when convection slowed down or stopped (warm subsurface South Atlantic).

The  $T_{100m}$  shift experienced during MIS 3/2 transition was the most significant event regarding the subsurface temperatures of the subtropical western South Atlantic. Not even the glacial-interglacial transition during last deglaciation produced a comparable temperature shift, since the  $T_{100m}$  during early-Holocene was rather similar to the temperatures reconstructed for MIS 2 (Figure 12 and 13). The strong shift in the  $T_{100m}$  leads us to propose that the interglacial subsurface pattern in this region was attained already during glacial period. This configuration provided an interglacial-like subsurface temperature in the middle of glacial period that could be transported for higher latitudes and contribute to alter the stability of glacial climate. In this case, not only the North Atlantic could be affected by this warm reservoir but equally the Southern Ocean and Antarctic climate. CROWLEY (2011a) argues that the 1 PW of heat accumulated in South Atlantic in response to stalled overturning is shunted southward by the Brazil Current and injected into southern high latitude via Brazil-Malvinas Confluence. This likely explains the rising temperature in the sub-Antarctic zone at the time of HS 1 and, potentially has implications for tapping deep ocean carbon reservoir due to kinematics change in  $CO_2$  solubility (CROWLEY, 2011). However, more subsurface reconstruction combining other temperature proxies (e. g. *G. inflata* Mg/Ca and  $TEX^{H}_{86}$ ) will



be necessary to estimate the extension of this glacial warmth in the western South Atlantic subtropical gyre.

## 5.6 REMARKS

As described in Chapter I, the subsurface western subtropical South Atlantic is also driven by an early warming trend initiated considerably prior to the end of glacial conditions. Here, the transition MIS 3/MIS 2 allocated an increase in subsurface temperature that left the subsurface subtropical western South Atlantic into its “interglacial” pattern, since from ~ 29 ka on any significant change in subsurface temperature was observed. Therefore, the ecological conditions that prevailed during Holocene already existed during glacial MIS 2. However, other factors beyond temperature control planktonic foraminifera distribution and could affect the  $T_{100m}$  estimation. If most of this warming is really a “temperature effect”, this could turn the subtropical western South Atlantic a source of warm waters to destabilize glacial climate at higher latitudes.

## 6 PRONOUNCED THERMOCLINE COOLING OF THE WESTERN SOUTH ATLANTIC DELAYED $\delta^{18}\text{O}$ SHIFT DURING THE LAST INTERGLACIAL

### 6.1 INTRODUCTION

As is clear from many  $\delta^{18}\text{O}$  records, the “saw-tooth” shaped glacial-interglacial cycles are characterized by long periods of ice growth/cooling followed by rapid deglaciations defined as Terminations (RAYMO, 1997). According to Asian Monsoon speleothem records, the terminations are separated by four or five Earth’s precession cycles, driving changes in the incoming solar energy and supporting the idea that the 100,000 year ice age cycle is an average of discrete numbers of precession cycles (CHENG et al., 2016).

In the context of the past 800 kyr, Termination II (TII) — the transition from the penultimate glacial to the previous interglacial — is considered one of the most rapid and abrupt transition of Quaternary period (LOTOTSKAYA AND GANSSEN, 1999). This interval is associated with the largest glacial–interglacial Antarctic temperature increase and a wide reorganization of southern hemisphere westerlies, allowing the most prominent intensification in Agulhas Leakage volume from mid- to late-Pleistocene (MASSON-DELMOTTE et al., 2010; CALEY et al., 2014).

There is continued support for a strong difference surrounding the sequence of events between Termination I (TI) (last deglaciation) and TII. The difference in maximum summer insolation at high southern latitudes is usually invoked as an explanation for the distinct spacing of the events that characterize such transitions (BROECKER AND HENDERSON, 1998). For instance, ice core  $\delta^{13}\text{CO}_2$  for Termination I and II accounts for different timings of decrease in iron supply and sea-ice extent modifications, leading to particular changes in the releasing of deep ocean carbon. Moreover,  $\delta^{13}\text{CO}_2$  appears 0.2 ‰ more depleted during TII compared to TI (LOURANTOU et al., 2010). Core GL-1090 denounces that different timing of events regarding penultimate and last Terminations are equally observed in the subtropical western South Atlantic. The results expressed in this chapter indicate that the most significant difference resides on subsurface/thermocline layer. *Globorotalia inflata*  $\delta^{18}\text{O}$ , which records the thermocline hydrology proprieties, presents continuous glacial heavy  $\delta^{18}\text{O}$  values for a long period within the Last Interglacial (MIS 5e). This pattern, not shared by surface and mid-depth  $\delta^{18}\text{O}$  evolution, might be related to an abrupt and strong resumption of South Atlantic thermocline circulation inherently linked to Agulhas Leakage return.

## 6.2 MATERIAL AND METHODS

This chapter employs the oxygen isotope composition ( $\delta^{18}\text{O}$ ) of the three foraminifera species described so far and the subsurface temperature ( $T_{100\text{m}}$ ) defined in Chapter II. *Cibicides wuellerstorfi* (250-300  $\mu\text{m}$  size fraction) and *Globigerinoides ruber* (white variety, *sensu stricto*, 250-300  $\mu\text{m}$ )  $\delta^{18}\text{O}$  analysis were described in Chapter I. *Globorotalia inflata*  $\delta^{18}\text{O}$  from 250 – 300  $\mu\text{m}$  size-fraction was performed with 5 to 10 shells for every sample. The analyses were performed at the MARUM – Center for Marine Environmental Sciences, University of Bremen, Germany using a Finnigan MAT251 gas isotope ratio mass spectrometer attached to a Kiel III automated carbonate preparation device. Data were calibrated against an in-house standard (Solnhofen limestone). The results are reported in per mil (‰, parts per thousand) versus Vienna Pee Dee belemnite (VPDB). The standard deviation based on replicate measurements of the in-house standard was 0.04 ‰.

## 6.3 RESULTS

Figure 14 presents the evolution of surface (*G. ruber*), thermocline (*G. inflata*) and mid-depth (*C. wuellerstorfi*)  $\delta^{18}\text{O}$  throughout late-MIS 6 (Figure 13D-F) and late-MIS 2 (Figure 14A-B). During TII (MIS 6/MIS 5e transition), surface and mid-depth  $\delta^{18}\text{O}$  exhibit their strongest amplitude at 130 ka, decreasing by 1.5 ‰ and 2.0 ‰, respectively. However, at 130 ka any noticeable change occurred in the glacial values of *G. inflata*  $\delta^{18}\text{O}$  (Figure 14E). As a result, the heavy isotopic values of the penultimate glacial invaded MIS 5e, leaving the Last Interglacial thermocline with glacial  $\delta^{18}\text{O}$  values for a period of approximately 7 kyr (Figure 14D-F). Only in late-MIS 5e *G. inflata*  $\delta^{18}\text{O}$  finally shifted to low values characteristic of interglacial climate. During TI (MIS 2/MIS 1 transition), all three  $\delta^{18}\text{O}$  curves shifted nearly simultaneous with amplitude of approximately 1.3 ‰, 0.8 ‰ and 1.5 ‰ for surface, thermocline and mid-depth ocean respectively (Figure 14A-C).

The  $T_{100\text{m}}$  during penultimate glacial MIS 6 was around 20 °C. At ca. 140 ka an increase of 2 °C elevated the  $T_{100\text{m}}$  to 22 °C, the warmest subsurface temperature of this time-slice (Figure 15B). This peak was followed by an accentuated  $T_{100\text{m}}$  cooling during TII that culminated in the coldest  $T_{100\text{m}}$  of this interval of 16 °C at 129 ka. The subsurface temperature then remained around 18 °C throughout Last Interglacial, substantially colder than during penultimate glacial (Figure 15B).

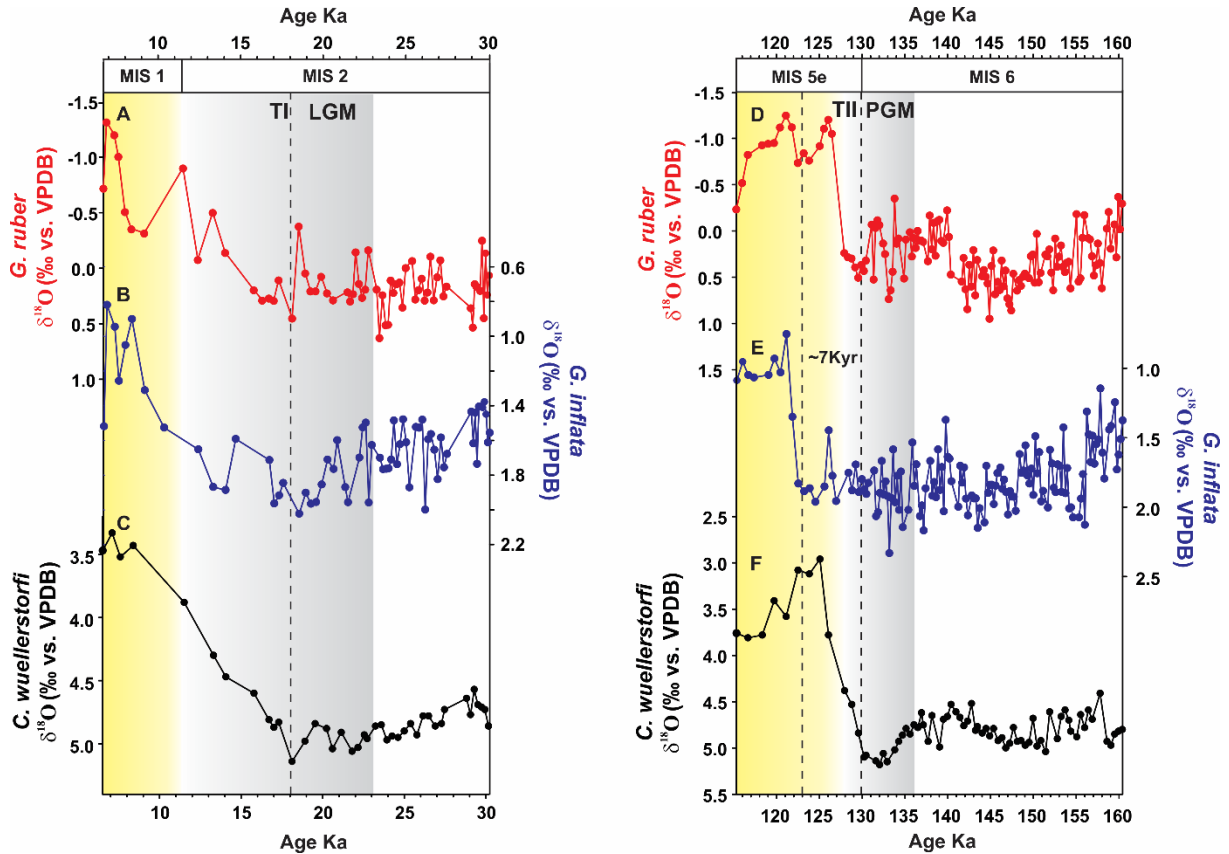


Figure 14 – Evolution of surface, thermocline and mid-depth  $\delta^{18}\text{O}$  throughout Termination I (A-C) and Termination II (D-F). A: *Globigerinoides ruber*  $\delta^{18}\text{O}$ . B: *Globorotalia inflata*  $\delta^{18}\text{O}$ . C: *Cibicides wuellerstorfi*  $\delta^{18}\text{O}$ . D: *Globigerinoides ruber*  $\delta^{18}\text{O}$ . E: *Globorotalia inflata*  $\delta^{18}\text{O}$ . F: *Cibicides wuellerstorfi*  $\delta^{18}\text{O}$ . Dashed line marks the onset of  $\delta^{18}\text{O}$  shift in each Termination.

## 6.4 DISCUSSION

The large  $\delta^{18}\text{O}$  change experienced by foraminifera carbonate during TII and I mostly reflect the wide ocean oxygen isotopic reorganization after the retreat of the large ice-sheet of the penultimate glacial and last glacial. However, a striking pattern related to *G. inflata*  $\delta^{18}\text{O}$  implies that the western South Atlantic thermocline did not react simultaneously with surface and mid-depth ocean at the end of penultimate glacial. Clearly, the significant impact of the sea level rise and ice-volume decay that control foraminifera oxygen fractionation has been masked in thermocline layer during the transition TII/MIS 5e.

$\delta^{18}\text{O}$  anomalies can be separated into a “meltwater” and a “circulation and climate” effect (BAGNIEWSKI et al., 2015). The “meltwater” effect derives from the addition of  $^{18}\text{O}$ -depleted meltwater and its subsequent propagation by the oceans (SHACKLETON, 1987). The “circulation and climate” effect describes the impact of modifications in precipitation/evaporation balance and in ocean circulation plus changes in water temperature,

as the isotopic fractionation during foraminifera calcification is temperature dependent (BAGNIEWSKI et al., 2015). If the *G. inflata*  $\delta^{18}\text{O}$  was firstly responding to the “meltwater” effect, the glacial-interglacial shift of TII/MIS 5e should have occurred at 130 ka, similar to *G. ruber* and *C. wuellerstorfi*  $\delta^{18}\text{O}$ . Thus, this delayed response likely involves changes in “circulation and climate” effect.

Regarding this later effect, changes in precipitation/evaporation balance unlikely play a significant role in this delayed response, since *G. inflata* is a thermocline dweller. Therefore, the explanation should reside on thermocline circulation and water temperature. The  $T_{100\text{m}}$  during late-MIS 6 is considerably high, overwhelming 20 °C (Figure 15B). This surprisingly warm subsurface likely result from the same conditions discussed for MIS 2 (Chapter II), i.e., a stagnated and poorly ventilated thermocline that allow the build-up of warm waters during glacial time and a reduced transfer of this heat towards northern Atlantic. At the demise of MIS 6, the  $T_{100\text{m}}$  dropped around 7 °C opposite to what occurred in surface, where the temperature vigorously warmed following the evolution of interglacial climate. This divergence between surface and subsurface temperatures ( $\Delta T$ ) leads to an impressive contrast that achieved 12 °C in its maximum (Figure 15A and B). The enhanced stratification is also apparent in  $\Delta\delta^{18}\text{O}$  (*G. inflata* – *G. ruber*), where a difference of almost 3.0 ‰ separates the surface and thermocline species, indicating an extremely weak vertical mixing (Figure 15C). Poor vertical mixing would further isolate the thermocline during Last Interglacial, contributing to preserve their cold waters and creating optimal conditions for the development of *Globigerina bulloides*, a planktonic foraminifera species directly associated with the SACW in Brazilian margin (LESSA et al., 2016), which has its population practically quadrupled during MIS 5e (Figure 15D). In addition, the reduced vertical mixing may have inhibited the propagation of  $^{18}\text{O}$ -depleted waters, retarding the *G. inflata*  $\delta^{18}\text{O}$  shift to late-MIS 5e.

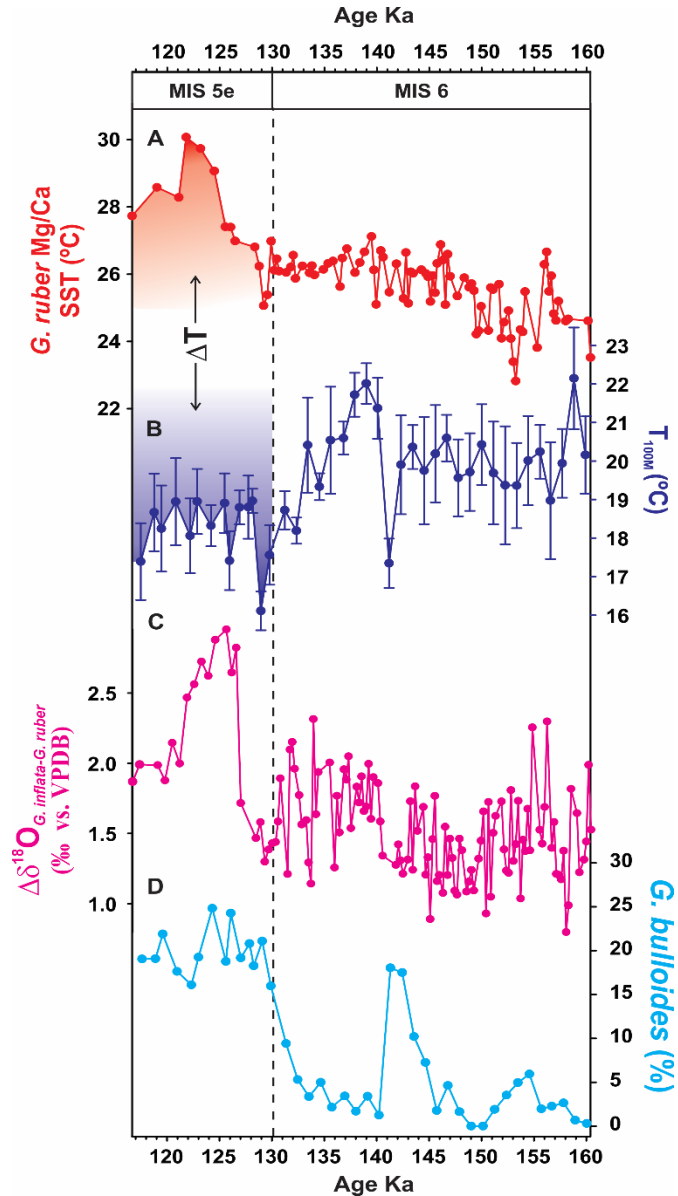


Figure 15 – Temperature contrast between surface and subsurface western South Atlantic. A: Surface Mg/Ca-derived SST (see Chapter I for more details). B: Subsurface temperature ( $T_{100m}$ ) derived from Modern Analogue Technique (MAT). C:  $\Delta\delta^{18}O$  (*Globorotalia inflata* – *Globigerinoides ruber*). D: Relative abundance (%) of *Globigerina bulloides*.

Therefore, the low temperature at the depth of the SACW is the most likely reason for the heavy *G. inflata*  $\delta^{18}O$  values during the Last Interglacial. Here, regional temperature effect overcame the global ice-volume  $\delta^{18}O$  effect for a period of  $\sim 7$  kyr. This very contrasting condition reveals that the SACW underwent an expressive change in its pattern from MIS 6 to MIS 5e. As previously mentioned in Chapter II, part of the SACW is Indian Ocean Central Water brought into the South Atlantic by eddies related to the Agulhas Current intrusions. A strong intensification of Agulhas transport towards the South Atlantic at the end of penultimate glacial has been showed by eastern South Atlantic surface (MARINO et al.,

2013) and thermocline (SCUSSOLINI et al., 2016) salinity reconstruction. This high salinity propagation in upper ocean via Agulhas Leakage is a straightforward evidence of a greater volume of thermocline waters available to feed the SACW (Figure 16A).

The water volume transported via Agulhas Leakage is strongly modulated by migrations of Subtropical Front (STF) and Southern Ocean westerlies. The STF impinged upon the southern African continent during extreme glacial periods and almost completely shut down the Agulhas Leakage (PEETERS et al., 2004). During glacial MIS 6, therefore, the volume transported in the upper water column was dramatically reduced, inhibiting the western South Atlantic thermocline circulation by the direct curtailment of Indian Ocean Central Water transport. The latitude of the STF, therefore, has the potential to influence the upper buoyancy fluxes of heat and salt (BARD AND RICKABY, 2009) towards the South Atlantic. In this way, a northern position of the STF closing the Agulhas corridor reduced the input of thermocline waters and favored the Tropical Water to occupy a large space in the water column, warming the subsurface western South Atlantic during a vast interval of MIS 6 (Figure 16E). The events regarding TII, i.e., southward displacement of STF/Southern Ocean westerlies and the resumption of upper waters transport have abruptly broken this pattern, regenerating the western South Atlantic thermocline ventilation and consequently dropping the subsurface temperature.

The increase in surface and thermocline salinity recorded in Walvis Ridge could be observed in western South Atlantic either, since salinity is a more persistent propriety of the Agulhas Leakage waters (SCUSSOLINI et al., 2015). Regarding the surface, core GL-1090

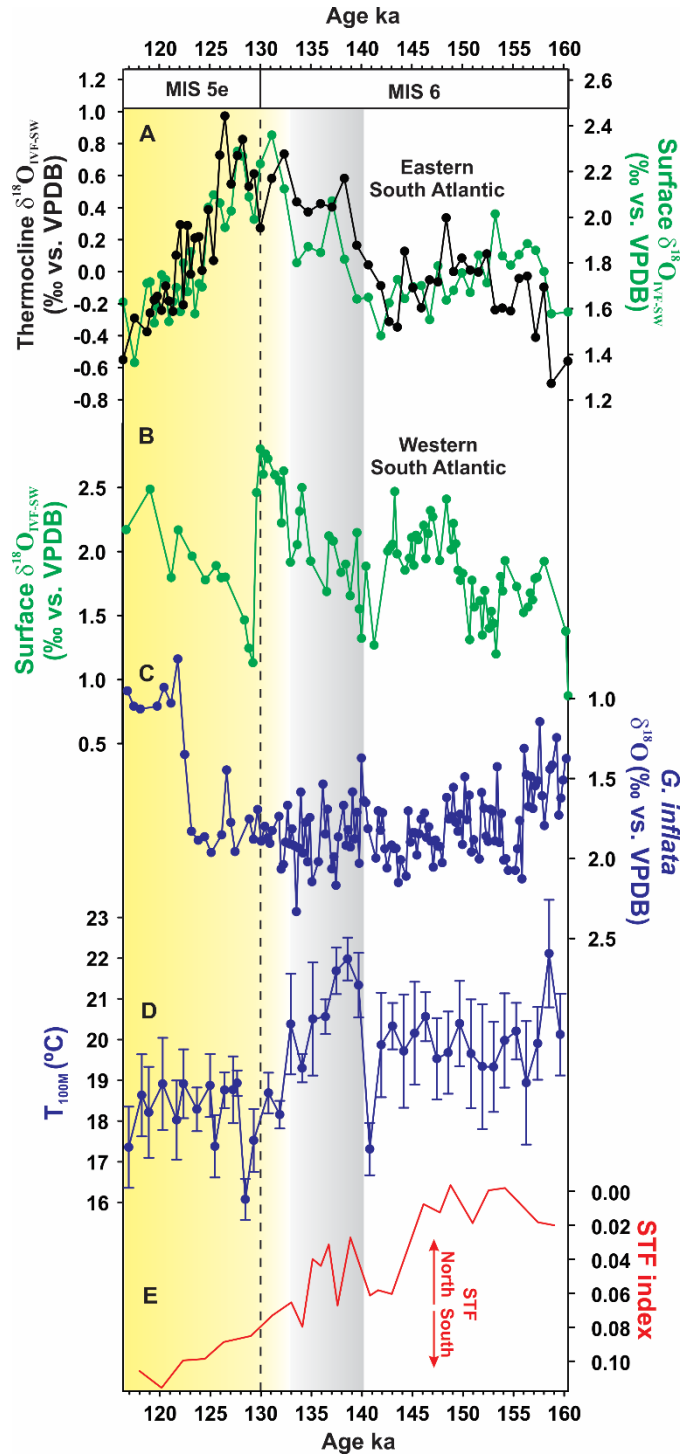


Figure 16 – A: Walvis Ridge surface (green) and thermocline (black)  $\delta^{18}\text{O}_{\text{IVF-SW}}$  (SCUSSOLINI et al., 2015). B: Western South Atlantic  $\delta^{18}\text{O}_{\text{IVF-SW}}$ . C: *G. inflata*  $\delta^{18}\text{O}$ . D: Subsurface temperature ( $T_{100\text{m}}$ ) derived from Modern Analogue Technique (MAT). E: Subtropical Front (STF) position (PEETERS et al., 2004).

exhibits an increase in salinity during TII coeval with Walvis Ridge reconstruction (Figure 16B). Eventually, part of the salt inputted into eastern South Atlantic circulated in the subtropical gyre and was transported to the BC via South Equatorial Current. If this is correct, we can suggest that the pronounced Agulhas Leakage resumption experienced during TII



contributed to produce the saltiest BC of the last 185 ka. Reasonably, an analogous reasoning could be applied for the thermocline, in which the SACW would receive a considerable amount of salt waters like the surface. Unfortunately, we did not reconstruct the thermocline  $\delta^{18}\text{O}_{\text{IVF-SW}}$  because this would result in large errors difficult to access. Furthermore, the subsurface temperature reflects the 100 m layer while the *G. inflata* dwells a depth slightly deeper and colder (CHIESSI et al., 2007) than that estimated by the MAT. This eventual high saline thermocline waters would act in the same direction of cold waters over the foraminifera fractionation and would contribute to keep the heavy values of *G. inflata*  $\delta^{18}\text{O}$  during the Last Interglacial (Figure 16D). The transport of this high salinity signal in thermocline from eastern to western South Atlantic would be even facilitated, since with increasing depth the South Equatorial Current flows at a southern latitude, turning its route more straightforward between the two sides of the South Atlantic (RODRIGUES et al., 2007).

Therefore, the southward movement of the STF favors the South Atlantic thermocline salinification and ventilation, thickening the SACW and reducing the subsurface temperature (Figure 15 and 16). These conditions likely are the main responsible for the *G. inflata* delayed  $\delta^{18}\text{O}$  shift. Allied to this, the Last Interglacial holds a strong AMOC resumption and may have restored the heat piracy from the upper layers of the South Atlantic towards the North Atlantic, cooling even more the SACW. The absence of this delayed *G. inflata*  $\delta^{18}\text{O}$  shift during TI may indicate that the return of Agulhas Leakage injection was not as pronounced as that recorded during TII (Figure 14). In this way, the “circulation and climate” effect over the *G. inflata*  $\delta^{18}\text{O}$  fractionation was superimposed by the “meltwater” effect, resembling what occurred at surface (*G. ruber*  $\delta^{18}\text{O}$ ) and mid-depth (*C. wuellerstorfi*  $\delta^{18}\text{O}$ ) western South Atlantic.

## 6.5 REMARKS

In this chapter, the evolution of penultimate and last deglaciations were investigated in order to identify divergent patterns between the last two Terminations. The results allow us to suggest that the events surrounding both transitions were not the same. Termination I  $\delta^{18}\text{O}$  evolution from surface to mid-depth exhibits nearly simultaneous  $\delta^{18}\text{O}$  shift from last glacial to Holocene values. On the other hand, during TII thermocline  $\delta^{18}\text{O}$  represented by *G. inflata* remained with heavy values characteristic of glacial climate for a long period of  $\sim 7$  kyr despite the Last Interglacial already have started. The strong Agulhas Leakage resumption that accompanied the southern displacement of the STF allowed a massive volume of Indian

Ocean central water enters the South Atlantic. Likely, the regeneration of thermocline circulation dropped the subsurface/thermocline temperature, masking the “meltwater” effect over foraminifera calcification. The non-observation of such pattern coeval with TI suggests that during this transition the volume of Agulhas Leakage was not so impressive like TII. In this way, the “meltwater” effect firstly control *G. inflata*  $\delta^{18}\text{O}$  fractionation, similar to *G. ruber* and *C. wuellerstorfi*.

## **7 EVALUATING THE REGIONAL FORCING ASSOCIATED WITH THE 21-KYR PRECESSIONAL CYCLE AND THE SOUTH AMERICAN SUMMER MONSOON**

### **7.1 INTRODUCTION**

Several climatological studies have focused on the feedbacks between the South America Convergence Zone (SACZ) and South Atlantic SSTs between 20 and 40 °S in order to determine cause-and-effect concerning the ocean-atmosphere coupling (BARROS et al., 2000; ROBERTSON et al., 2003; CHAVES AND NOBRE, 2004; ALMEIDA et al., 2007; JORGETTI et al., 2014). Continental and marine paleoclimatic reconstructions could greatly improve the knowledge about this coupling but, until this moment, no extensive marine temperature curve was available to allow such comparison.

In this last chapter, we propose that a possible coupling between sea surface and precipitation related to the South America monsoon may be observed in long-time scale reconstructions. Our data suggest that strong precipitation and consequent protuberance of the SACZ over the ocean contribute to create a negative feedback between atmosphere circulation and surface ocean, in which intensified SACZ would be coeval with a colder and fresher BC. However, this coupling is not pervasive along the entire GL-1090 record but rather confined in a specific interval, where apparently the AMOC forcing was less prominent.

### **7.2 ATMOSPHERIC CIRCULATION**

The atmospheric circulation over SE South America is marked by strong seasonal variability. During the austral summer (January-March) a NW-SE oriented zone (20° - 40 °S, 50 – 20 °W) of low-level convergence, upper-level divergence and intense convection is established over SE South America (BARROS et al., 2000). This zone is known as the SACZ (see Figure 4, Chapter I), and it is the predominant feature of the South America Summer Monsoon. The SACZ has been defined as a transient phenomenon with an elongated convective band extending from the Amazon basin towards SE Brazil and protruding into the subtropical western South Atlantic (CARVALHO et al., 2004; ALMEIDA et al., 2007). During the austral winter (July-September), the low-level convergence is generally weak and, consequently, a convergence zone is rarely formed and low precipitation rates are observed. The weak SACZ is accompanied by positive outgoing long-wave radiation anomalies over tropical South America and negative outgoing long-wave radiation anomalies over SE South America (CARVALHO et al., 2004). Recent observations from 1986 to 2015 comparing days

during January with and without SACZ prove that when the SACZ is present the underlying surface ocean is colder (Figure 17). Taking into account that the *G. ruber* Mg/Ca-SST likely is bias to austral summer temperatures, it is reasonable think that periods of strong presence of the SACZ would result in colder summer temperatures recorded by the foraminifera shell.

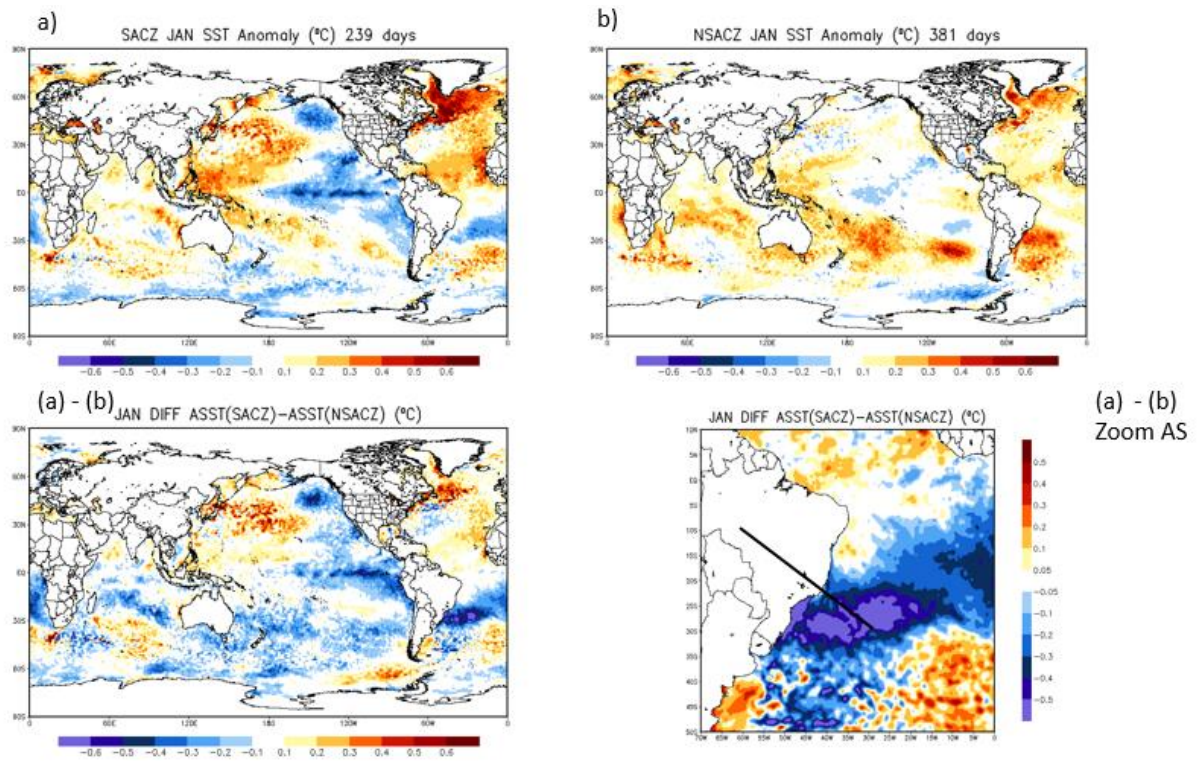


Figure 17 – A: average daily anomaly SST during January from 1986 to 2015 with SACZ. B: average daily anomaly SST during January from 1986 to 2015 without SACZ. Lower left panel shows the subtraction of days with minus days without SACZ. Lower right panel shows a zoom for the South Atlantic. Note that the band of negative SST includes the region where GL-1090 was collected. Optimum Interpolation (OI) SST v2 high resolution daily average (0.25° x 0.25°) (REYNOLDS et al., 2007). Configuration series Boletim Climanálise CPTEC/INPE (<http://climanalise.cptec.inpe.br/~rclimanl/boletim/>). Courtesy of David Nielsen.

### 7.3 MATERIAL AND METHODS

In order to identify harmonic patterns in the SST and  $\delta^{18}\text{O}_{\text{IVF-SW}}$  record, we performed REDFIT (SCHULZ AND MUDELSEE, 2002) and Wavelet time-series analyses (HAMMER et al., 2009). The resulting spectral peaks were tested at 95 % and 99 % confidence levels based on a first-order autoregressive model (SCHULZ AND MUDELSEE, 2002). We chose the Welch-overlapped-segments-averaging algorithm, with oversampling of four and three segments. A Monte-Carlo simulation was performed to investigate a possible random distribution of peaks at the 99 % confidence level. Before the Wavelet transform, the SST

data was regularly interpolated each 0.3 ka based on the nearest neighbor method. The analysis used the Morlet function and a lag of 0.5 with one segment.

#### 7.4 RESULTS

REDFIT spectral analysis reveals cycles in the band of 21 ka and 41 ka above the 99 % and 95 % confidence levels, respectively (Figure 18A). The 21 ka peak is associated with precession and 41 ka with obliquity cycle. The precession cycle presented the highest power. However, Wavelet transform shows that precession is not a permanent band throughout GL-1090. This cycle is limited to the period between 136 ka and 40 ka (Figure 18B), apparently disappearing when full glacial climate is running.

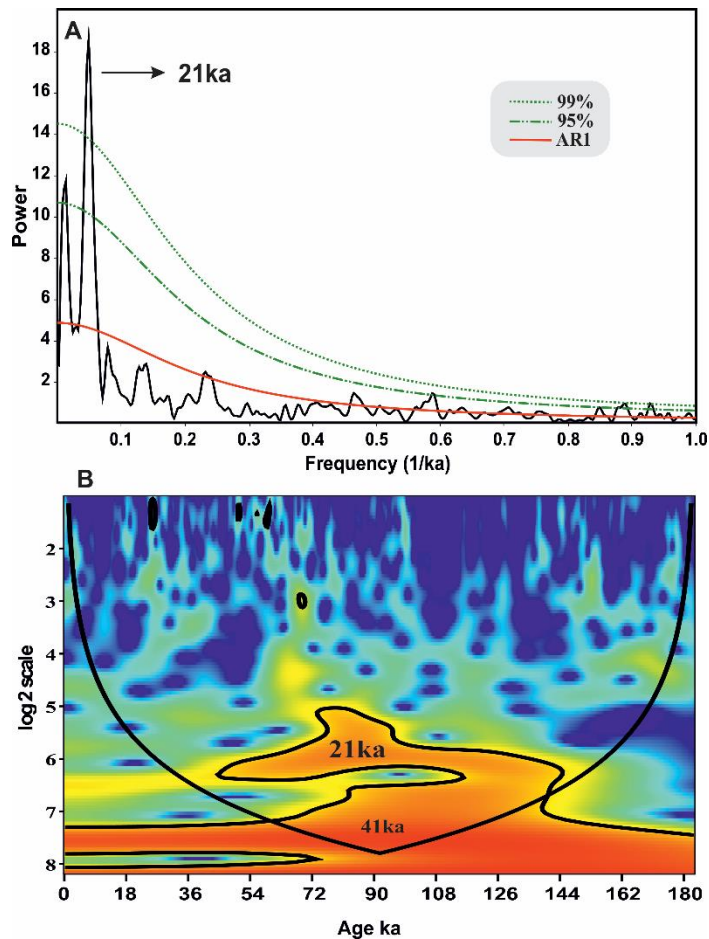
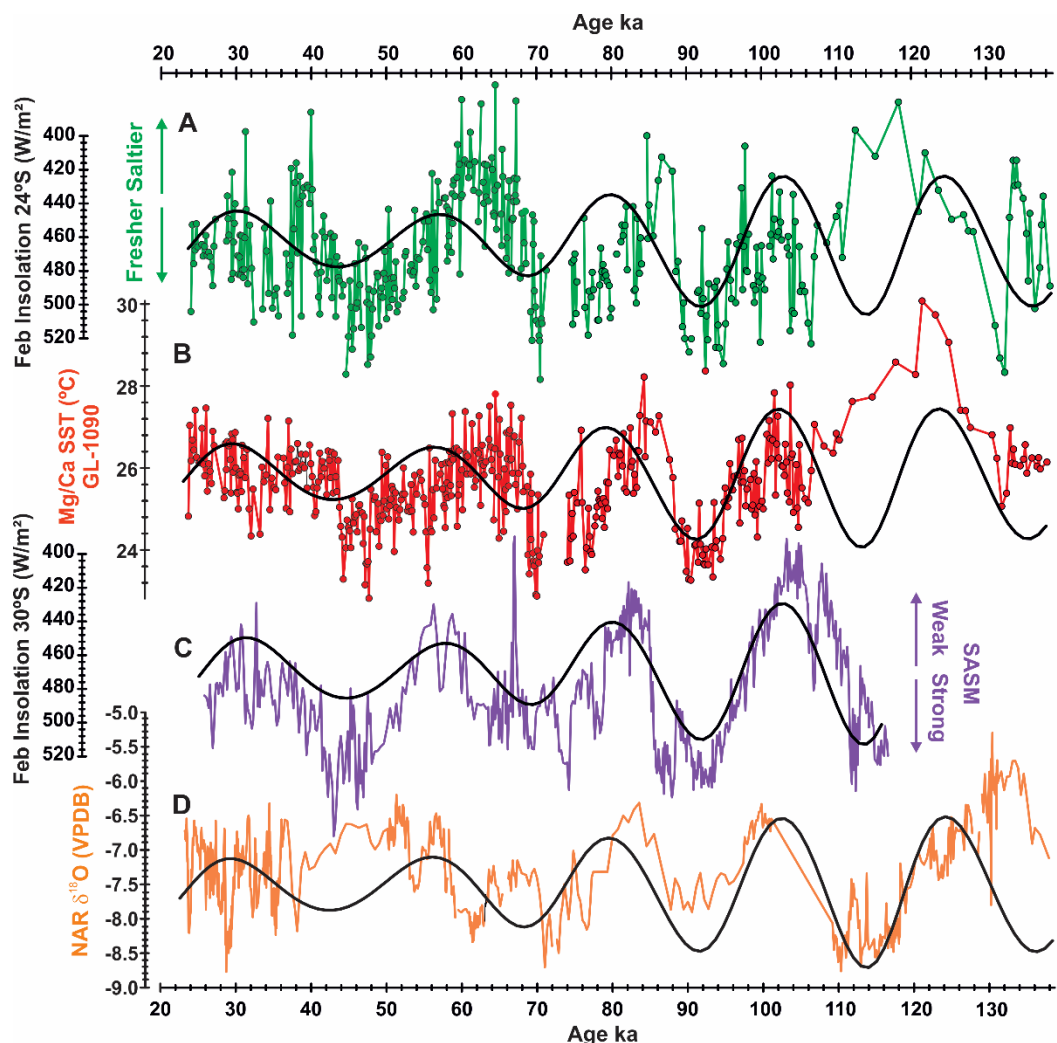


Figure 18 – Time-series analysis over the *Globigerinoides ruber* Mg/Ca-SST and  $\delta^{18}\text{O}_{\text{IVF-SW}}$  of core GL-1090. A: REDFIT spectral peaks at 95 % confidence level (long dashed line) and 99 % (short dashed line) and auto-regressive AR1 model (continuous red line). B: Wavelet transform with Morlet function and one segment. Black line bounds 95% significance level.

## 7.5 DISCUSSION

Speleothem-based reconstructions of the strength of the SASM for the last 116 ka close to our study area (Botuverá cave – subtropical Brazil) and for the last 250 ka (Cueva del Diamante - western Amazonia) show that intervals of intensified SASM activity (depleted  $\delta^{18}\text{O}$ ) coincided with maxima in austral summer insolation controlled by precession (CRUZ et al., 2005; CHENG et al., 2013) (Figure 19C and D). REDFIT time-series analysis of the GL-1090 SST record also shows strong precession (21 kyr) cyclicity (Figure 18A), which within age-model errors, aligns well with changes in February insolation at 24 °S (Figure 19B). A similar pattern is also present for the  $\delta^{18}\text{O}_{\text{IVF-SW}}$  record from GL-1090 (Figure 19A). When we compare GL-1090 SST and  $\delta^{18}\text{O}_{\text{IVF-SW}}$  with SASM/SACZ reconstructions, it is possible to observe that insolation maxima and strong precipitation are synchronous with low values of SST and  $\delta^{18}\text{O}_{\text{IVF-SW}}$  (Figure 19). If periods of strong SASM/SACZ are synchronous with a colder and fresher western South Atlantic, we can suggest that a negative feedback between the ocean surface and atmospheric circulation acts on orbital time-scales, where the atmospheric circulation associated with austral summer precipitation might collaborate to produce a colder and fresher BC.



Intensified SACZ has been found to be predominantly accompanied by cold SST anomalies around 10 °S - 30 °S due to a large local thermodynamic forcing realized by the atmosphere (ROBERTSON et al. 2003). Indeed, atmospheric circulation associated with the SACZ reduces the net radiative energy input over a specific sector of the western South Atlantic and, consequently, decreases the SST (CHAVES AND NOBRE, 2004). JORGETTI et al. (2014) separated the SACZ into northern (SACZN) and southern (SACZS) modes, with oceanic variations in the latter mode being a response to the atmospheric conditions related to convective activity. Since our data indicate a forcing of the atmosphere over the surface of the ocean, we can infer that the process involving the SACZS is more prevalent in the region and

Intensified SACZ has been found to be predominantly accompanied by cold SST anomalies around 10 °S - 30 °S due to a large local thermodynamic forcing realized by the atmosphere (ROBERTSON et al. 2003). Indeed, atmospheric circulation associated with the SACZ reduces the net radiative energy input over a specific sector of the western South Atlantic and, consequently, decreases the SST (CHAVES AND NOBRE, 2004). JORGETTI et al. (2014) separated the SACZ into northern (SACZN) and southern (SACZS) modes, with oceanic variations in the latter mode being a response to the atmospheric conditions related to convective activity. Since our data indicate a forcing of the atmosphere over the surface of the ocean, we can infer that the process involving the SACZS is more prevalent in the region and

became recorded in the sediment at orbital time-scales. The intensity of the summer monsoon is also related to the strength of the temperature gradient due to contrasting land-sea heat (CHOU, 2003). The negative SST anomalies in our record simultaneous to high insolation might arise from a stronger thermal gradient between the ocean and adjacent continent, so that the transport of moisture from the ocean towards the continent could have been enhanced, thereby intensifying the monsoon (CHOU, 2003). In this way, part of the variability found for the surface temperature and salinity might come from regional climate associated with an extended SACZ over the western South Atlantic in periods of strong SASM.

However, wavelet transform shows that the 21-kyr cycle is not present throughout the record, but is rather concentrated between 136 and 40 ka (Figure 18B). Apparently, the precessional control was weaker during the penultimate and part of the last glacial period than during the period between 136 and 40 ka. What could make the SACZ reduces its influence over the surface ocean it is difficult to precise only with our data. Into the Chapter I, we discussed the influence of ice-volume and AMOC condition near to glacial maximum climate. In a scenario like this, the AMOC state would support western South Atlantic heat piracy, leading to the early warming trend previously described. Likely, when this state is working the AMOC strength becomes the prevalent mechanism, masking the influence of the SACZ/SASM. Therefore, when AMOC is fully active (“warm mode”) associated with reduced ice-volume/freshwater input other forcing, like the SACZ/SASM, would also have space to influence the surface ocean. Another reason could be related to the amplitude of precessional signal. During MIS 5, the eccentricity lies in values considerably high, which also propitiates an accentuated precessional variability. This high precession contributed to increase the seasonality in GL-1090 region, which also creates a larger amplitude of the SST during MIS 5 compared to MIS 3. During MIS 3, the eccentricity assumes a flattened pattern, which consequently damped the amplitude of precession. This change could have contributed to weaken the seasonality at the same time that the AMOC variability initiated its dominant role in Atlantic heat distribution. Still, further paleoclimate and modeling investigations are needed to test this hypothesis.

## 7.6 REMARKS

At the end of penultimate glacial GL-1090 Mg/Ca-SST assumes a pattern highly tied to precession cyclicity that disappears when the last glacial approaches its maximum. REDFIT spectral analysis confirms that the 21-kyr precession cycle is present but confined



between  $\sim 136$  ka and 40 ka. Into this interval, where precession responds by the long-term evolution of surface data, both Mg/Ca-SST and  $\delta^{18}\text{O}_{\text{IVF-SW}}$  resembled the speleothem  $\delta^{18}\text{O}$ , mainly the proximal Botuverá cave. This similar evolution could indicate that the presence of 21-kyr cycle in our data is modulated by atmosphere circulation related to SACZ, since earlier studies showed that the summer insolation regulated by precession is the strongest mechanism controlling long time-scale precipitation. Modern observations concerning the presence of SACZ and cold SST during austral summer, give us subsidence to propose that enhanced precipitation could contribute in order to produce a colder and fresher BC. However, this negative feedback apparently did not occur near to glacial maximum conditions, where likely the AMOC “cold mode” raised as the central forcing modulating the surface ocean evolution. More paleoclimate reconstructions and modeling efforts are needed to fully test this idea.

## 8 CONCLUSIONS AND FUTURE CHALLENGES

Core GL-1090 permitted the first high-resolution reconstruction of the BC covering the last two glacial-interglacial transitions. Undoubtedly, the most striking pattern that emerges with these results relies on the early glacial warming – an apparently resilient characteristic present in both glacial periods which anticipated by thousands of years the penultimate and last deglaciations. Such pattern was observed in surface and subsurface layer by two independent methods to estimate past ocean temperature, confirming that this occurrence is not merely related to planktonic foraminifera seasonality. The evolution of the subtropical western South Atlantic warming then was initially promoted by (i) favorable orbital conditions at late-MIS 3 and continuously sustained by (ii) gradual AMOC weakening when climate approaches the maximum glacial conditions. Likely, the AMOC slow down is the most important aspect for the early warming, since the orbital configuration during late-MIS 6 was relatively dissimilar from that of late-MIS 3. The good agreement of upper waters temperature increase with decreasing mid-depth ocean ventilation supports the idea that gradual warm waters build up is result of reduced deep-water convection at high northern latitudes.

The South Atlantic warm waters build up has long been recognized, but its occurrence was related to abrupt millennial-scale events that deeply disturb the AMOC. Our findings imply that the beginning of this warm pool is not only related to abrupt events, but equally to the long-term glacial progression. This means that this pattern is much more sensible than previously thought and small changes in deep water convection, and consequently, in the extra-tropical heat exchange is enough to trigger the warming. Herewith, possibilities of future investigations are open focusing in both paleoclimate/paleoceanography understanding and future climate projections. Concerning past climate variability, the consequences of the BC early warming should be investigated in-depth through ocean-atmosphere coupled models in order to clarify the potential impacts of this temperature increase still during glacial climate. As the South Atlantic is the only ocean transmitting waters toward North Atlantic through the subtropical gyre, the warm surface and subsurface waters could have favored instabilities of North Atlantic ice-cover and accelerated the finish of glacial periods. At the same time, natural flowing of the BC waters towards Brazil-Malvinas Confluence and then South Atlantic Current might have approximated this heat to the subantarctic region, altering water solubility and promoting CO<sub>2</sub> tapping. These two plausible pictures evidence the capacity of the South Atlantic to interact with high southern and northern latitudes.

Obviously, additional long-time scale and high-resolution paleoceanography studies are imperative to confirm the occurrence of such pattern along entire extension of the BC. In terms of future scenarios, a similar pattern may be running right now in the BC, since the recent human-made temperature raising has leading to an AMOC slow down (RAHMSTORF et al., 2015) with an expressive response of the western boundary currents (WU et al., 2012). Therefore, paleoceanography and modern observations are converging toward the same conclusion, i.e., small AMOC reductions is already enough to produce BC warming. How will respond the South America continent and especially Brazilian regional precipitations patterns to a warmer ocean?

Additionally, GL-1090 data exhibit that South Atlantic/Indian Ocean exchange performed by Agulhas Leakage is fundamental to reestablish the South Atlantic thermohaline circulation during glacial Terminations. Particularly, the TII (the strongest transition of mid- to late-Pleistocene) is marked by a sharp subsurface temperature reduction, which indicates a vigorous SACW production that was maintained during Last Interglacial MIS 5e. Likely, this was the condition that kept the *G. inflata*  $\delta^{18}\text{O}$  with glacial heavy values for a long period within the Last Interglacial. Future paleoceanography attempts will correlate both eastern and western South Atlantic, providing deeper insights about this oceanic teleconnection. In this way, geochemical proxies to estimate subsurface temperatures will be mandatory.

## 9 REFERENCES

- ALLEY, R. B.; MAROTZKE, J.; NORDHAUS, W. D.; et al. Abrupt climate change. **Science**, v. 299, n. 5615, p. 2005–10, 2003.
- ALMEIDA, R. A F. DE; NOBRE, P.; HAARSMA, R. J.; CAMPOS, E. J. D. Negative ocean-atmosphere feedback in the South Atlantic Convergence Zone. **Geophysical Research Letters**, v. 34, n. 18, p. 1–5, 2007.
- ALVAREZ-SOLAS, J.; ROBINSON, A.; MONTOYA, M.; RITZ, C. Iceberg discharges of the last glacial period driven by oceanic circulation changes. **Proceedings of the National Academy of Sciences of the United States of America**, v. 110, n. 41, p. 16350–4, 2013.
- ANDERSON, D. M. Paleooceanography. **Encyclopedia of Quaternary Science**, p. 1599–1609, 2007.
- ANDERSON, R. F.; ALI, S.; BRADTMILLER, L. I.; et al. Wind-driven upwelling in the Southern Ocean and the deglacial rise in atmospheric CO<sub>2</sub>. **Science**, v. 323, n. 5920, p. 1443–1448, 2009.
- ANGULO, R. J.; REIMER, P. J.; SOUZA, M. C. DE; et al. A Tentative Determination of Upwelling Influence on the Paleo-Surficial Marine Water Reservoir Effect in Southeastern Brazil. **Radiocarbon**, v. 49, n. 3, p. 1255–1259, 2007.
- ARBUSZEWSKI, J.; DEMENOCAL, P.; KAPLAN, A.; FARMER, E. C. On the fidelity of shell-derived  $\delta^{18}\text{O}$  seawater estimates. **Earth and Planetary Science Letters**, v. 300, n. 3–4, p. 185–196, 2010.
- ARZ, H. W.; PÄTZOLD, J.; WEFER, G. The deglacial history of the western tropical Atlantic as inferred from high resolution stable isotope records off northeastern Brazil. **Earth and Planetary Science Letters**, v. 167, n. 1–2, p. 105–117, 1999.
- BAGNIEWSKI, W.; MEISSNER, K. J.; MENVIEL, L.; BRENNAN, C. E. Quantification of factors impacting seawater and calcite  $\delta^{18}\text{O}$  during Heinrich Stadials 1 and 4. **Paleoceanography**, v. 30, n. 7, p. 895–911, 2015.
- BARD, E.; RICKABY, R. E. M. Migration of the subtropical front as a modulator of glacial climate. **Nature**, v. 460, n. 7253, p. 380–3, 2009.
- BARKER, S.; CHEN, J.; GONG, X.; et al. Icebergs not the trigger for North Atlantic cold events. **Nature**, v. 520, n. 7547, p. 333–336, 2015.
- BARKER, S.; DIZ, P. Timing of the descent into the last Ice Age determined by the bipolar seesaw. **Paleoceanography**, v. 29, n. 6, p. 489–507, 2014.
- BARKER, S.; GREAVES, M.; ELDERFIELD, H. A study of cleaning procedures used for foraminiferal Mg/Ca paleothermometry. **Geochemistry, Geophysics, Geosystems**, v. 4, n. 9, p. 1–20, 2003.
- BARROS, V. Y.; GONZALEZ, M.; LIEBMANN, B.; CAMILLONI, I. Y. Influence of the South Atlantic convergence zone and South Atlantic Sea surface temperature on interannual summer rainfall variability in Southeastern South America. **Theoretical and Applied Climatology**, v. 67, p. 123–133, 2000.
- BASSINOT, F. C. Oxygen Isotope Stratigraphy of the Oceans. **Encyclopedia of Quaternary Science**, v. 18, n. 2000, p. 1740–1748, 2007.

- BAY, R. C.; BRAMALL, N.; PRICE, P. B. Bipolar correlation of volcanism with millennial climate change. **Proceedings of the National Academy of Sciences of the United States of America**, v. 101, n. 17, p. 6341–6345, 2004.
- BAZIN, L.; LANDAIS, A.; LEMIEUX-DUDON, B.; et al. An optimized multi-proxy, multi-site Antarctic ice and gas orbital chronology (AICC2012): 120–800 ka. **Climate of the Past**, v. 9, n. 4, p. 1715–1731, 2013.
- BEREITER, B.; LUTHI, D.; SIEGRIST, M.; et al. Mode change of millennial CO<sub>2</sub> variability during the last glacial cycle associated with a bipolar marine carbon seesaw. **Proceedings of the National Academy of Sciences**, v. 109, n. 25, p. 9755–9760, 2012.
- BIJMA, J.; HEMLEBEN, C.; HUBER, B. T.; ERLLENKEUSER, H.; KROON, D. Experimental determination of the ontogenetic stable isotope variability in two morphotypes of *Globigerinella siphonifera* (d'Orbigny). **Marine Micropaleontology**, v. 35, n. 3–4, p. 141–160, 1998.
- BLAAUW, M.; CHRISTENY, J.A. Flexible paleoclimate age-depth models using an autoregressive gamma process. **Bayesian Anal.** 6, 457–474, 2011.
- BLUNIER, T.; BROOK, E. J. Timing of millennial-scale climate change in Antarctica and Greenland during the last glacial period. **Science**, v. 291, n. 5501, p. 109–12, 2001.
- BÖHM, E.; LIPPOLD, J.; GUTJAHR, M.; et al. Strong and deep Atlantic meridional overturning circulation during the last glacial cycle. **Nature**, v. 517, n. 7534, p. 73–76, 2015.
- BOND, G. A Pervasive Millennial-Scale Cycle in North Atlantic Holocene and Glacial Climates. **Science**, v. 278, n. 5341, p. 1257–1266, 1997.
- BOUDAGHER-FADEL, M. K. Na Introduction to planktonic foraminifera. In: **Biostratigraphic and Geological Significance of Planktonic Foraminifera**, 2<sup>a</sup> Ed., UCLPRESS, 2012.
- BRADTMILLER, L. I.; MCMANUS, J. F.; ROBINSON, L. F. 231Pa/230Th evidence for a weakened but persistent Atlantic meridional overturning circulation during Heinrich Stadial 1. **Nature Communications**, v. 5, p. 5817, 2014.
- BRAUN, H.; DITLEVSEN, P.; CHIALVO, D. R. Solar forced Dansgaard-Oeschger events and their phase relation with solar proxies. **Geophysical Research Letters**, v. 35, n. 6, p. 1–5, 2008.
- BROECKER, W. S. Massive iceberg discharges as triggers for global climate change. **Nature**, 1994.
- BROECKER, W. S.; HENDERSON, G. M. The sequence of events surrounding termination II and their implications for the causes of glacial interglacial CO<sub>2</sub> changes. **Paleoceanography**, v. 13, n. 4, p. 352–364, 1998.
- CALEY, T.; PEETERS, F. J. C.; BIASTOCH, A.; et al. Quantitative estimate of the paleo-Agulhas leakage. **Geophysical Research Letters**, p. 1238–1246, 2014.
- CALVO, E.; VILLANUEVA, J.; GRIMALT, J. O.; BOELAERT, A.; LABEYRIE, L. New insights into the glacial latitudinal temperature gradients in the North Atlantic. Results from U<sup>K</sup><sub>37</sub> sea surface temperatures and terrigenous inputs. **Earth and Planetary Science Letters**, v. 188, n. 3–4, p. 509–519, 2001.
- CAMPOS, E. J. D.; VELHOTE, D.; SILVEIRA, I. C. A DA. Shelf break upwelling driven by

- Brazil current cyclonic meanders. **Geophysical Research Letters**, v. 27, n. 6, p. 751–754, 2000.
- CARLSON, A. E.; OPPO, D. W.; CAME, R. E.; et al. Subtropical Atlantic salinity variability and Atlantic meridional circulation during the last deglaciation. **Geology**, v. 36, n. 12, p. 991–994, 2008.
- CARVALHO, L. M. V.; JONES, C.; LIEBMANN, B. The South Atlantic Convergence Zone: Intensity, Form, Persistence, and Relationships with Intraseasonal to Interannual Activity and Extreme Rainfall. **Journal of Climate**, v. 17, n. 1, p. 88–108, 2004.
- CHAVES, R. R.; NOBRE, P. Interactions between sea surface temperature over the South Atlantic Ocean and the South Atlantic Convergence Zone. **Geophysical Research Letters**, v. 31, n. 3, p. 1–4, 2004.
- CHENG, H.; EDWARDS, R. L.; SINHA, A.; et al. The Asian monsoon over the past 640,000 years and ice age terminations. **Nature**, v. 534, n. 7609, p. 640–646, 2016.
- CHENG, H.; SINHA, A.; CRUZ, F. W.; et al. Climate change patterns in Amazonia and biodiversity. **Nature Communications**, v. 4, p. 1411, 2013.
- CHIESSI, C. M.; MULITZA, S.; MOLLENHAUER, G.; et al. Thermal evolution of the western South Atlantic and the adjacent continent during Termination 1. **Climate of the Past**, v. 11, n. 6, p. 915–929, 2015.
- CHIESSI, C. M.; MULITZA, S.; PAUL, A.; et al. South Atlantic interocean exchange as the trigger for the Bølling warm event. **Geology**, v. 36, n. 12, p. 919–922, 2008.
- CHIESSI, C. M.; ULRICH, S.; MULITZA, S.; PÄTZOLD, J.; WEFER, G. Signature of the Brazil-Malvinas Confluence (Argentine Basin) in the isotopic composition of planktonic foraminifera from surface sediments. **Marine Micropaleontology**, v. 64, n. 1–2, p. 52–66, 2007.
- CHOU, C. Land-sea heating contrast in an idealized Asian summer monsoon. **Climate Dynamics**, v. 21, n. 1, p. 11–25, 2003.
- CORTESE, G.; ABELMANN, A.; GERSONDE, R. The last five glacial-interglacial transitions: A high-resolution 450,000-year record from the subantarctic Atlantic. **Paleoceanography**, v. 22, n. 4, p. 1–14, 2007.
- CROWLEY, T. J. Paleoclimate Reconstruction Challenge: Available for participation. **PAGES news**, v. 19, p. 71–72, 2011a.
- CROWLEY, T. J. Paleoclimate Reconstruction Challenge: Available for participation. **PAGES news**, v. 19, p. 71–72, 2011b.
- CRUZ, F. W.; BURNS, S. J.; KARMANN, I.; et al. Insolation-driven changes in atmospheric circulation over the past 116,000 years in subtropical Brazil. **Nature**, v. 434, n. 7029, p. 63–66, 2005.
- CURRY, W. B.; OPPO, D. W. Glacial water mass geometry and the distribution of  $\delta^{13}\text{C}$  of  $\Sigma\text{CO}_2$  in the western Atlantic Ocean. **Paleoceanography**, v. 20, n. 1, p. 1–12, 2005a.
- DEKENS, P. S. Core top calibration of Mg/Ca in tropical foraminifera: Refining paleotemperature estimation. **Geochemistry Geophysics Geosystems**, v. 3, n. 4, 2002.
- DEPLAZES, G.; LÜCKGE, A.; PETERSON, L. C.; et al. Links between tropical rainfall and North Atlantic climate during the last glacial period. **Nature Geoscience**, v. 6, n. 2, p. 1–5,

2013.

DUEÑAS-BOHÓRQUEZ, A.; ROCHA, R. E. DA; KUROYANAGI, A.; BIJMA, J.; REICHAERT, G. J. Effect of salinity and seawater calcite saturation state on Mg and Sr incorporation in cultured planktonic foraminifera. **Marine Micropaleontology**, v. 73, n. 3–4, p. 178–189, 2009.

EMÍLSSON, I. The shelf and coastal waters off southern Brazil. **Boletim do instituto oceanográfico**, v. 11, n. 2, p. 101–112, 1961.

EPICA COMMUNITY MEMBERS. Eight glacial cycles from an Antarctic ice core. **Nature**, v. 429, n. 6992, p. 623–628, 2004.

EZAT, M. M.; RASMUSSEN, T. L.; GROENEVELD, J. Persistent intermediate water warming during cold stadials in the southeastern Nordic seas during the past 65 k.y. **Geology**, v. 42, n. 8, p. 663–666, 2014.

FAIRBANKS, R. G.; WIEBE, P. H.; BÉ, A. W. Vertical distribution and isotopic composition of living planktonic foraminifera in the Western north atlantic. **Science**, 4, 1980.

GEBBIE, G. How much did Glacial North Atlantic Water shoal? **Paleoceanography**, v. 29, n. 3, p. 190–209, 2014.

GORDON, A. L. South Atlantic thermocline ventilation. **Deep Sea Research Part A, Oceanographic Research Papers**, v. 28, n. 11, p. 1239–1264, 1981.

GORDON, A. L.; WEISS, R. A. Y. F.; SMETHIE, W. M.; WARNER, M. J. Thermocline and Intermediate Water Communication Between the South Atlantic and Indian Oceans. **Journal of Geophysical Research**, v. 97, n. C5, p. 7223–7240, 1992.

GOTTSCHALK, J.; SKINNER, L. C.; MISRA, S.; et al. Abrupt changes in the southern extent of North Atlantic Deep Water during Dansgaard–Oeschger events. **Nature Geoscience**, v. 8, n. 12, p. 950–954, 2015.

GOVIN, A.; CHIESSI, C. M.; ZABEL, M.; et al. Terrigenous input off northern South America driven by changes in Amazonian climate and the North Brazil Current retroflexion during the last 250 ka. **Climate of the Past**, v. 10, n. 2, p. 843–862, 2014.

GRANT, K. M.; ROHLING, E. J.; BAR-MATTHEWS, M.; et al. Rapid coupling between ice volume and polar temperature over the past 150,000 years. **Nature**, v. 491, n. 7426, p. 744–747, 2012.

GROENEVELD, J.; CHIESSI, C. M. Mg/Ca of *Globorotalia inflata* as a recorder of permanent thermocline temperatures in the South Atlantic. **Paleoceanography**, 2011.

HAMMER, Ø.; HARPER, D.; RYAN, P. PAST-PALaeontological STatistics, ver. 1.89. **University of Oslo, Oslo**, n. 1999, p. 1–31, 2009.

HEMMING, S. R. Heinrich events: Massive late Pleistocene detritus layers of the North Atlantic and their global climate imprint. **Reviews of Geophysics**, v. 42, n. 2003, p. 1–43, 2004.

HENRY, L. G.; HENRY, L. G.; MCMANUS, J. F.; et al. North Atlantic ocean circulation and abrupt climate change during the last glaciation. **Science**, v. 353, n. 6298, p. 470–474, 2016.

HERTZBERG, J. E.; SCHMIDT, M. W. Refining *Globigerinoides ruber* Mg/Ca paleothermometry in the Atlantic Ocean. **Earth and Planetary Science Letters**, v. 383, p.

123–133, 2013.

HODELL, D. A.; MINTH, E. K.; CURTIS, J. H.; et al. Surface and deep-water hydrography on Gardar Drift (Iceland Basin) during the last interglacial period. **Earth and Planetary Science Letters**, v. 288, n. 1–2, p. 10–19, 2009.

HODELL, D. A.; VENZ, K. A.; CHARLES, C. D.; NINNEMANN, U. S. Pleistocene vertical carbon isotope and carbonate gradients in the South Atlantic sector of the Southern Ocean. **Geochemistry, Geophysics, Geosystems**, v. 4, n. 1, p. 1–19, 2003.

HÖNISCH, B.; ALLEN, K. A.; LEA, D. W.; et al. The influence of salinity on Mg/Ca in planktic foraminifers - Evidence from cultures, core-top sediments and complementary  $\delta^{18}\text{O}$ . **Geochimica et Cosmochimica Acta**, v. 121, p. 196–213, 2013.

HOOGAKKER, B. A. A.; ROHLING, E. J.; PALMER, M. R.; TYRRELL, T.; ROTHWELL, R. G. Underlying causes for long-term global ocean  $\delta^{13}\text{C}$  fluctuations over the last 1.20 Myr. **Earth and Planetary Science Letters**, v. 248, n. 1–2, p. 1–15, 2006.

HOOGAKKER, B. A. A.; SMITH, R. S.; SINGARAYER, J. S.; et al. Terrestrial biosphere changes over the last 120 kyr. **Climate of the Past**, v. 12, n. 1, p. 51–73, 2016.

HOWE, J. N. W.; PIOTROWSKI, A. M.; NOBLE, T. L.; et al. North Atlantic Deep Water Production during the Last Glacial Maximum. **Nature Communications**, v. 7, p. 11765, 2016.

HUT, G. Stable Isotope Reference Samples for Geochemical and Hydrological Investigations. Consultant Group Meeting IAEA. **Report to the Director General, International Atomic Energy Agency**, 16–18, 1987.

HUTSON, W. H. The agulhas current during the late pleistocene: analysis of modern faunal analogs. **Science**, v. 207, n. 4426, p. 64–6, 1980.

JONKERS, L.; MOROS, M.; PRINS, M. A.; et al. A reconstruction of sea surface warming in the northern North Atlantic during MIS 3 ice-rafting events. **Quaternary Science Reviews**, v. 29, n. 15–16, p. 1791–1800, 2010.

JONKERS, L.; PRINS, M. A.; MOROS, M.; et al. Temporal offsets between surface temperature, ice-rafting and bottom flow speed proxies in the glacial (MIS 3) northern North Atlantic. **Quaternary Science Reviews**, v. 48, p. 43–53, 2012.

JORGETTI, T.; SILVA DIAS, P. L. DA; FREITAS, E. D. DE. The relationship between South Atlantic SST and SACZ intensity and positioning. **Climate Dynamics**, v. 42, n. 11–12, p. 3077–3086, 2014.

KAISER, J.; LAMY, F.; HEBBELN, D. A 70-kyr sea surface temperature record off southern Chile (Ocean Drilling Program Site 1233). **Paleoceanography**, v. 20, n. 4, p. 1–15, 2005.

KANFOUSH, S.; HODELL, D.; CHARLES, C.; et al. Millennial-scale instability of the antarctic ice sheet during the last glaciation. **Science**, v. 288, n. 5472, p. 1815–8, 2000.

KIM, J. H.; ROMERO, O. E.; LOHMANN, G.; et al. Pronounced subsurface cooling of North Atlantic waters off Northwest Africa during Dansgaard-Oeschger interstadials. **Earth and Planetary Science Letters**, v. 339–340, p. 95–102, 2012.

KUCERA, M.; ROSELL-MELÉ, A.; SCHNEIDER, R.; WAELBROECK, C.; WEINELT, M. Multiproxy approach for the reconstruction of the glacial ocean surface (MARGO). **Quaternary Science Reviews**, v. 24, n. 7–9, p. 813–819, 2005.



- KUCERA, M.; WEINELT, M.; KIEFER, T.; et al. Reconstruction of sea-surface temperatures from assemblages of planktonic foraminifera: multi-technique approach based on geographically constrained calibration data sets and its application to glacial Atlantic and Pacific Oceans. **Quaternary Science Reviews**, v. 24, n. 7–9, p. 951–998, 2005.
- LESSA, D. V.; VENANCIO, I. M.; SANTOS, T. P. DOS; et al. Holocene oscillations of Southwest Atlantic shelf circulation based on planktonic foraminifera from an upwelling system (off Cabo Frio, Southeastern Brazil). **The Holocene**, v. 26, n. 8, p. 1175–1187, 2016.
- LISIECKI, L. E.; RAYMO, M. E. A Pliocene-Pleistocene stack of 57 globally distributed benthic  $\delta^{18}\text{O}$  records. **Paleoceanography**, v. 20, n. 1, p. 1–17, 2005.
- LOCARNINI, R. A., et al. World Ocean Atlas, Volume 1: Temperature. **NOAA Atlas NESDIS**, 68, 184 pp, 2010.
- LOTOTSKAYA, A.; GANSEN, G. M. The structure of Termination II (penultimate deglaciation and Eemian) in the North Atlantic. **Quaternary Science Reviews**, v. 18, n. 14, p. 1641–1654, 1999.
- LOUBERE, P.; FARIDUDDIN, M.; RICHAUD, M. Glacial marine nutrient and carbon redistribution: Evidence from the tropical ocean. **Geochemistry, Geophysics, Geosystems**, v. 12, n. 8, p. 1–16, 2011.
- LOURANTOU, A.; CHAPPELLAZ, J.; BARNOLA, J. M.; MASSON-DELMOTTE, V.; RAYNAUD, D. Changes in atmospheric  $\text{CO}_2$  and its carbon isotopic ratio during the penultimate deglaciation. **Quaternary Science Reviews**, v. 29, n. 17–18, p. 1983–1992, 2010.
- LUND, D. C.; TESSIN, A. C.; HOFFMAN, J. L.; SCHMITTNER, A. Southwest Atlantic water mass evolution during the last deglaciation. **Paleoceanography**, v. 30, n. 5, p. 477–494, 2015.
- LYNCH-STIEGLITZ, J.; SCHMIDT, M. W.; GENE HENRY, L.; et al. Muted change in Atlantic overturning circulation over some glacial-aged Heinrich events. **Nature Geoscience**, v. 7, n. 2, p. 1–7, 2014.
- LYNCH-STIEGLITZ, J.; STOCKER, T. F.; BROECKER, W. S.; FAIRBANKS, R. G. The influence of air-sea exchange on the isotopic composition of oceanic carbon: Observations and modeling. **Global Biogeochemical Cycles**, v. 9, n. 4, p. 653–665, 1995.
- MARCOTT, S. A.; CLARK, P. U.; PADMAN, L.; et al. Ice-shelf collapse from subsurface warming as a trigger for Heinrich events. **Proceedings of the National Academy of Sciences of the United States of America**, v. 108, n. 33, p. 13415–13419, 2011.
- MARINO, G.; ZAHN, R.; ZIEGLER, M.; et al. Agulhas salt-leakage oscillations during abrupt climate changes of the Late Pleistocene. **Paleoceanography**, v. 28, n. 3, p. 599–606, 2013.
- MARTÍNEZ-MÉNDEZ, G.; ZAHN, R.; HALL, I. R.; et al. Contrasting multiproxy reconstructions of surface ocean hydrography in the Agulhas Corridor and implications for the Agulhas Leakage during the last 345,000 years. **Paleoceanography**, v. 25, n. 4, p. 1–12, 2010.
- MASSON-DELMOTTE, V.; STENNI, B.; BLUNIER, T.; et al. Abrupt change of Antarctic moisture origin at the end of Termination II. **Proceedings of the National Academy of Sciences of the United States of America**, v. 107, n. 27, p. 12091–4, 2010.

- MCMANUS, J. F.; FRANCOIS, R.; GHERARDI, J.; KEIGWIN, L. D. Collapse and rapid resumption of Atlantic meridional circulation linked to deglacial climate changes. **Nature**, v. 428, n. April, p. 1–4, 2004.
- MENVIEL, L.; JOOS, F.; RITZ, S. P. Simulating atmospheric CO<sub>2</sub>, <sup>13</sup>C and the marine carbon cycle during the Last Glacial-Interglacial cycle: Possible role for a deepening of the mean remineralization depth and an increase in the oceanic nutrient inventory. **Quaternary Science Reviews**, v. 56, p. 46–68, 2012.
- MIGNOT, J.; GANOPOLSKI, A.; LEVERMANN, A. Atlantic subsurface temperatures: Response to a shutdown of the overturning circulation and consequences for its recovery. **Journal of Climate**, v. 20, n. 19, p. 4884–4898, 2007.
- MORTYN, P. G. Planktonic foraminifera and their proxies for the reconstruction of surface-ocean climate parameters. **Contributions to Science**, v. 3, n. 3, p. 371–383, 2007.
- MULITZA, S.; BOLTOVSKOY, D.; DONNER, B.; et al. Temperature: <sup>δ18</sup>O relationships of planktonic foraminifera collected from surface waters. **Palaeogeography, Palaeoclimatology, Palaeoecology**, v. 202, n. 1–2, p. 143–152, 2003.
- MULITZA, S.; PAUL, A.; WEFER, G. Paleoceanography, records/Late Pleistocene South Atlantic. **Encyclopedia of Quaternary Science**, n. 2004, p. 1816–1831, 2007.
- MURRAY-WALLACE, C. V. Sea level studies/Eustatic Sea-Level Changes, Glacial-Interglacial Cycles. **Encyclopedia of Quaternary Science**, , n. 1998, p. 3024–3034, 2007.
- NGRIP COMMUNITY MEMBERS. High-resolution record of Northern Hemisphere climate extending into the last interglacial period. **Nature**, v. 431, n. 7005, p. 147–151, 2004.
- NINNEMANN, U. S.; CHARLES, C. D. Changes in the mode of Southern Ocean circulation over the last glacial cycle revealed by foraminiferal stable isotopic variability. **Earth and Planetary Science Letters**, v. 201, n. 2, p. 383–396, 2002.
- OLSON, D. B.; PODEST, G. P.; EVANS, R. H.; BROWN, O. B. Temporal variations in the separation of Brazil and Malvinas Currents. **Deep Sea Research Part A, Oceanographic Research Papers**, v. 35, n. 12, p. 1971–1990, 1988.
- OPPO, D. W.; CURRY, W. B.; MCMANUS, J. F. What do benthic <sup>13</sup>C and <sup>18</sup>O data tell us about Atlantic circulation during Heinrich Stadial 1? , p. 353–368, 2015.
- PADOS, T.; SPIELHAGEN, R. F.; BAUCH, D.; MEYER, H.; SEGL, M. Oxygen and carbon isotope composition of modern planktic foraminifera and near-surface waters in the Fram Strait (Arctic Ocean): A case study. **Biogeosciences**, v. 12, n. 6, p. 1733–1752, 2015.
- PAHNKE, K.; SACHS, J. P. Sea surface temperatures of southern midlatitudes 0–160 kyr B.P. **Paleoceanography**, v. 21, n. 2, p. 1–17, 2006.
- PEETERS, F. J. C.; ACHESON, R.; BRUMMER, G.-J. A.; et al. Vigorous exchange between the Indian and Atlantic oceans at the end of the past five glacial periods. **Nature**, v. 430, n. 7000, p. 661–5, 2004.
- PETERSON, C. D.; LISIECKI, L. E.; STERN, J. V. Deglacial whole-ocean <sup>δ13</sup>C change estimated from 480 benthic foraminiferal records. **Paleoceanography**, v. 29, n. 6, p. 549–563, 2014.
- PETERSON, R. G.; STRAMMA, L. Upper-level circulation in the South Atlantic Ocean. **Progress in Oceanography**, v. 26, n. 1, p. 1–73, 1991.

- PIOTROWSKI, A. M.; GOLDSTEIN, S. L.; HEMMING, S. R.; FAIRBANKS, R. G. Temporal relationships of carbon cycling and ocean circulation at glacial boundaries. **Science**, v. 307, n. 5717, p. 1933–1938, 2005.
- RAHMSTORF, S.; BOX, J. E.; FEULNER, G.; et al. Exceptional twentieth-century slowdown in Atlantic Ocean overturning circulation. **Nature Climate Change**, v. 5, n. 5, p. 475–480, 2015.
- RASMUSSEN, T. L.; THOMSEN, E.; MOROS, M. North Atlantic warming during Dansgaard-Oeschger events synchronous with Antarctic warming and out-of-phase with Greenland climate. **Scientific Reports**, v. 6, 2016.
- RAYMO, M. E. The timing of major climate terminations. **Paleoceanography**, v. 12, n. 4, p. 577, 1997.
- REIMER, P. J.; BARD, E.; BAYLISS, A.; et al. IntCal13 and Marine13 Radiocarbon Age Calibration Curves 0–50,000 Years cal BP. **Radiocarbon**, v. 55, n. 4, p. 1869–1887, 2013.
- REYNOLDS, R. W.; SMITH, T. M.; LIU, C.; et al. Daily high-resolution-blended analyses for sea surface temperature. **Journal of Climate**, v. 20, n. 22, p. 5473–5496, 2007.
- ROBERTSON, A. W.; FARRARA, J. D.; MECHOSO, C. R. Simulations of the Atmospheric Response to South Atlantic Sea Surface Temperature Anomalies. **Journal of Climate**, v. 16, p. 2540–2551, 2003.
- RODRIGUES, R. R.; ROTHSTEIN, L. M.; WIMBUSH, M. Seasonal Variability of the South Equatorial Current Bifurcation in the Atlantic Ocean: A Numerical Study. **Journal of Physical Oceanography**, v. 37, n. 1, p. 16–30, 2007.
- ROSENTHAL, Y.; LINSLEY, B. Paleoceanography, physical and chemical proxies/Mg/Ca and Sr/Ca Paleothermometry. **Encyclopedia of Quaternary Science**, p. 1723–1731, 2007.
- RUDDIMAN, W. F. Orbital changes and climate. **Quaternary Science Reviews**, v. 25, n. 23–24, p. 3092–3112, 2006.
- SÁNCHEZ GOÑI, M. F.; BARD, E.; LANDAIS, A.; ROSSIGNOL, L.; D'ERRICO, F. Air–sea temperature decoupling in western Europe during the last interglacial–glacial transition. **Nature Geoscience**, v. 6, n. 10, p. 837–841, 2013.
- SANTOS, T. P.; LESSA, D. O.; VENANCIO, I. M.; et al. Prolonged warming of the Brazil Current precedes deglaciations. **Earth and Planetary Science Letters**, v. 463, p. 1–12, 2017.
- SCHLITZER, R. Interactive analysis and visualization of geoscience data with ocean data view. **Computers & Geosciences**, 28 (10), 1211–1218, 2002.
- SCHMIDT, M. W.; SPERO, H. J. Meridional shifts in the marine ITCZ and the tropical hydrologic cycle over the last three glacial cycles. **Paleoceanography**, v. 26, n. 1, p. 1–15, 2011.
- SCHMITTNER, A.; LUND, D. C. Early deglacial Atlantic overturning decline and its role in atmospheric CO<sub>2</sub> rise inferred from carbon isotopes ( $\delta^{13}\text{C}$ ). **Climate of the Past**, v. 11, n. 2, p. 135–152, 2015.
- SCHULZ, M.; MUDELSEE, M. REDFIT: estimating red-noise spectra directly from unevenly spaced paleoclimatic time series. **Computers & Geosciences**, v. 28, n. 3, p. 421–426, 2002.
- SCUSSOLINI, P.; MARINO, G.; BRUMMER, G.-J. A.; PEETERS, F. J. C. Saline Indian

Ocean waters invaded the South Atlantic thermocline during glacial termination II. **Geology**, v. 43, n. 2, p. 139–142, 2015.

SÉVELLEC, F.; FEDOROV, A. V. Unstable AMOC during glacial intervals and millennial variability: The role of mean sea ice extent. **Earth and Planetary Science Letters**, v. 429, p. 60–68, 2015.

SIGMAN, D. M.; BOYLE, E. A. Glacial/Interglacial Variations In Atmospheric Carbon Dioxide. **Nature**, v. 407, n. 6806, p. 859–869, 2000.

SHACKLETON, N. J. Oxygen isotopes, ice volume and sea level. **Quaternary Science Reviews**, v. 6, n. 3–4, p. 183–190, 1987.

SKINNER, L. C.; ELDERFIELD, H. Rapid fluctuations in the deep North Atlantic heat budget during the last glacial period. **Paleoceanography**, v. 22, n. 1, p. 1–9, 2007.

STENNI, B.; JOUZEL, J.; MASSON-DELMOTTE, V.; et al. A late-glacial high-resolution site and source temperature record derived from the EPICA Dome C isotope records (East Antarctica). **Earth and Planetary Science Letters**, v. 217, n. 1–2, p. 183–195, 2004.

STOCKER, T. F.; JOHNSEN, S. J. A minimum thermodynamic model for the bipolar seesaw. **Paleoceanography**, v. 18, n. 4, p. n/a-n/a, 2003.

STRAMMA, L.; ENGLAND, M. On the water masses and mean circulation of the South Atlantic Ocean. **Journal of Geophysical Research: Oceans**, v. 104, n. C9, p. 20863–20883, 1999.

TALLEY, L. D. Some aspects of ocean heat transport by the shallow, intermediate and deep overturning circulations. **Geophys. Mono. Ser.**, 1999.

TELFORD, R. J.; ANDERSSON, C.; BIRKS, H. J. B.; JUGGINS, S. Biases in the estimation of transfer function prediction errors. **Paleoceanography**, v. 19, n. 4, p. 1–5, 2004.

TELFORD, R. J.; BIRKS, H. J. B. The secret assumption of transfer functions: problems with spatial autocorrelation in evaluating model performance. **Quaternary Science Reviews**, v. 24, n. 20–21, p. 2173–2179, 2005.

TESSIN, A. C.; LUND, D. C. Isotopically depleted carbon in the mid-depth South Atlantic during the last deglaciation. **Paleoceanography**, v. 28, n. 2, p. 296–306, 2013.

TOLEDO, F. A. L.; COSTA, K. B.; PIVEL, M. A. G. Salinity changes in the western tropical South Atlantic during the last 30 kyr. **Global and Planetary Change**, v. 57, n. 3–4, p. 383–395, 2007.

TOMCZAK, M.; GODFREY, J.S. Regional Oceanography: An Introduction. **Pergamon**, p. 390, 1994.

VERES, D.; BAZIN, L.; LANDAIS, A.; et al. The Antarctic ice core chronology (AICC2012): An optimized multi-parameter and multi-site dating approach for the last 120 thousand years. **Climate of the Past**, v. 9, n. 4, p. 1733–1748, 2013.

WAELEBROECK, C.; LABEYRIE, L.; MICHEL, E.; et al. Sea-level and deep water temperature changes derived from benthic foraminifera isotopic records. **Quaternary Science Reviews**, v. 21, n. 1–3, p. 295–305, 2002.

WEBER, S. L.; DRIJFHOUT, S. S.; ABE-OUCHI, A.; et al. The modern and glacial overturning circulation in the Atlantic ocean in PMIP coupled model simulations. **Climate of the Past Discussions**, v. 2, n. 5, p. 923–949, 2006.

WELDEAB, S.; SCHNEIDER, R. R.; KÖLLING, M. Deglacial sea surface temperature and salinity increase in the western tropical Atlantic in synchrony with high latitude climate instabilities. **Earth and Planetary Science Letters**, v. 241, n. 3–4, p. 699–706, 2006.

WOODGATE, R. A.; WEINGARTNER, T.; LINDSAY, R. The 2007 Bering Strait oceanic heat flux and anomalous Arctic sea-ice retreat. **Geophysical Research Letters**, v. 37, n. 1, p. 1–5, 2010.

WU, L.; CAI, W.; ZHANG, L.; et al. Enhanced warming over the global subtropical western boundary currents. **Nature Climate Change**, v. 2, n. 3, p. 161–166, 2012.

YU, J.; MENVIEL, L.; JIN, Z. D.; et al. Sequestration of carbon in the deep Atlantic during the last glaciation. **Nature Geoscience**, v. 9, n. 4, p. 319–324, 2016.

ZAHN, R., WINN, K., SARNTHEIN, M. Benthic foraminiferal  $\delta^{13}\text{C}$  and accumulation rates of organic carbon: *Uvigerina peregrina* group and *Cibicidoides wuellerstorfi*. **Paleoceanography** 1, 27–42, 1986.

ZHANG, R. Coherent surface-subsurface fingerprint of the Atlantic meridional overturning circulation. **Geophysical Research Letters**, v. 35, n. 20, p. 1–6, 2008.